UNIVERSITATEA LUCIAN BLAGA DIN SIBIU

Medical doctoral school

Doctoral field: Medicine

DOCTORAL THESIS

Histopathological alterations and immunohistochemical and molecular analysis of the SARS-CoV-2 infection

Ph.D. candidate:
GEORGE-CĂLIN, OPRINCA

Ph.D. supervisor:
Prof. Univ. Dr. MANUELA, MIHALACHE

SIBIU2023

CONTENTS

INTRODUCTION

Given the pandemic context of previous years and the ongoing global efforts of authorities to understand the interaction of the new coronavirus with the human body through scientific methods, it is of utmost importance to research all the changes that this virus manages to induce at the tissue level.

Through a detailed analysis of the macroscopic changes obtained from autopsies, the microscopic tissue alterations, and the immunological interactions highlighted through immunohistochemical techniques, this work serves as a piece of the puzzle in the scientific world, contributing to the understanding of the void created by this pandemic that has taken the entire humanity by surprise. The microscopic footprint of a microorganism, as well as its mode of interaction with each host cell, can unveil all the weapons it possesses that can cause irreversible damage at the tissue level. Moreover, precise knowledge of a microorganism can even reveal the hidden mechanisms it uses to activate immunological evasion, allowing us to compare this virus to a "shadow assassin." All these viral "weapons" can be unveiled through next-generation analyses (immunohistochemistry and molecular analyses).

Even though the pandemic has come to an end, the virus is still active in the general population. Although its aggressiveness towards the human host has significantly diminished, it still leads to fatalities in many cases, especially in individuals with comorbidities. Over the years, the concept of "long-COVID" has emerged, characterized by the persistence of symptoms in some individuals previously infected with the SARS-CoV-2 virus. Given that infection with the aforementioned virus has had and continues to have an impact on the population, we aim to identify the cellular changes that this pathogen induces in an attempt to meet the medical world's needs in finding new weapons in the fight against the SARS-CoV-2 virus.

CURRENT STATE OF KNOWLEDGE

1. FUNDAMENTAL CONCEPTS OF VIROLOGY

1.1. BRIEF HISTORY OF MODERN VIROLOGY

The microbial theory had its conceptual foundations as early as the 19th century, under the research of the anatomist Jacob Henle, who first described the etiology of certain diseases as being caused by microorganisms too small to be observed with an optical microscope.[2] However, it took the research of Louis Pasteur and Robert Koch in the late 1800s for the microbial theory to become widely accepted. Pasteur made significant progress by analyzing fermentation caused by various microorganisms, and Robert Koch, the father of solid culture media, was the first to describe the etiological agent of anthrax and tuberculosis. He also formulated a set of postulates that became the foundation of modern microbiology, stating that: a) the microorganism must be constantly observed in the lesion; b) it must be isolated in pure culture; c) inoculation of the microorganism into a new host must induce the disease; d) the microorganism must be isolated again from the last host. Furthermore, the discovery of certain diseases that presented clear evidence of an infectious etiology but challenged Koch's postulates led to the identification of new, often more dangerous microorganisms.[1]

Dimitri Iwanowsky managed to discover, through the study of tobacco mosaic disease, that the condition was caused by a pathogenic agent that could pass through the porcelain filter (Chamberland filter) and did not adhere to Koch's postulates. Subsequently, by repeating the experiment, Martinus Beijerinck became convinced that he was dealing with a pathogenic agent different from bacteria and defined it as "contagium vivum fluidum." [3]

1.2. VIRAL BIOMASS: FROM ANCIENT VIRAL GENOMES TO SYMBIOTIC AND PATHOGENIC VIRUSES

The term "virus" originates from the Latin word "virus," which means "poison." It represents a nanoparticle or, more precisely, a complex molecular structure incapable of self-

replication, needing to invade, parasitize, and take control of the components of a living cell to multiply. The viral biomass consists of numerous viral populations, with the majority living in a symbiotic relationship with the host cell and being harmless to living organisms. However, although few in number, some viruses are pathogenic, causing a range of pathologies from mild, even asymptomatic infections to severe, debilitating, and even fatal illnesses. In addition to active pathogenic viruses and those in symbiosis with the host cell, dormant viruses and even genomic remnants of ancient viruses that integrated into the host genome long ago have been discovered. [4]

1.3. VIRAL MORPHOLOGICAL STRUCTURE

Viral particles can be defined as carriers of viral genetic material, a biological machinery capable of entering the host cell, taking over some of its functions, reproducing, escaping from the infected cell, and surviving extracellularly until the next "invasion" when the viral cycle resumes. [1]

Structurally, a viral particle is composed of viral genetic material in the form of DNA or RNA in various representations, almost always surrounded by protein subunits that are folded protein chains forming asymmetric structural units, resulting in the viral capsid or nucleocapsid. Some viruses have an external lipid envelope called a viral envelope to which surface receptors are attached, playing a major role in adhesion and penetration mechanisms into the host cell. When we refer to the nucleocapsid, we are talking about enveloped viruses in which the capsid serves a subunitary role, enveloping the genetic material without direct contact with the extracellular environment. Viral particles are always metastable, existing in a stable form outside the host cell, but they must transition to an unstable form at the cellular entry point to be disassembled. [5]

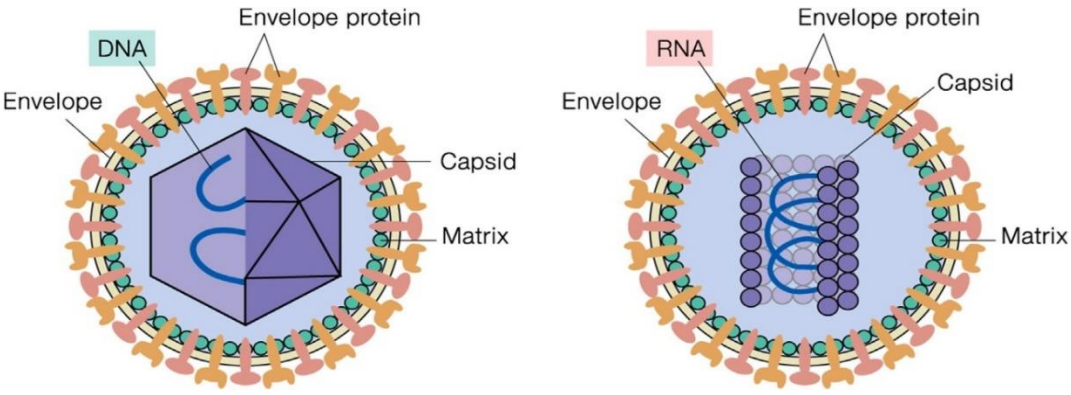

Figure 1. Example of viral morphological structure. [2]

Each nucleic acid molecule can be single-stranded (monocatenary) or double-stranded (double-catenary). Based on this principle, a virus can have DNA as its genetic material, either single-stranded (ssDNA) or double-stranded (dsDNA), or it can have RNA as its genetic material, either single-stranded (ssRNA) or double-stranded (dsRNA). The Baltimore classification categorizes viruses into seven classes based on their genetic material, namely dsDNA (double-stranded DNA), ssDNA (single-stranded DNA), dsRNA (double-stranded RNA), ss(-)RNA (single-stranded negative-sense RNA), ss(+)RNA (single-stranded positive-sense RNA), ssRNA with attached intermediate DNA, and dsDNA with attached intermediate RNA, known as "gapped DNA." [6]

The capsid is composed of multiple copies of the same protein, forming a complex designed to protect the viral genetic material from external environmental factors and the immune system of the host cell. This protein structure is encoded by a relatively short sequence in the viral genome but can encapsulate a large number of nucleic acids. This is beneficial for the microorganism because it relieves the virus from the burden of encoding a large molecular structure protein, but it presents the challenge of assembling multiple protein subunits. [7]

The viral envelope is not consistently present in all types of viruses. It is an external membrane or capsule designed to protect the viral genetic content and the nucleocapsid (whether helical or icosahedral) and is formed from a double lipid bilayer derived from the host cell. The viral genome is incapable of encoding the information required for the development of the lipid-synthesizing machinery. Therefore, the newly formed virion by the infected host cell assimilates part of the cytoplasmic membrane, nuclear membrane, Golgi apparatus, or endoplasmic reticulum to create the viral envelope.

For a virus to be active, it is necessary for it to have on its surface glycoproteins responsible for adhesion, fusion, and cell penetration. In some cases, a single type of glycoprotein can perform all three functions combined, as is the case with the hemagglutinin (HA) of the influenza virus. Other functions of glycoproteins include destroying cell receptors after adhesion or mediating immune evasion. [13]

In addition to the main structures mentioned above, a viral particle can also contain other proteins, such as enzymes like polymerases, integrases, proteases, topoisomerases, as well as cellular components like transfer RNA (tRNA), lipids, or histones. These additional components

can play various roles in the viral replication cycle, including genome replication, integration into the host genome, and modulation of host cell processes.

2. HOST IMMUNE RESPONSE IN VIRAL INFECTIONS

2.1. CHEMICAL AND ANATOMICAL BARRIERS

The pseudostratified epithelium of the bronchial mucosa is exposed not only to pathogenic microbiological agents but also to toxic particles present in inhaled air. Therefore, in addition to columnar cells, the epithelium also contains goblet cells which, along with the glandular epithelium in the submucosa, secrete mucus. This fluid contains gel-forming mucins as well as antimicrobial molecules, antiproteases, and antioxidants, forming a chemical barrier. The presence of oligomeric mucins MUC5AC and MUC5B helps capture and neutralize pathogens and foreign particles, which are then eliminated through the action of cilia. [16] At the alveolar level, the inner wall is composed of two cell types: type I alveolar cells (ATI) and type II alveolar cells (ATII). While ATI cells dominate in terms of distribution, ATII cells, although fewer in number, play a major role in local antimicrobial defense. In addition to secreting surfactant, which is necessary for alveolar inflation, ATII cells are involved in tissue regeneration, maintaining fluid balance, and trans-epithelial ion transport. [17]

At the intestinal level, the mucosa is lined with a simple columnar epithelium composed of several subtypes of cells, including M cells, goblet cells, Paneth cells, enterochromaffin cells, and columnar cells. This epithelium serves as a physical barrier that separates the luminal external environment from the intestinal wall. However, this barrier is often found to be inefficient. To enhance protection at this level, similar to the bronchial epithelium, there is a secretion of mucus composed of numerous bioactive molecules, mucins, glycoproteins, antimicrobial peptides, and immunoglobulin A. Given the presence of numerous commensal bacteria in the digestive tract that live in symbiosis with the host organism, this physico-chemical barrier takes on a special status. Continuous interaction and close collaboration between the commensal bacterial flora, the intestinal epithelial cells, and local immune cells are necessary to maintain homeostasis.

2.2. INTRINSIC IMMUNITY

The earliest evolved structures in this type of immunity are under the coordination of RNA-mediated interference (RNAi) and CRISPR (Clustered Regularly Interspaced Short Palindromic Repeats) sequences. RNA interference (RNAi) is the predominant mechanism of antiviral defense in plants and invertebrates, but it can also be observed in vertebrates. In cellular responses to RNA viruses, long double-stranded RNA (dsRNA) fragments are produced, which are structurally different from the single-stranded, short RNA of the host cell.

Interferons are another class of proteins with a role in innate immunity, acting as a bridge between autonomous cellular immunity and innate immunity. They belong to the category of cytokines and are produced by cells exposed to pathogens, serving as a biochemical alarm system. There are three distinct families of interferons: Type I, composed of INF-α (interferon alpha) and INF-β (interferon beta); Type II, represented by a single member, INF-γ (interferon gamma); and Type III, composed of INF-λ (interferon lambda) 1, 2, 3, and 4. [21]

Autophagy, another key element of intrinsic immunity, is a mechanism for the sequestration and lysosomal degradation of cytoplasmic structures, including damaged organelles or invasive microorganisms. Autophagy begins with the sequestration of a portion of the cytoplasm containing organelles or pathogens into a double-membrane vesicle called an autophagosome. Subsequently, the autophagosome fuses with lysosomes, forming an autolysosome, where its contents are degraded. [23] The mechanism underlying autophagy is represented by autophagy-related proteins (ATG proteins). ATG proteins target all stages of pathogen entry, including endosome escape, viral replication within the cytosol, and evasion of viruses into the cytosol. [24]

Apoptosis, or programmed cell death, plays a crucial role in the defense against viral pathogens and lies at the border between intrinsic and adaptive immunity, under the strict coordination of both internal cellular mechanisms and immune system cells. That being said, apoptosis is triggered by two major pathways: an intrinsic pathway (coordinated by intracellular genetic machinery) and an extrinsic pathway (coordinated by the immune system), with the central role in both pathways being played by apoptotic caspases. [25]

2.3. INNATE IMMUNITY

The formation of the antigen-receptor complex leads to the release of cytokines, especially interferons, from the cell that encounters the viral pathogen. To achieve this result, the antigen-

receptor complex activates specific biochemical signaling pathways designed to trigger massive releases of immune "alarm" molecules. After recognizing pathogen-associated molecular patterns (PAMPs), the cytoplasmic TIR domain (Toll-Interleukin 1 receptor) recruits signaling adapters like MyD88 (Myeloid differentiation primary response 88), TIRAP (TIR domain-containing adapter protein), TRAM (TRIF-related adaptor molecule), or TRIF (TIR-domain-containing adaptor inducing interferon-β), followed by the recruitment and activation of various kinases, such as IRAK1, IRAK2, IRAK4 (interleukin-1 receptor-associated kinases), TBK1 (TANK-binding kinase), IKK1 (inhibitor of kappaB kinase), and ubiquitin ligases, including TRAF6 (tumor necrosis factor receptor-associated factor 6) or pellino1, which are necessary for the transcription of INF genes. [29,30]

Dendritic cells are part of the innate immune system, but they also serve as the primary link between innate and adaptive immunity. These cells have a morphological structure with numerous cytoplasmic extensions, giving them a dendritic appearance, similar to neuronal dendrites, which is where they got their name. They are found in the interstitium of every organ except the brain, as well as in the blood and lymph nodes, but their primary location is in mucosal tissues, in close proximity to epithelia. Dendritic cells can extend their protrusions through the intercellular spaces of epithelial cells to the lumen where, using numerous surface receptors, they scan the area to detect non-self antigens. When an antigen binds to a receptor on the surface of dendritic cells, it becomes activated and migrates through the tissue to reach the lymphatic vessels. From there, it travels to the nearest lymph node, where it activates T cells using the previously collected antigen. [5]

Natural Killer (NK) cells are the effector lymphocytes of the innate immune system. These sentinel cells are found in both lymphoid and non-lymphoid tissues, and their primary purpose is to destroy virally infected cells or cells in a certain state of distress. The regulatory mechanisms of NK cells are based on two types of receptors: activating receptors and inhibitory receptors. Activating receptors detect the presence of ligands on the surface of distressed cells, such as stress-induced ligands recognized by NKG2D (Natural Killer Group 2D) receptors, Toll-like receptor ligands, or non-self infectious ligands. NK cells also express low-affinity for the Fc (crystallizable fragment) of CD16 (Cluster of Differentiation 16) receptors, allowing them to detect antibody-coated target cells and destroy them through antibody-dependent cellular cytotoxicity (ADCC). As their name suggests, NK cells are designed to destroy, and their braking system is dependent

on inhibitory receptors, including KIRs (killer cell immunoglobulin-like receptors) or CD94-NKG2A heterodimers. The ability of these receptors is to detect MHC class I molecules (Major Histocompatibility Complex class I) that are constantly expressed on healthy cells. In the case of a viral infection, the virus inhibits the production of MHC class I, and NK cells are no longer restrained from destroying the infected cell. However, some viruses produce MHC class I as an evasion mechanism against NK cells. [33]

The complement system is comprised of a diverse group of proteins that are part of the innate immune system. It functions as a rapid-response immunosurveillance system in the case of an infection. The classical activation pathway is triggered by certain isotypes of antibodies such as IgM or IgG bound to antigens. The lectin activation pathway is generated by pattern recognition receptors (PRRs), and the alternative pathway is activated by the spontaneous hydrolysis of C3. Regardless of the activation pathway, the main effects include initiating or supporting inflammation, opsonization, and direct cell lysis through the formation of the membrane attack complex. [34]

Neutrophils are small cells among the polymorphonuclear granulocytes (the most numerous of these cells), classified as such due to their bi or tri-lobed nuclear morphology and numerous intracytoplasmic enzyme-containing granules. Their migration to the battlefield occurs indirectly through endothelial cells, stimulated by cytokines like TNF (tumor necrosis factor) or IL-1β (interleukin 1 beta) which activate endothelial cells to express adhesion molecules that neutrophils adhere to. They cross the barrier of the vascular wall through diapedesis and reach the site of tissue damage. Neutrophils have an indirect role in viral infections through the secretion of cytokines and chemokines, which play a major role in activating other immune cells and supporting inflammation. An important advantage of neutrophils on the battlefield is the formation of NETs (neutrophil extracellular traps), which, according to recent studies, can capture viral particles or, at the very least, slow down their mobilization. [35]

The primary fuels that drives the innate immune response are cytokines, which are released in large quantities in damaged areas and trigger the five cardinal signs of inflammation: rubor (redness), tumor (swelling), calor (heat), dolor (pain), and functio lesa (loss of function). These cytokines can diffuse throughout the entire body, causing general symptoms such as fever, chills, fatigue, joint pain, and muscle aches. These cytokines are categorized into three groups:

proinflammatory cytokines like IL-1, TNF, IL-6, IL-12; anti-inflammatory cytokines like IL-4, IL-10, TGF-β (transforming growth factor); and chemokines like IL-8. [5]

2.4. ADAPTIVE IMMUNITY

The key player in cell-mediated immunity is the T lymphocyte (T cell), and the process of T cell development begins in the bone marrow and continues in the thymus, where they undergo numerous processes of maturation, differentiation, and selection. The production of T cells in the thymus begins in the late stages of embryonic development and continues until puberty. Genes encoding the T cell receptor (TCR) chains are formed in immature thymocytes through constant and variable gene segment rearrangements. Most T cells at this stage will express αβ TCR receptors, and the specificity of T cell clones is to recognize MHC (major histocompatibility complex) class I or class II. Over time, several types of CD4+ T helper cells have been identified, including T-helper 1 (Th1), T-helper 2 (Th2), T-helper 17 (Th17), T-follicular helper (Tfh), Type 1 regulatory T cells (Tr1), induced regulatory T cells (iTreg), and T-helper 9 (Th9). Their differentiation is driven by a complex network of cytokine signals and specific transcription factors, followed by epigenetic changes. [37]

Humoral immunity plays an essential role in both combating acute viral infections and protecting the host organism against reinfection with the same pathogen. The key coordinator of this type of immunity is the B lymphocyte, and this coordination is mediated through the production of special proteins called antibodies. B lymphocytes are produced in the bone marrow, and after maturation, they are found in an inactive state in the follicular area of the lymph node. Their activation occurs when a specific antigen binds to the B cell receptor (BCR). It's worth noting that B lymphocytes can recognize not only antigens presented by antigen-presenting cells but also soluble antigens. The encounter between the antigen and the receptor can occur both in the lymph node and the spleen. Upon activation, B lymphocytes process the antigen and, in the end, can present it on the cell surface via MHC class II, demonstrating that B cells can recruit CD4+ T helper lymphocytes in the fight against the pathogen. [40]

Antibodies, the secret weapon of B cell-mediated immunity, are protein molecules known as immunoglobulins. The classic structure of these molecules consists of two light protein chains and two heavy protein chains, linked together by disulfide bridges. Each chain contains constant regions (CH or CL), which are unchangeable, and variable regions (VH or VL), which have the

capacity to change over time. Both constant and variable regions are present in the Fab region (antigen binding domain), while only constant regions are present in the Fc region (crystallizable fragment). The function of Fab is the effective attachment to the antigen, while Fc represents the binding region to the host cell's membrane receptors, such as macrophages, as well as the region for binding to complement. [5]

3. SARS-CoV-2 VIRUS: VIROLOGICAL ASPECTS

3.1. GENERAL CONSIDERATIONS

Structural studies have revealed two important characteristics of SARS-CoV-2. The virus appears to be optimized for binding to ACE2 (Angiotensin Conversion Enzyme 2) receptors, and the Spike protein, used as a key to enter host cells, has a functional polybasic cleavage site at the S1-S2 junction due to the insertion of 12 nucleotides. The receptor-binding domain (RBD) on the Spike protein represents the most variable structure in the coronavirus genome. Six amino acids in the RBD have been found to play a critical role in attaching to ACE2 receptors, and five of them are entirely different from the previous SARS-CoV virus. Although the Spike protein binds with high affinity to ACE2 receptors, molecular analysis reveals that this interaction is not optimal, so these changes are most likely a result of natural selection, allowing the virus to create other optimal binding solutions over time. The transition of the virion from animals to humans was marked by rapid mutations in these six amino acids within the RBD. The bat's horseshoe crab coronavirus RaTG13 shares a similar nucleotide structure with SARS-CoV-2 up to 96%, but it lacks the mutations in these six amino acids, which are instead found in samples obtained from pangolins. However, there is no evidence of recent genomic recombination. [47] [48]

3.2. VIRION STRUCTURE

From a structural perspective, the SARS-CoV-2 virus has a diameter of approximately 65-125 nm. It is encapsulated externally by an envelope that displays numerous spike proteins, giving the virion its characteristic appearance resembling a solar corona. The viral genome consists of a single-stranded positive-sense RNA. There are four major structural components that form the viral particle: the spike glycoprotein (S), the membrane glycoprotein (M), the envelope

glycoprotein (E), and the nucleocapsid (N). In addition to these, several accessory proteins are also present. [50]

The spike protein (S) plays a crucial role in the process of cellular invasion by effectively attaching the virion to the cell membrane receptors. In the case of the SARS-CoV-2 virus, it binds to ACE2 receptors (angiotensin-converting enzyme 2 receptors). The spike protein is a type I membrane glycoprotein that forms a trimer anchored to the viral envelope. After binding to the ACE2 receptors on the host cell, the protein undergoes numerous structural rearrangements to facilitate the fusion of the viral particle. It is heavily glycosylated, with each protomer containing 22 N-linked glycosylation sites.

The envelope protein (E) represents a structure of considerable importance and a key component in the assembly, escape, and virulence phases of the SARS-CoV-2 virus's reproductive cycle. It is composed of 75 amino acids, making it a relatively small protein, and it contains two distinct domains: an N-terminal transmembrane (TM) domain followed by a C-terminal domain. In addition to its structural role in coordinating virion assembly with the M protein, the E protein also mediates the host's immune response. [52] Being a hydrophobic protein, it oligomerizes in the host cell's membrane, forming hydrophilic pores that facilitate membrane remodeling and viral assembly. Recombinant coronaviruses lacking the E protein exhibit low titers and are incompetent in terms of propagation, demonstrating the crucial role of this structural protein in the viral replication process. [53]

The membrane protein M represents the most abundant protein on the surface of the viral particle, and its main purpose is to determine the shape of the viral envelope. Additionally, this protein can attach to other structural proteins, such as the N protein, which stabilizes the nucleocapsid and the RNA-protein N complex inside the virion. [50] Structurally, the M protein consists of an N-terminal amino domain, a transmembrane domain (TMD), and a C-terminal carboxyl domain. The N-terminal domain contains 10 amino acids, followed by an extended hydrophobic region of approximately 90 amino acids at the TMD level, and it finishes with a hydrophilic carboxyl terminal composed of 100 amino acids. [54]

The N protein consists of 419 amino acids and is organized in a modular fashion, divided into intrinsically disordered regions (IDRs) and structurally conserved regions. The IDRs include three modules: an N-arm, a central flexible Ser/Arg (serine/arginine)-rich linker region (LKR), and

a C-tail. Meanwhile, the conserved region is composed of an N-terminal domain (NTD) and a C-terminal domain (CTD). [55]

In addition to these four structural proteins, the viral genome also encodes a series of non-structural proteins (nsps) observed in other coronaviruses. Most of these non-structural proteins have enzymatic roles, such as genome viral genome correction, stimulation of exon activities, protein adhesion, interference signaling inhibition, host RNA translation blockade, RNA-dependent RNA polymerase replication, cytokine expression promotion, and viral polyprotein cleavage. [50]

3.3. ORGANIZATION AND STRUCTURE OF THE VIRAL GENOME

After the discovery of the first cases of atypical pneumonia at the end of 2019 in Wuhan, China, sequential analysis of specimens collected from the lower respiratory tract revealed the presence of a previously unidentified coronavirus, with a sequence that was 75% identical to the SARS-CoV virus. By January 2020, the entire genomic sequence of the new virus had been decoded. Like other Coronaviridae, the SARS-CoV-2 virus is constructed based on a single-stranded positive-sense RNA, with a length of approximately 29 kb (kilobases), which is a little over 29,800 nucleotides. The genetic material is packaged by the N protein into an extended ribonucleoprotein complex and further enclosed within a lipid viral envelope. The genome is composed of two open reading frames (ORFs) for the formation of non-structural proteins (Nsps) and nine smaller open reading frames that code for structural proteins, as well as accessory genes. The entire ORF region is flanked by 5' and 3' untranslated regions that contain conserved RNA structures with important functional roles in the viral replication cycle. [56][57]

3.4. VIRAL REPLICATION CYCLE

In the process of attaching to the cell membrane, the SARS-CoV-2 virus uses the spike protein from its viral envelope. The structure of this protein consists of a trimer with three receptor-binding heads (S1) positioned on a trimeric stalk for membrane fusion (S2). The S1 heads contain the receptor-binding domain (RBD), which specifically recognizes the ACE2 receptors (angiotensin-converting enzyme 2) on the surface of the host cell. Consistently, the RBD switches between an upright position, necessary for receptor binding, and a lying position for immune evasion. After effective binding to the receptor, the spike protein undergoes conformational

changes mediated by cell surface proteases like TMPRSS2 and lysosomal proteases such as cathepsins, changes necessary for the fusion process. This entire process is mediated by the pre-activation of furin, a proteolytic enzyme capable of increasing affinity and, subsequently, the invasion process in certain ACE2 receptor-expressing cells. [63]

The release of the viral genome into the cytoplasm triggers a complex and well-organized gene expression program. The first step involves the translation of the RNA sequences to produce non-structural proteins. As previously mentioned, these sequences are included in open reading frames (ORF1a and ORF1b). The pp1ab protein is produced due to a ribosomal frameshift between ORF1a and ORF1b, which is specific to the SARS-CoV-2 virus. Through co-translational and post-translational mechanisms, and with the help of proteases like nsp3 and nsp5, 16 non-structural proteins are released from the cleaved pp1a and pp1ab. Of these, 15 form the replication and transcription complex (RTC), which is essential for the next steps. Genomic replication is initiated by transcribing a full-length negative-sense RNA strand, which serves as a template for producing positive-sense RNA. This newly generated negative-sense RNA also produces more non-structural proteins and RTC. Transcription regulatory sequence leaders (TRS-L) serve as signals for the transcription of subgenomic messenger RNA, while each transcriptional unit of the genomic RNA is preceded by TRS-B. Once subgenomic mRNA particles are produced, nsp16, in strict coordination with nsp10, methylates the 5' end of viral mRNA to create a 5'-methyl cap. These subgenomic RNA molecules are further translated to form structural proteins, as well as some non-structural proteins, and the entire intermediate negative-sense RNA is transcribed again, this time in its entirety, into a positive-sense RNA that forms the basis of the newly formed virion's genome.[61]

1. INTRODUCTION

Since the declaration of the COVID-19 pandemic, researchers have been working to unravel all the pathological mechanisms underlying this new viral infection, which has had a significant global impact. Although the number of newly reported infection cases has been steadily decreasing, the initial phase was devastating, with numerous cases of patients experiencing post-infection complications from the SARS-CoV-2 virus, including death. Similar to the original SARS-CoV virus and the MERS-CoV virus, SARS-CoV-2 has aggressively and repeatedly jumped from animals to humans, making the possibility of future jumps to other species a constant concern. While the viral morphology, pathogenesis, and clinical and pathological alterations during the acute phase are relatively well understood, the same cannot be said for fulminant cases with a high mortality rate or for the subacute or "chronic" phase, which clinicians refer to as "long COVID." In this phase, patients may suffer from irreversible organ damage and a range of nonspecific chronic symptoms. It is essential for researchers, pathologists, and medical professionals to have multiple pathological models of the disease tailored to individual cases. Our study is based on 56 autopsies conducted on patients who died directly or indirectly due to COVID-19 at the Sibiu County Emergency Clinical Hospital. The goal of our study was to outline a morphopathological pattern of SARS-CoV-2 infection at a systemic level by evaluating each major organ in the body using histopathology, immunohistochemistry, and molecular analysis. Additionally, the initial results will be compared and correlated with the patients' age and gender, comorbidities, the time interval between symptom onset and death, and the number of days of hospitalization, thus establishing histopathological patterns of SARS-CoV-2 infection. In this way, we can construct the histopathological criteria necessary for the histopathological diagnosis of COVID-19.

2. RESEARCH PURPOSE AND OBJECTIVES

The purpose of this study is to determine the main pathogenetic mechanisms by which the SARS-CoV-2 virus interacts with the human host. This will be achieved by detecting microscopic tissue and cellular changes that occur as a result of the infection and by determining the morphopathological evolutionary forms through the study of dynamic lesions.

The main objectives of the study include:

- Highlighting microscopic lesions in patients who have died as a result of SARS-CoV-2 virus infection.
    - Histopathological examination, using hematoxylin and eosin staining, of specimens collected from the lung, heart, kidney, liver, spleen, and intestine.
- Determining the level of viral genome detection in the major organs and systems studied.
    - Molecular analysis, using real-time reverse transcription-polymerase chain reaction (rt-PCR), on specimens collected from the lung, heart, kidney, liver, spleen, and intestine, to detect the N, S, and ORF1ab genes of the SARS-CoV-2 virus.
- Determining the degree of viral invasion in different tissues and organs, as well as the cell types for which the SARS-CoV-2 virus has the highest affinity.
    - Immunohistochemical analysis on specimens collected from the lung, heart, kidney, liver, spleen, and intestine, using a monoclonal antibody against SARS-CoV-2 nucleocapsid, to detect viral nucleocapsid at the cellular level.
    - Immunohistochemical analysis using antibodies against CK5/6, CK7, TTF1, CD68, CK AE1/AE3, CK MNF 116, CD3, CD5, CD20, to highlight the cell type in which the viral nucleocapsid has been observed or which plays a major role in the pathogenic mechanism of the viral infection.
- Analyzing the trend of changes in the histopathological pattern over time and the degree of detection of the viral nucleocapsid and viral genome, depending on the time interval from the onset of the disease to death.
    - Classifying the microscopic lesions detected through classic histopathological examination, rt-PCR results, and immunohistochemistry, based on the time interval between the onset of the disease and death.

These objectives will help provide critical knowledge for understanding COVID-19, its histopathological diagnosis, and the development of more effective management and treatment strategies.

3. MATERIALS AND METHODS

3.1. SELECTION OF CASES

The current doctoral research is conducting a prospective study that began approximately 4 years ago, at the beginning of the SARS-CoV-2 pandemic, namely in 2020. All cases included in this thesis are derived from the case records of the Clinical Laboratory of Pathological Anatomy within the Emergency County Hospital of Sibiu, as well as from the records of the County Forensic Medicine Departament of Sibiu. Patients who were admitted to the Emergency County Hospital of Sibiu, confirmed with SARS-CoV-2 virus infection, and who subsequently passed away were selected. The number of autopsies on this category of patients was severely limited since, at that time, legislative regulations called for avoiding autopsies of SARS-CoV-2 positive patients to minimize exposure to the infectious agent. Nevertheless, a total of 56 autopsy cases of patients with SARS-CoV-2 infection were compiled, with infection confirmed within a timeframe ranging from one day to 68 days.

3.2. THE AUTOPSY

All autopsies in the study group were conducted in the Clinical Pathological Anatomy Laboratory of the Sibiu County Emergency Clinical Hospital, in the red zone - the Prosecture Department, strictly following the legal provisions of that period and using appropriate protective equipment. A total of 56 autopsies were performed for the study group, of which 39 were thoraco-abdomino-pelvic, 15 also included the cranial cavity, and 2 cases were minimally invasive, solely for the purpose of tissue sampling for further examination. Real-time descriptive analysis of external and internal examinations was conducted using a voice recorder, and autopsy photographs were taken using a Sony Alpha a6000 camera. The main modifications were photographed and described in detail within the autopsy report.

3.3. TISSUE SAMPLE COLLECTION

During each autopsy, tissue samples were collected from each organ for laboratory examinations, with the first sample being of a larger volume (approximately 2.5/2.5/2 cm) for embedding in paraffin blocks for histopathological and immunohistochemical examination. These samples were submerged in a 10% formaldehyde solution. For molecular examinations, smaller tissue samples were collected (approximately 2 mm in diameter). The latter samples were collected immediately after opening the cavities, in situ, using sterile tools for each organ to prevent cross-contamination with viral RNA from one organ to another. Immediately after collection, the tissue specimen was submerged in an RNA capture reagent (RNA-lock Reagent) for the preservation and stabilization of viral RNA. Subsequently, the tissue materials were stored at -30 degrees Celsius until they were molecularly evaluated.

3.4. PREPARATION OF HISTOPATHOLOGICAL SLIDES

In order to create histopathological slides, the tissue samples collected from each autopsy underwent chemical processes of fixation, dehydration, and processing, as well as mechanical processes of embedding and micrometric sectioning, followed by staining processes. Before the actual processing, following the initial fixation of the tissue samples in a 10% formaldehyde solution for at least 48 hours, the collected tissues were sliced to a thickness of approximately 2-3 mm, shaped and macroscopically oriented, and then placed into traditional histological cassettes with lids. After the tissue materials were processed, they were embedded in paraffin blocks for subsequent microtome sectioning. Sections were made using a manual microtome, then stretched using a warm water bath and placed on slides with a positive charge. All histopathological slides in the current study were stained only with the standard Hematoxylin and Eosin stain, using an automated histological stainer.

3.5. PREPARATION OF IMMUNOHISTOCHEMICAL SLIDES

The basic immunohistochemical analysis used in all autopsied cases, on tissue samples collected from the cerebral, pulmonary, cardiac, renal, hepatic, splenic, and intestinal levels, was aimed at detecting the viral nucleocapsid of the SARS-CoV-2 virus. This detection was performed using a mouse monoclonal antibody of IgG2b isotype. For positive control, five lung tissues infected in vitro with the SARS-CoV-2 BSB-3701-CS virus were acquired, sectioned, and mounted on Hydrophilic Plus slides. Two negative controls were obtained for each organ and for

each case separately. One negative control utilized tissue from the same patients but without the primary antibody incubation, while the other used specimens recovered from another patient who had been confirmed as negative through molecular techniques. [79]

3.6. RT-PCR EXAMINATION (REVERSE TRANSCRIPTION POLYMERASE CHAIN REACTION)

RNA was extracted from the specimens stored in RNA capture reagent at -20°C using the QIAamp viral RNA extraction kit (Qiagen, Hilden, Germany), following the manufacturer's recommendations. The RNA was then eluted in a final volume of 60 μL using elution buffer. In vitro-created MS2 bacteriophage RNA (Emesvirus zinderi) was introduced into the specimen lysis buffer and served as a control for the RNA extraction step, as well as for control in the absence of inhibitors in the RT-qPCR reactions. The presence and quantity of the viral genes N (nucleocapsid), S (spike), and Orf1ab (Open Reading Frame 1ab) of SARS-CoV-2, as well as the MS2 control, were determined using quantitative reverse transcription polymerase chain reaction (RT-qPCR) with the TaqPath COVID-19 CE-IVD RT-PCR kit (Thermo-Fisher Scientific, Waltham, MA, USA), following the manufacturer's recommendations and utilizing the QuantStudio 5 Real-Time PCR system (Applied Biosystems, Waltham, MA, USA).

3.7. DIGITIZING MICROSCOPIC SLIDES

Each microscopic slide was evaluated using a traditional microscope. Subsequently, the slides that displayed the most pronounced and specific changes were re-cataloged and digitized in 4K format to facilitate a more in-depth histopathological analysis. The digitization of the microscopic slides was performed using a digital scanner, specifically the Pannoramic Desk II DW (3dHistech).

3.8. HISTOPATHOLOGICAL AND IMMUNOHISTOCHEMICAL EXAMINATION

Each histopathological specimen was assessed using a traditional microscope, and the slides displaying the most specific and prominent alterations were further analyzed digitally. Following these meticulous evaluations, a microscopic description of each histopathological and immunohistochemical slide was prepared, along with the histopathological and immunohistochemical diagnosis.

3.9. REZULTS ANALYSIS

Each case in the study group was included in a database that primarily encompassed the structure of the group divided by gender and age, as well as clinical and pathological data such as the length of hospitalization (in days), the time interval between the onset of symptoms and death (in days), comorbidities, cause of death, and associated diagnoses. Another aspect of the database comprised the primary histopathological changes observed in the Hematoxylin and Eosin stained specimens, categorized by each organ and each case in the study group. The next segment of the database consisted of immunohistochemical profiles, specifically the presence or absence of viral nucleocapsid at the cellular level in the collected specimens. This data was categorized by each organ, each type of cell exhibiting positivity, and, of course, each case in the study group. The last part of the database contained molecular analyses through rt-PCR, where the results were categorized as positive or negative for each of the three studied genes. This data was organized by each organ, encompassing every case in the study group. After completing the database, a descriptive analysis of each microscopic alteration was conducted. The results of molecular and immunohistochemical analyses were described in detail. Furthermore, correlating the histopathological results with the duration of hospitalization and the time interval between the onset of the disease and death provided valuable information regarding microscopic alterations over time. Statistical analysis of the data was performed using the chi-square (X2) calculation and the phi coefficient (Φ).

4. RESULTS

4.1. GENERAL DATA OF THE STUDY SAMPLE

In the study group, there were a total of 40 male patients and 16 female patients. Among all the cases, 5 patients were between 21 and 40 years old, 7 patients were between 41 and 60 years old, and 7 patients were over 81 years old. The most numerous cases were found in the 61-80 age category, with a total of 33 patients.

Most patients had a hospitalization period ranging from 1 to 3 days. The next most frequent category was represented by patients hospitalized for over 21 days. There were 10 cases with a hospitalization period between 15 and 21 days, 4 cases with a hospitalization period of 4-7 days, and 3 cases with a hospitalization period of 8-14 days. In conclusion, the average duration of hospitalization was 12.3 days.

Regarding the time interval between the onset of the disease and death, the results appear more evenly distributed compared to the previous categorization. There were 11 cases of death in the 1-3 days category, 8 cases of death in the 4-7 days category, 5 cases of death in the 8-14 days category, again 11 cases of death, this time in the 15-21 days category, and the most numerous cases, with over 21 days from the onset of the first symptoms, totaling 21 cases. In conclusion, the average interval between the onset of the infection and death was 21.4 days in the current study group.

Regarding comorbidities, the most numerous patients had cardiovascular diseases, such as coronary or systemic atherosclerotic disease, hypertension, or chronic heart failure, totaling 26 cases.

The primary cause of death following autopsy and histopathological analysis was determined to be viral pneumonia in the case of 34 patients in the study group. In only 8 patients, it was established that the underlying cause of death was triggered by bacterial superinfection. 5 patients suffered a massive pulmonary embolism, which led to their demise. In 4 cases, the primary cause of death was determined to be perforation or necrosis of the digestive tract.

4.2. PULMONARY HISTOPATHOLOGICAL EXAMINATION

The acute changes were further categorized into cellular inflammatory lesions (presence of inflammatory infiltrates), alveolar lesions, vascular changes or lesions, and hemodynamic changes. Concerning the inflammatory infiltrate, the majority of cases were characterized by the presence of a lymphomonocytic inflammatory infiltrate, observed in 44 cases. The diffuse or focal form was equally represented in the study group, with 22 cases for each category. Of these, 15 cases showed a rich lymphomonocytic inflammatory infiltrate with a focal disposition, and 12 cases had a rich inflammatory infiltrate with a diffuse disposition. A much smaller proportion of cases presented a slightly increased lymphomonocytic inflammatory infiltrate, with 10 cases having a diffuse disposition and only 7 cases with a focal disposition. In the study group, there were 35 cases where microscopic examination of the lungs revealed the presence of a predominantly neutrophilic polymorphonuclear inflammatory infiltrate. Among these, 19 specimens had a diffuse distribution of the infiltrate, and 16 specimens showed a focal distribution of the infiltrate. 10 cases had a rich focal polymorphonuclear inflammatory infiltrate, 9 cases had a reduced focal polymorphonuclear

inflammatory infiltrate, and 8 cases each presented a diffuse polymorphonuclear inflammatory infiltrate, both rich and slightly increased.

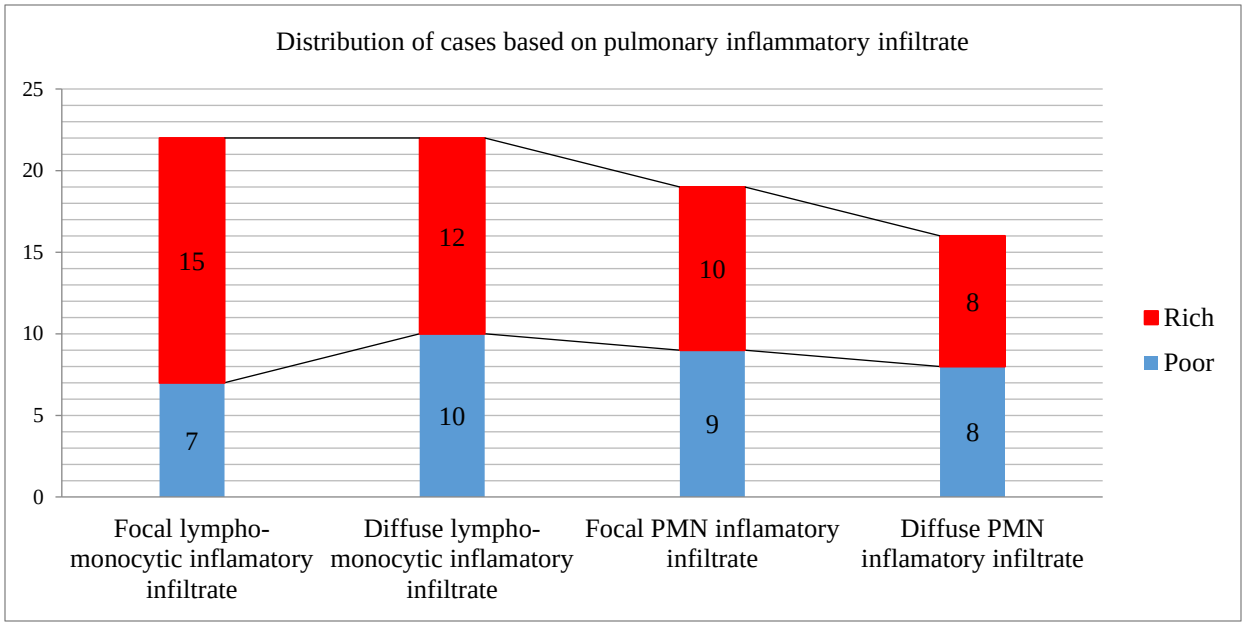

Figure 10: Distribution of cases based on pulmonary inflammatory infiltrate

In a total of 52 patients, the histopathologically examined specimens presented at least one change secondary to alveolar lesions, with the most common being represented by the hyperplasia of type II pneumocytes. In 51 cases in the study group, a marked increase in the number of type II pneumocytes was observed, many of them detached from the basement membrane and observed within the alveolar spaces (Figure 11).

Among the patients who exhibited histopathological changes suggestive of hyperplasia of type II pneumocytes, in a variable proportion, cytopathic effects were observed in 38 cases (Image 1).

In a total of 31 collected specimens that exhibited pneumocyte hyperplasia with viral cytopathic effects, it was observed that, in some areas, these altered cells fused and formed the so-called syncytia. These were referred to as pneumocyte aggregate formation with giant cell-like appearance or syncytial giant cell-like aggregates, and they could be easily confused with multinucleated giant cells of histiocytic origin (Image 2).

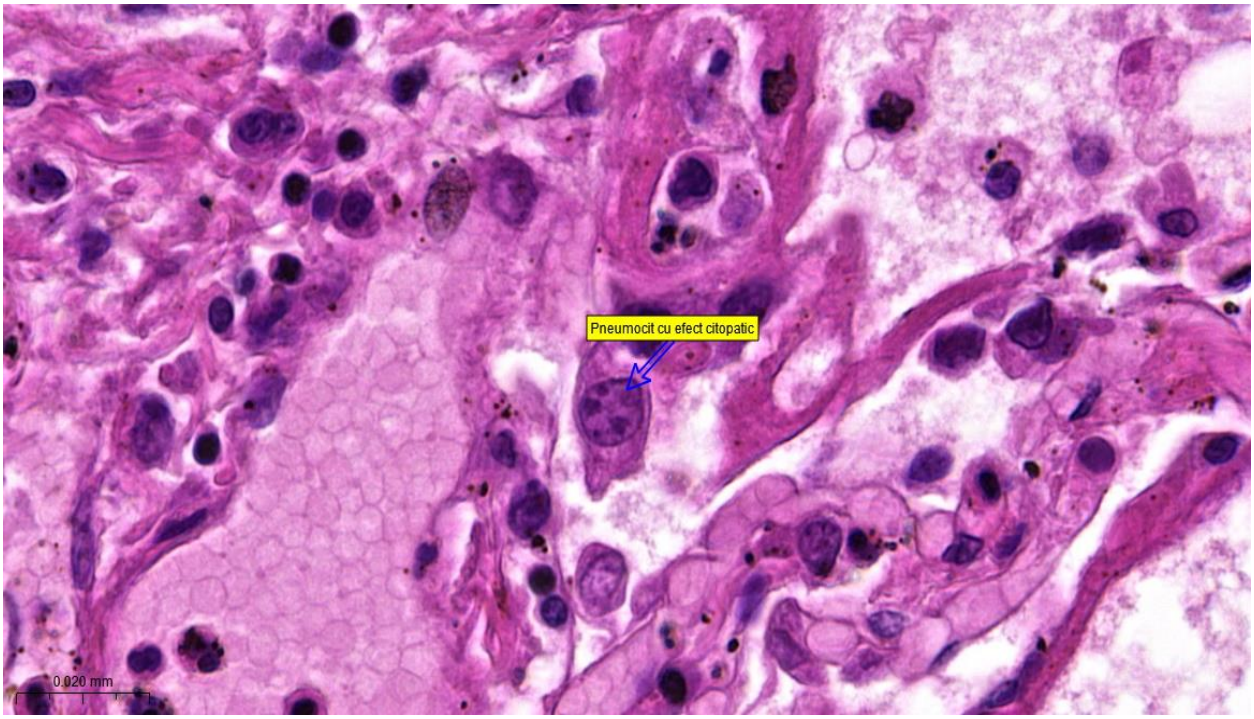

Image 1 - HE Staining 73X (Lung): Pneumocyte with viral cytopathic effect

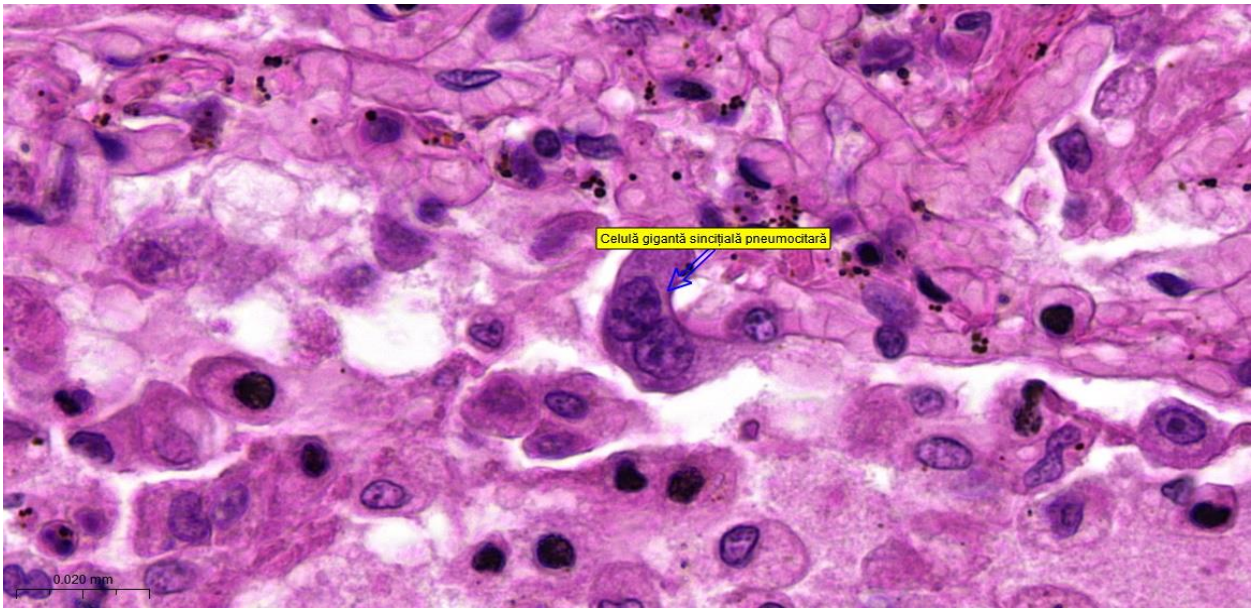

Image 2 - HE Staining 73X (Lung): Pneumocytic syncytial giant cell

Another important histopathological change within the spectrum of diffuse alveolar lesions is the formation of hyaline membranes, which was observed in 34 cases (Figure 11). Due to their diffuse formation and structure, hyaline membranes are an integral part of diffuse alveolar lesions.

The last histopathological change included in the spectrum of alveolar lesions is megakaryocytic hyperplasia. In our study group, 5 patients were identified to exhibit this lesion (Figure 11).

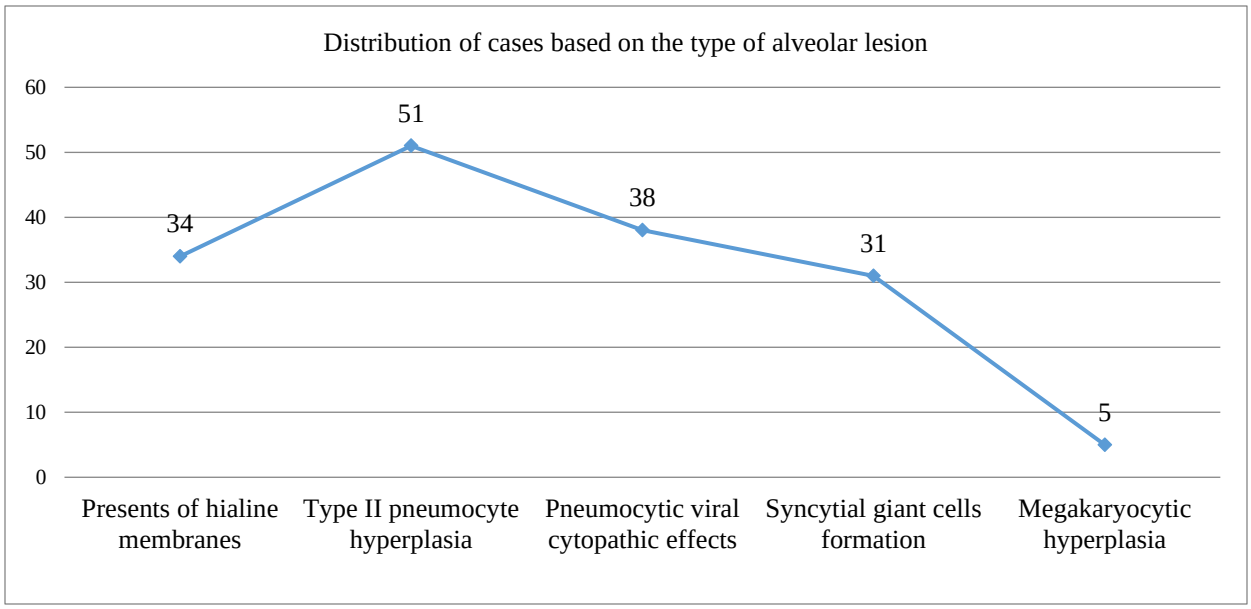

Figure 11: Distribution of cases based on the type of alveolar lesion

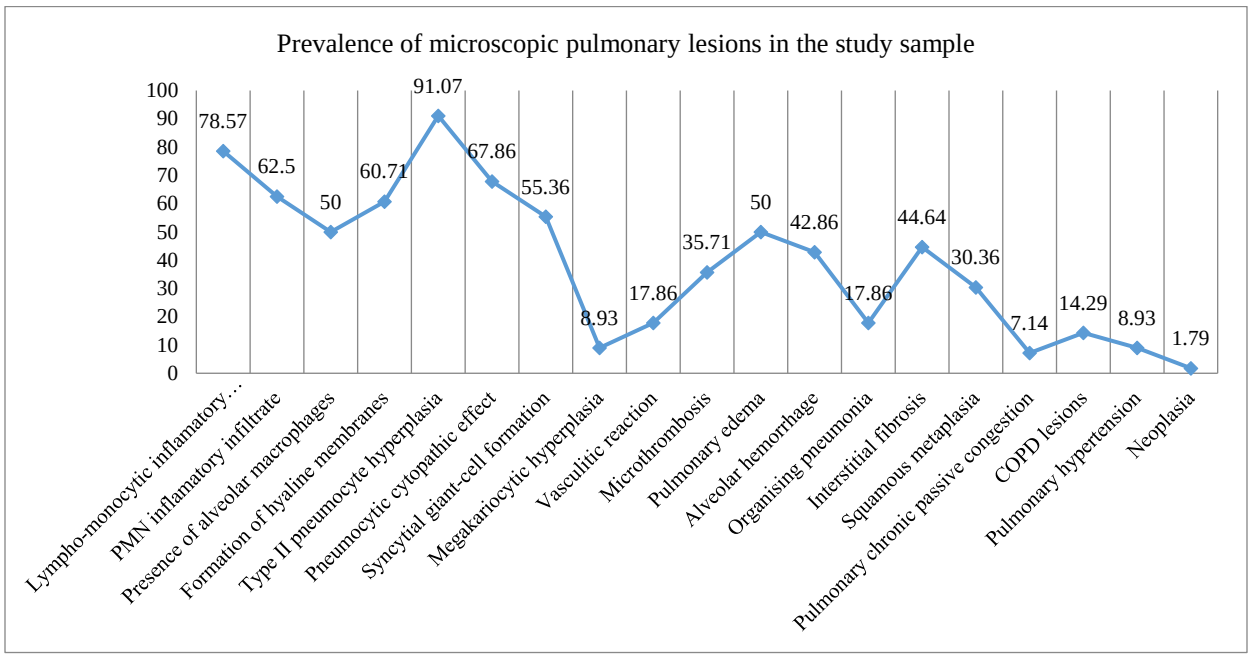

Figure 12: Prevalence of microscopic pulmonary lesions in the study sample

The next acute changes addressed and observed in the current case study were vascular lesions, including microthromboses and vasculitic reaction. The presence of vascular thrombi, both small and larger in caliber, was observed in 20 cases, with 5 patients experiencing massive pulmonary embolism.

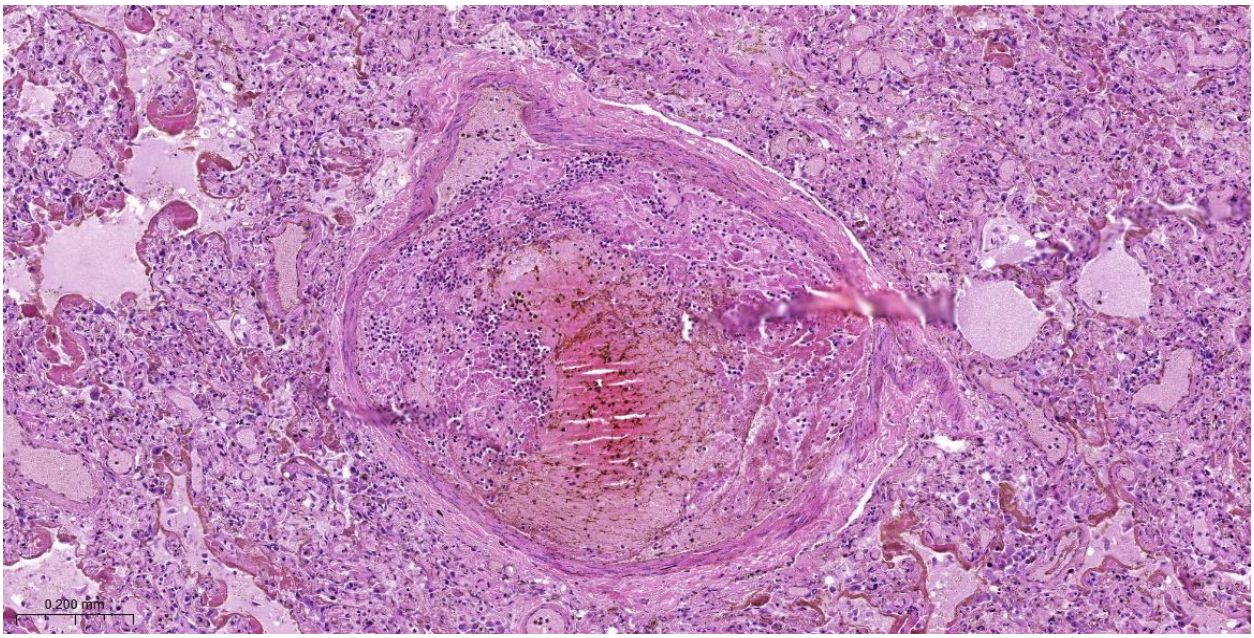

Image 3 - HE Staining 6.4X (Lung): Thrombosis in pulmonary arterial vessel

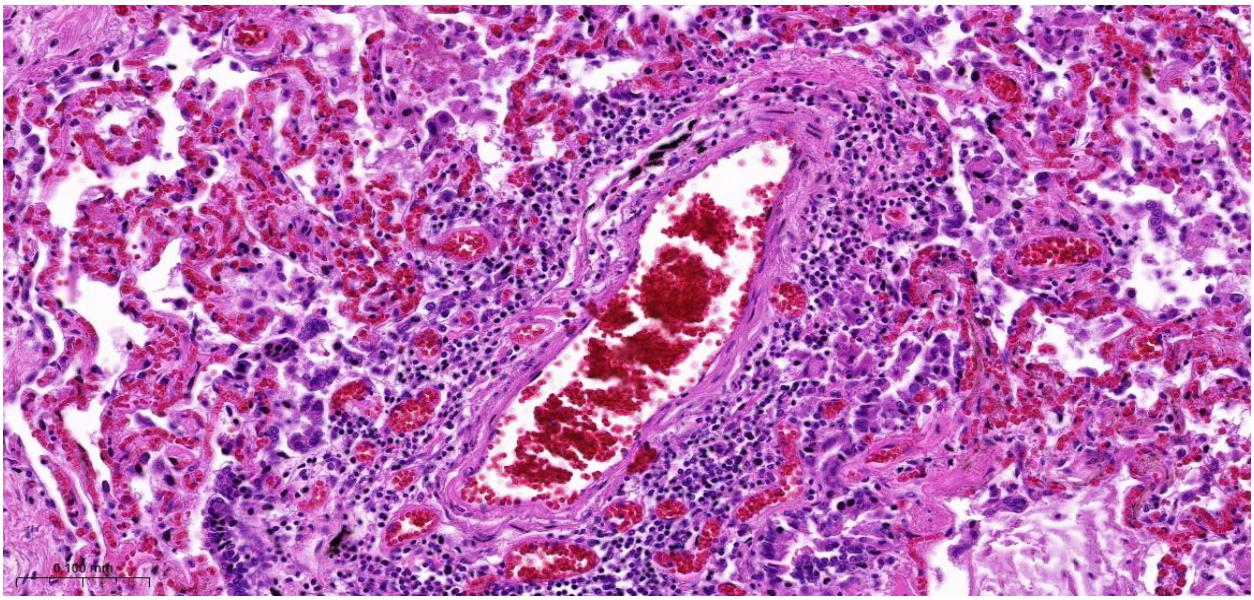

Image 4 - HE Staining 14.6X (Lung): Lymphocytic inflammatory reaction at and around the vascular wall

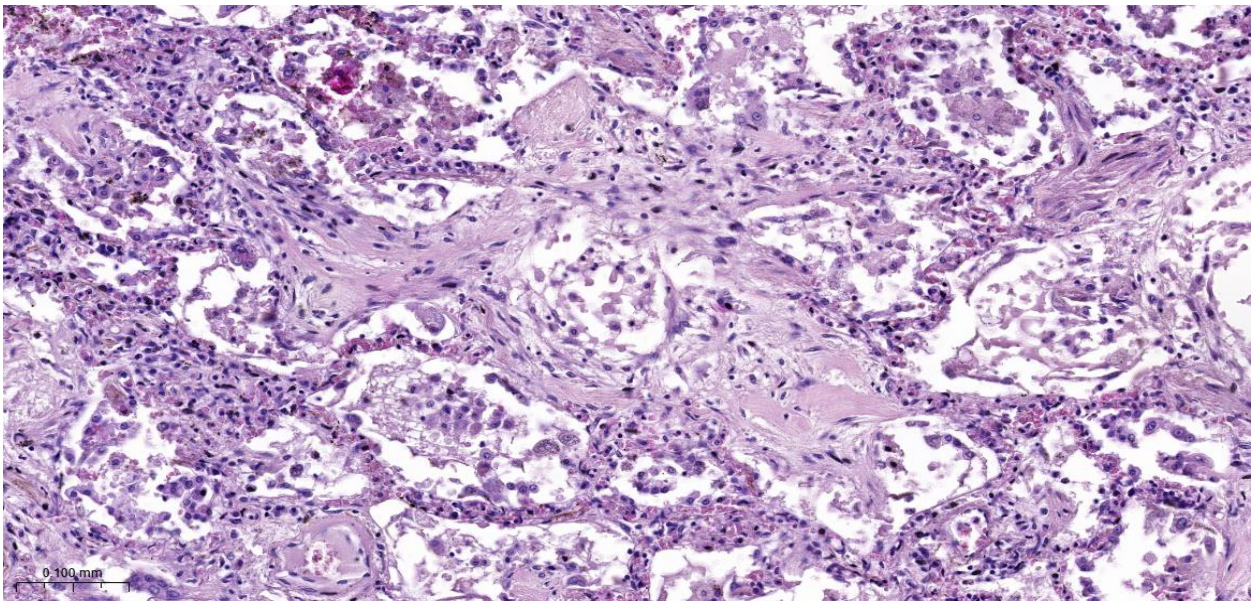

Image 5 - HE Staining 12.3X (Lung): Organizing pneumonia

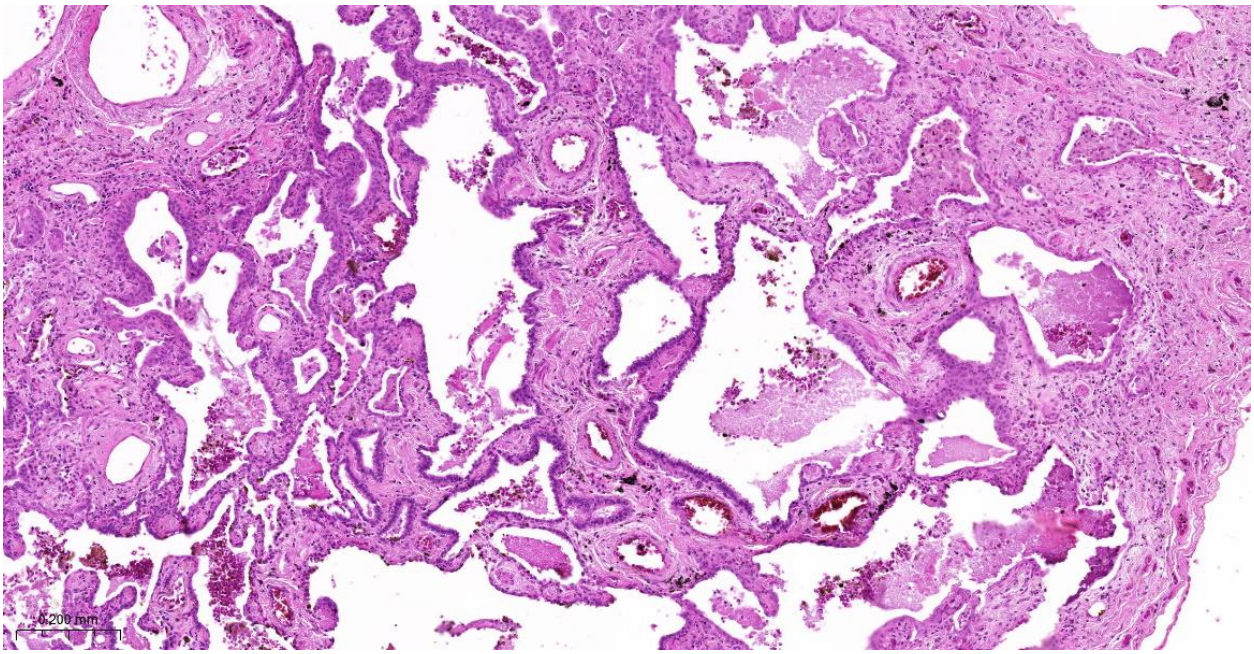

Image 6 - HE Staining 5.7X (Lung): Interstitial fibrosis with extensive areas of squamous metaplasia

The aberrant regenerative lesions follow the acute exudative phase, including hyaline membranes, type II pneumocyte hyperplasia, alveolar hemorrhage, inflammatory infiltrate, and fall within the spectrum of the proliferative organizing phase of acute alveolar lesions. In the study group, a total of 30 cases exhibited at least one form of aberrant regenerative change (Figure 12). Among these, 10 cases presented organizing pneumonia, 25 cases showed interstitial fibrosis, and

17 cases had squamous metaplasia (Figure 15). Organizing pneumonia was observed in 6 cases in patients with an infection onset over 21 days before death and in 3 cases with an onset between 15 and 21 days before death. In 16 out of 25 cases with interstitial fibrosis, the onset was more than 21 days before death, and in 5 cases, the onset was between 15 and 21 days before death. In 2 cases, the lesion was observed in patients with symptom onset between 4 and 7 days before death. Squamous metaplasia was observed in 11 cases in patients with an infectious onset over 21 days and in 4 cases with an onset within the 15-21 day range (Figure 16).

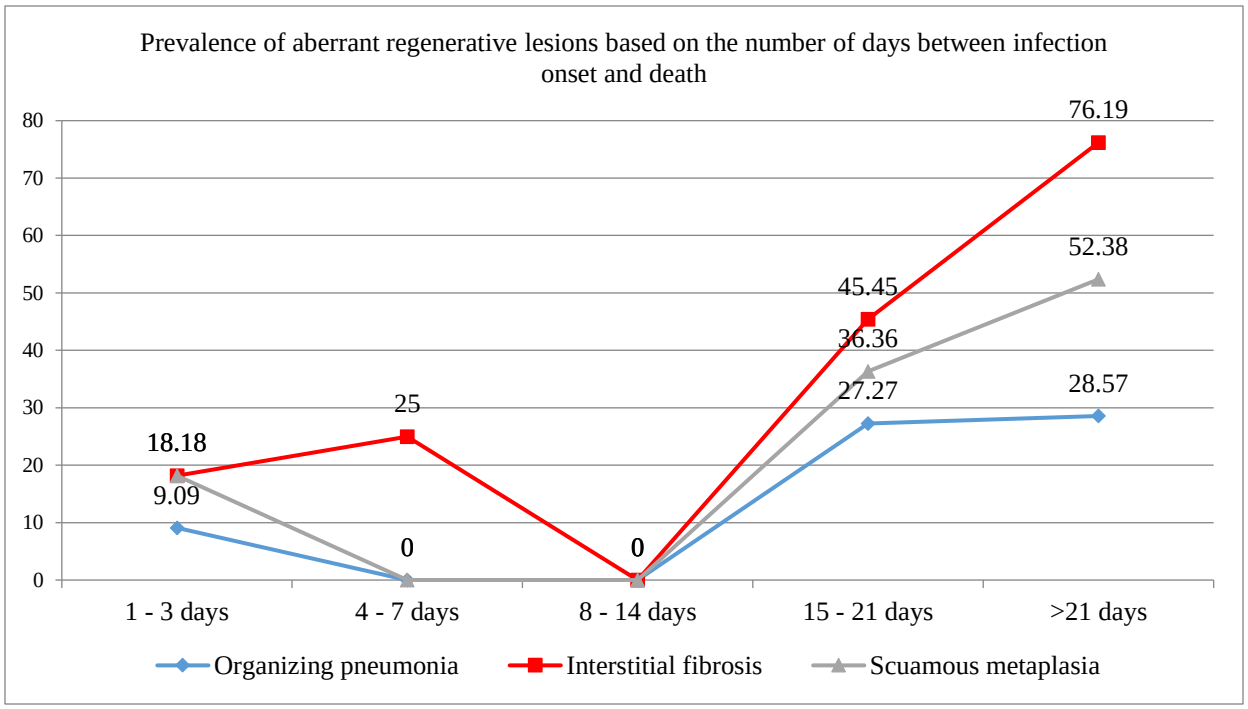

Figure 16: Prevalence of aberrant regenerative lesions based on the number of days between infection onset and death

4.3. CARDIAC HISTOPATHOLOGICAL EXAMINATION

Following the microscopic examination of specimens collected from the hearts of autopsied patients who had died as a result of SARS-CoV-2 infection, multiple lesions were described, each classified based on the type of tissue affected. The initial lesions included myocardial tissue, specifically myocytes, and were classified as acute myocytic lesions, observed in a total of 37 patients (Figure 18). These lesions were characterized by myocytic microstructural changes, myocytic necrosis, or myocytic suffering (myocytic cytopathic effects). In all 37 cases, at least one form of myocytic microstructural change was identified, manifested as wavy and/or

fragmented myocardial fibers, myocyte ballooning or vacuolization, cytoplasmic hyper-eosinophilia, or nuclear pyknosis (Image 7). These microstructural changes are nonspecific and are observed in many cases of prolonged agony, resulting in multiple nonspecific cardiac microischemias (Figure 19).

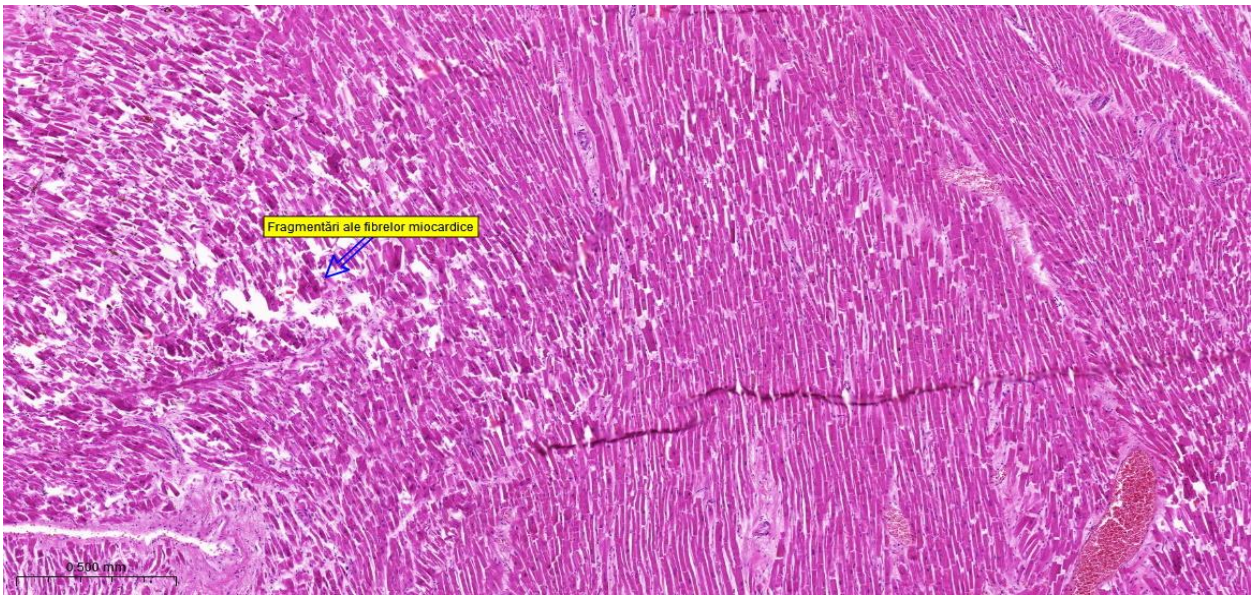

Image 7 - HE Staining 3.6X (Heart): Fragmentation of myocardial fibers

True myocardial necrosis was observed in only 7 patients, with 6 of them being male and one female, aged between 36 and 85 years (Figure 19). The hospitalization period for these patients was short, with 4 cases having a hospitalization period ranging from 1 to 3 days, one case with a 5-day hospitalization, and two patients hospitalized for 6 and 15 days, respectively. Regarding the number of days between the onset of infection and death, there was no significant correlation, as the patients with observed myocardial necrosis had an onset-to-death interval ranging from 1 day to 28 days.

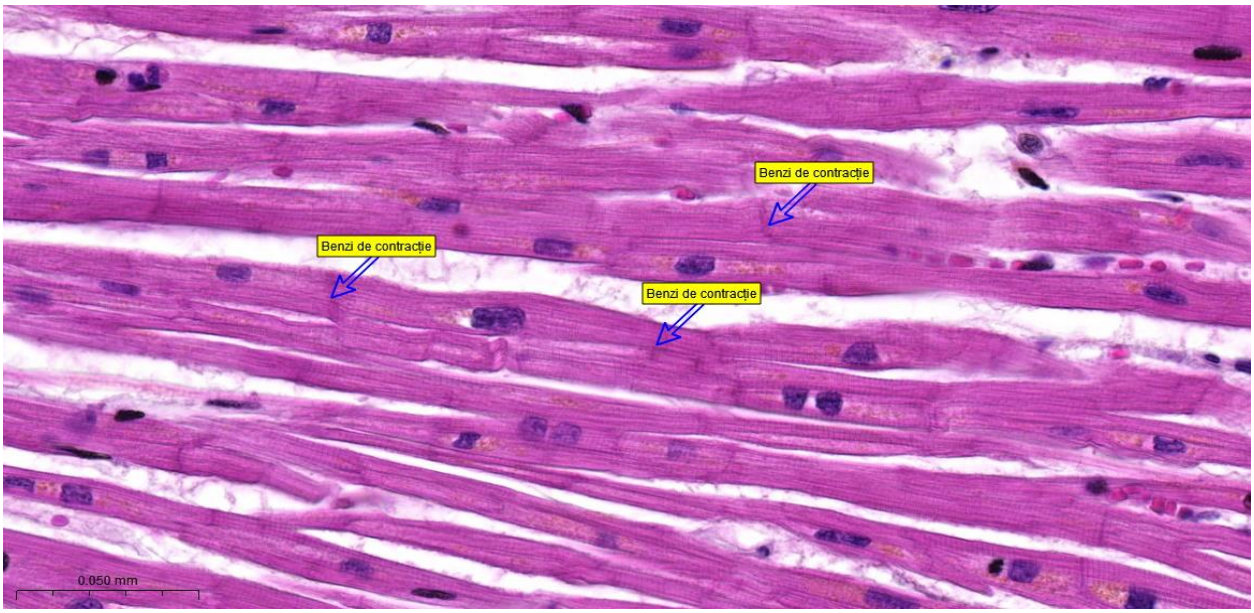

Image 8 - HE Staining 41.4X (Heart): Presence of contraction bands

Myocyte suffering, manifested by cellular swelling with the presence of large, quadrilateral, angular, irregular nuclei, inhomogeneous chromatin, and central nucleoli, was present in 11 cases. Lesions corresponding to myocarditis were observed in only 4 patients, with three of them showing cytopathic myocytes with cellular swelling, large quadrilateral, angular, irregular nuclei, inhomogeneous chromatin, and central nucleoli. Lymphocytic inflammatory reaction in the subepicardial space was observed in 15 patients and included both minimal changes represented by a slightly augmented inflammatory infiltrate with focal disposition and more evident inflammation with an abundant lymphocytic reaction and diffuse disposition. Vascular inflammation or the presence of neutrophilic conglomerates in the vascular lumen was observed in 8 cases. In all 8 cases, the presence of neutrophilic inflammatory infiltrate in the pulmonary parenchyma was simultaneously observed. The presence of neutrophils in the blood vessel lumens was associated with the diagnosis of superimposed bacterial bronchopneumonia in 3 cases and pulmonary thromboembolism in one case, while the remaining four cases were associated with the diagnosis of viral pneumonia. As for vascular lesions, two significant modifications were identified in the cardiac specimens collected in the study group: mild vasculitic reaction mediated by lymphocytes and myocardial vascular microthromboses. Six patients had microthrombi in the lumen of small arteries, and in all of these cases, the presence of microthrombi in the pulmonary vascular branches was also observed. Among these, 3 were diagnosed with pulmonary thromboembolism after autopsy, while the rest were diagnosed with viral pneumonia..

4.4. RENAL HISTOPATHOLOGICAL EXAMINATION

In the case of 13 patients, lesions of the nephrons in the form of acute tubular necrosis were observed (Figure 20). There was no significant association between the presence of acute tubular necrosis and the patients' age or gender. Additionally, the hospitalization period varied from one day to 39 days, and the interval from the onset of infectious symptoms to death ranged from one day to 68 days.

Vascular changes in the kidneys were representative for a total of 20 patients (Figure 21) and were subdivided into three main forms: vasculitic reaction, microthrombosis, and marked vascular congestion. The latter was the most common, observed in 16 patients. Microthrombosis of small renal vessels was only observed in 4 patients, and vasculitic reaction of vascular walls mediated by lymphocytes was seen in only 3 patients. (Figure 20) Among these, 2 patients had both microthrombi in the renal vascular tree and pulmonary vessels, but microthrombi were not detected in intramyocardial vessels. Inflammatory lesions consisted of the presence of lymphocytes or polymorphonuclear cells in the interstitium, around glomeruli, or renal tubules. Thus, 21 patients had inflammatory lesions represented only by interstitial infiltration predominantly with lymphocytes, and in only 2 patients an inflammatory infiltrate composed only of predominantly neutrophilic polymorphonuclear cells could be detected. (Figure 20)

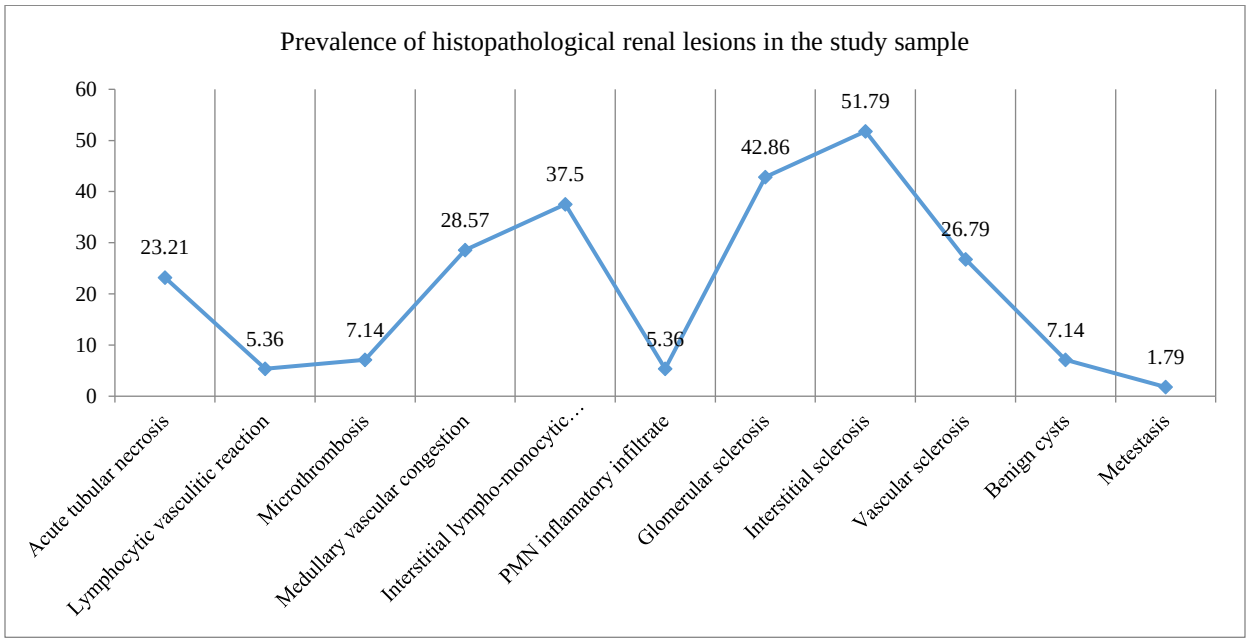

Figure 20: Prevalence of histopathological renal lesions in the study sample

4.5. HEPATIC HISTOPATHOLOGICAL EXAMINATION

In most cases, microscopic alterations were nonspecific, with the largest proportion represented by the presence of lymphomonocytic inflammatory infiltrate in the portal space or subcapsular level, in a total of 23 patients. (Figure 23) More specific hepatocellular changes observed in the study and which can demonstrate the liver parenchyma's reaction to virion invasion included hepatocellular cytopathic effects (Image 10). Thus, the study observed the presence of granulo-vacuolar hepatocytic dystrophy in 11 collected specimens, with the same number for hepatocellular cytopathic changes. Of these, only 3 specimens showed both forms of hepatocellular lesions. Hepatocellular cytopathic effects were associated in 7 out of 11 cases with cytopathic effects at the pneumocyte level, and in 6 cases with the presence of multinucleated pneumocyte syncytial cells, which is over 50% of cases.

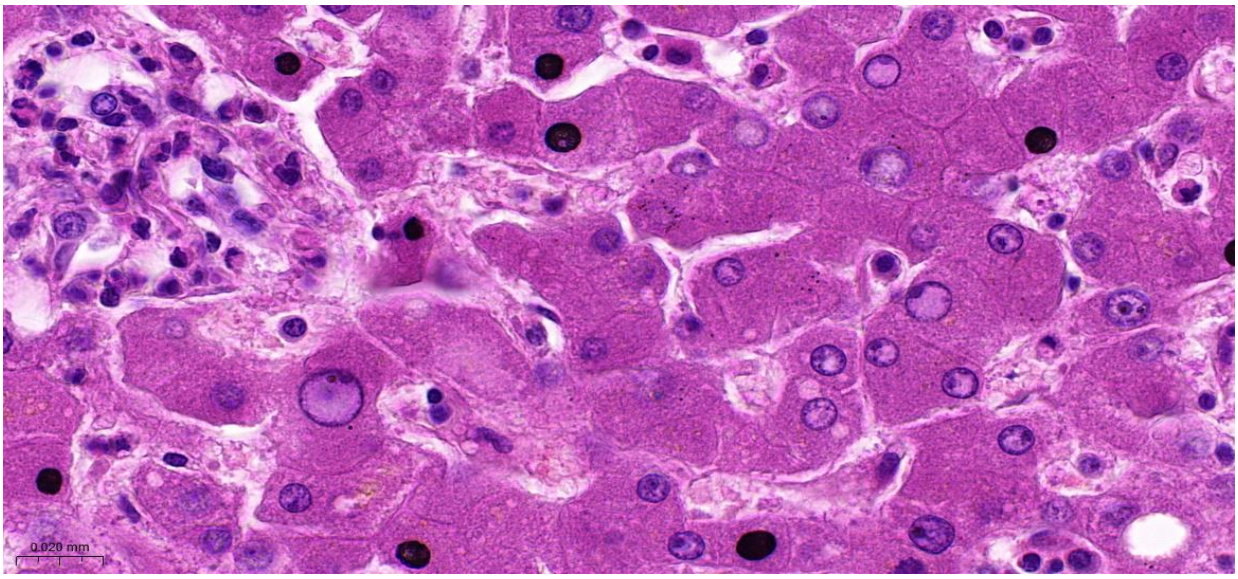

Image 10 - HE Staining 48.4X (Liver): Hepatocyte cytopathic effects

Another form of microscopic lesion detected in hepatic histopathological examination was the presence of neutrophils in the lumen of hepatic vessels, either centrilobular veins, sinusoidal capillaries, or veins and arteries at the portal space level, observed in 6 cases. (Figure 23) The presence of neutrophils in the lumen of hepatic vessels was associated in 50% of cases with the presence of neutrophils in myocardial vessels and in 100% of cases with the presence of diffuse-disposition neutrophilic inflammatory infiltrate in the lungs. Vascular lesions, like in the case of other organs, were divided into vasculitic reactions or microthromboses. (Image 11) The first type was not observed in any specimen collected from hepatic tissue. The presence of thrombi in hepatic

vessels, primarily centrilobular veins or blood vessels at the portal space level, was observed in 5 hepatic tissue samples. (Figure 23)

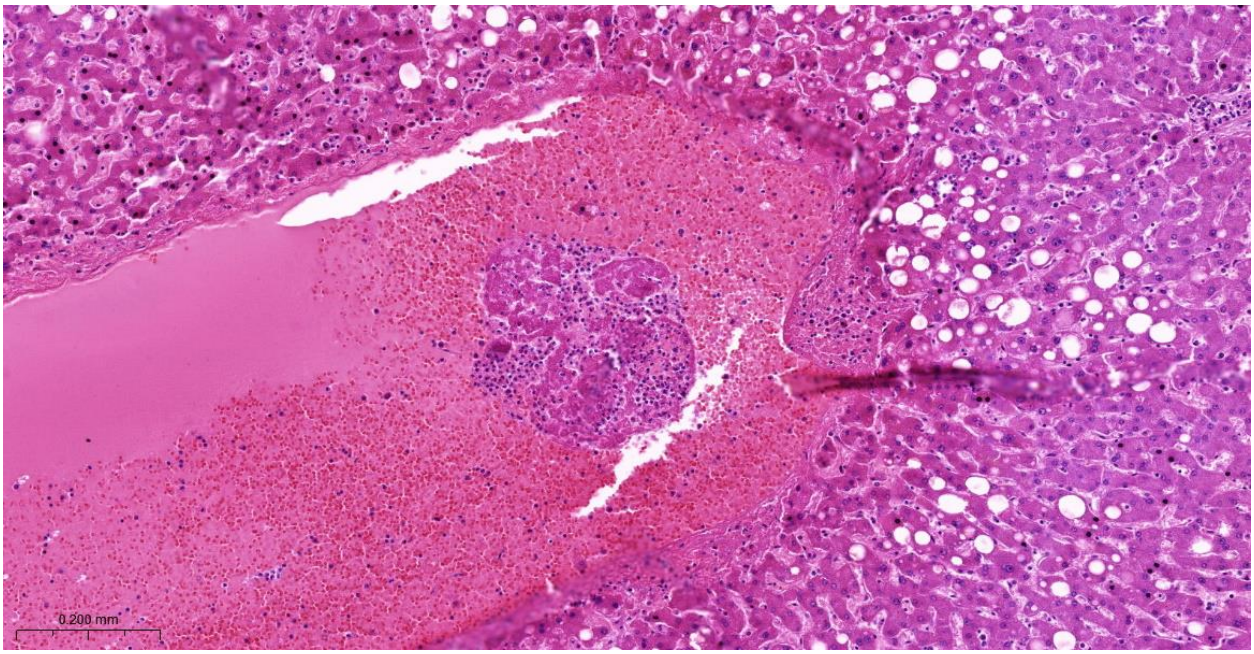

Image 11 - HE Staining 8.2X (Liver): Hepatic venous thrombosis

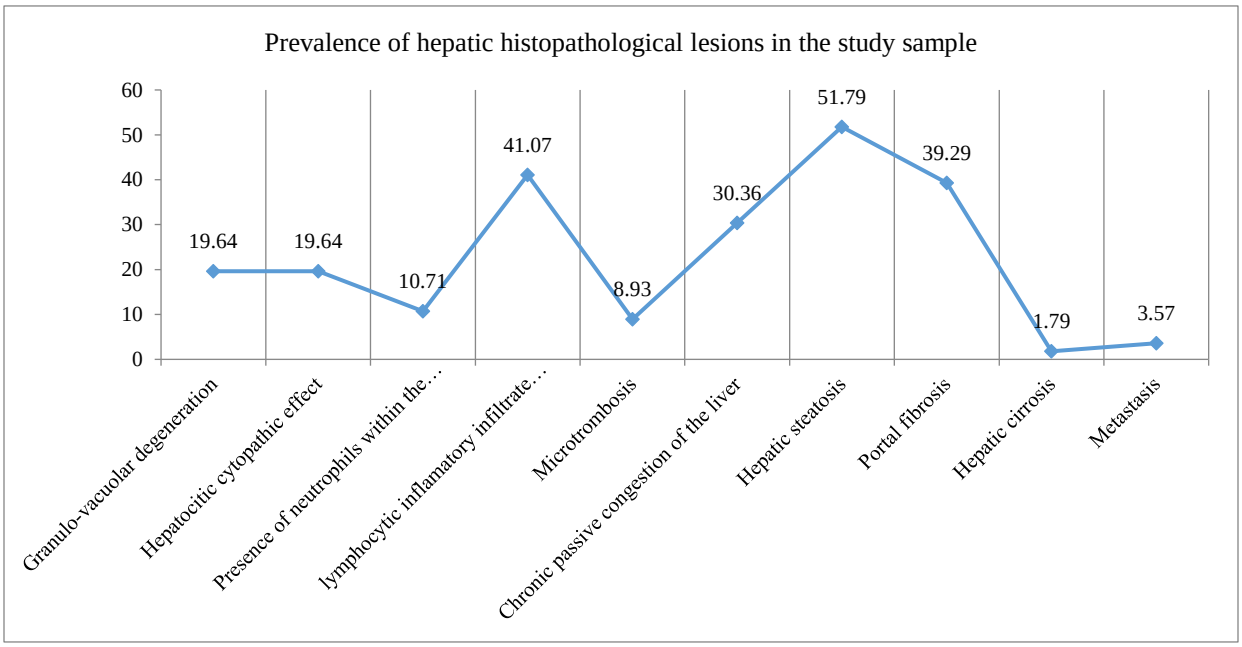

Figure 23: Prevalence of hepatic histopathological lesions in the study sample

4.6. SPLENIC HISTOPATHOLOGICAL EXAMINATION

The changes in splenic parenchyma mostly involved disorganization in both white pulp and red pulp. Mild hypoplasia of the white pulp was observed in 13 cases, while atrophy was observed in 31 cases. Hyperplasia of splenic lymphoid tissue was only seen in 8 cases. (Figure 24) Disorganization in the red pulp only included marked congestion, represented by an increased sequestration of red blood cells in a larger volume. This change was detected in 43 patients. (Figure 24) Atrophy of the white pulp had a direct proportional relationship with the unfavorable slow progression of viral infection, being present in just over 50% of cases with an infectious onset more than 21 days before death and in only 7 of 19 patients with a rapid, fulminant progression, with an infectious onset between 1 and 7 days before death. On the other hand, mild hypoplasia of the white pulp was correlated with a medium-term infectious progression. No association was found between hyperplasia of the white pulp and the interval between the infectious onset and death, with this interval ranging from 2 days to 36 days for these 6 patients. (Figure 25)

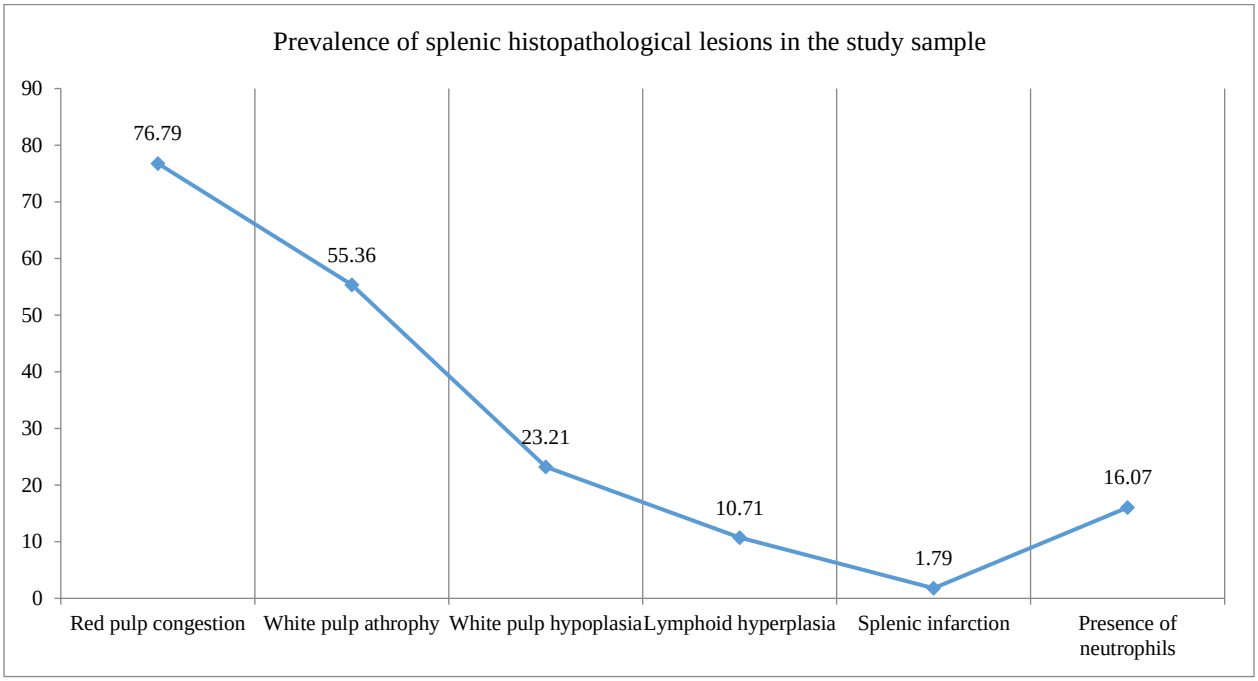

Figure 24: Prevalence of splenic histopathological lesions in the study sample

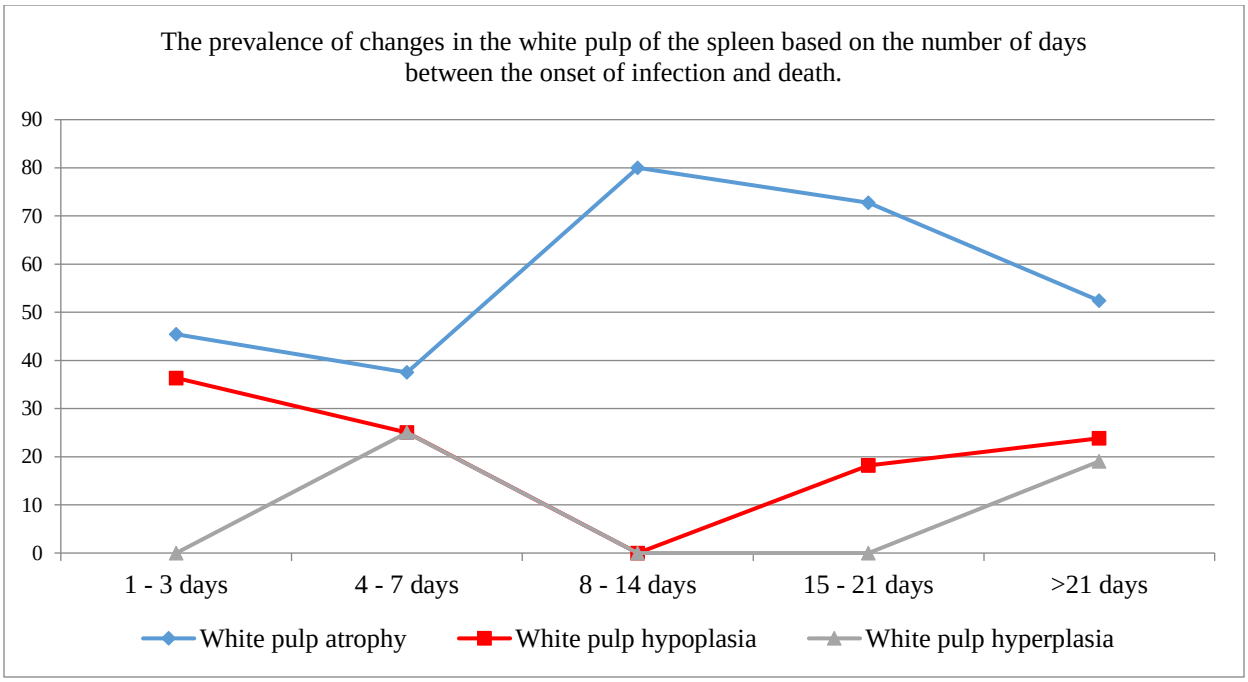

Figure 25: The prevalence of changes in the white pulp of the spleen based on the number of days between the onset of infection and death.

4.7. INTESTINAL HISTOPATHOLOGICAL EXAMINATION

After histopathological analysis of all collected specimens using standard hematoxylin-eosin staining, it was found that two patients presented inflammatory neutrophilic lesions in the small intestine, one with a diffuse disposition of the infiltrate and the other with a focal, patchy disposition. In the colon, the same type of lesion was observed in a larger proportion, with six specimens showing these features. Several cases exhibited inflammatory lesions mediated by a lymphomonocytic infiltrate, with a total of 21 cases in the small intestine and 24 cases in the colon. Out of these, six cases represented a focal/patchy lymphomonocytic infiltrate in the small intestine and seven cases in the colon. A diffuse disposition of lymphocytes was evident in 15 cases in the small intestine and 17 cases in the colon. (Figure 27) Among all these patients, 18 showed lymphomonocytic inflammatory lesions both in the colon and the small intestine. Mucosal erosions were observed in 16 patients in the small intestine and 17 patients in the colon, with the combination of intestinal and colonic erosions being seen in only ten patients.

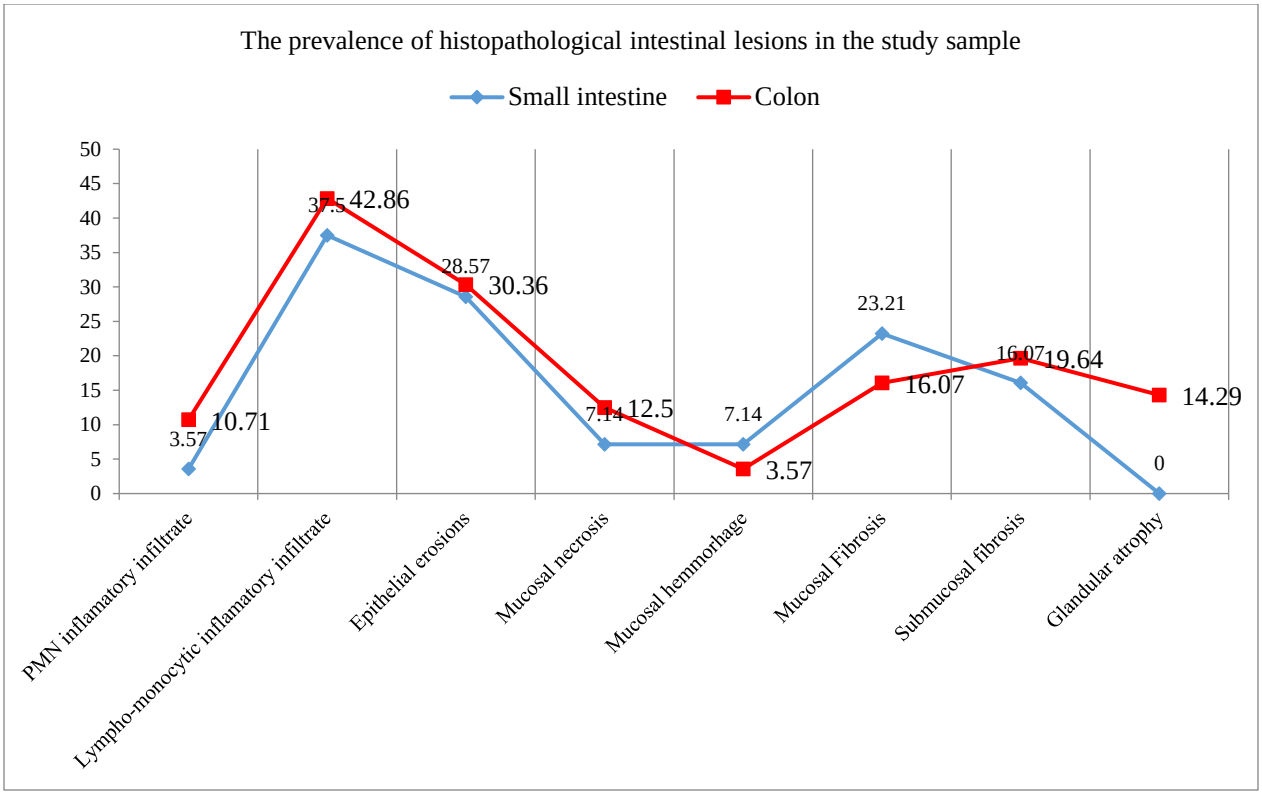

Figure 28: The prevalence of histopathological intestinal lesions in the study sample.

4.8. MOLECULAR EXAMINATIONS FOR VIRAL GENOME DETECTION

The molecular examinations, such as reverse transcription polymerase chain reaction (rt-PCR), were conducted on 35 patients from the study group using tissue samples collected from both lungs, as well as from the heart, kidneys, liver, spleen, and intestines. The molecular analysis involved the detection of three viral genes: the S, N, and ORF1ab genes. To confirm a positive result, all three viral genes needed to be present in the examined tissue samples. At the pulmonary level, the detection of all three viral genes was established in 33 out of 35 patients. Only one patient showed positivity for two out of the three viral genes, and one patient was completely negative, with none of the viral genes detected. (Figure 29) An important aspect is that the presence of all three viral genes in the tissue samples collected from the lungs was observed even in patients with unfavorable slow progression, including one patient with an infectious onset 68 days before their demise.

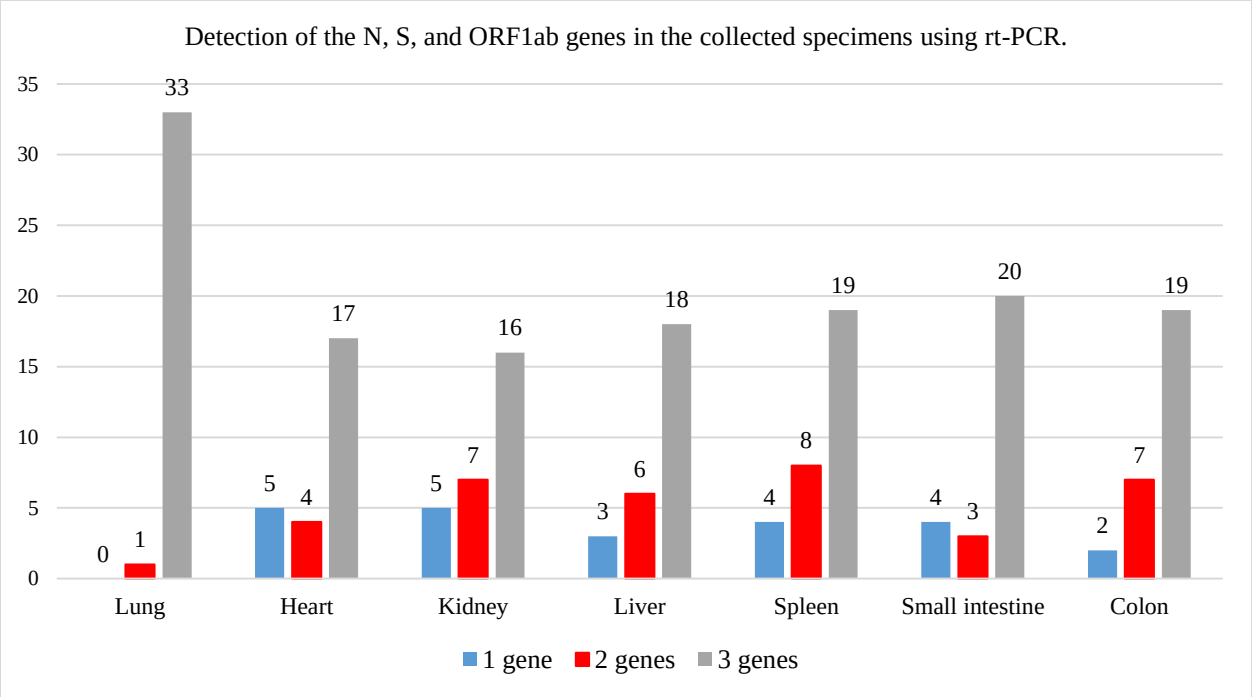

Figure 29: Detection of the N, S, and ORF1ab genes in the collected specimens using rt-PCR.

The rt-PCR examination at the cardiac level for the 35 patients in the study group, positivity for all three viral genes was found in 17 patients. Four patients showed positivity for two out of the three studied viral genes, and five patients exhibited positivity for only one of them. (Figure 29) For the remaining patients, a total of 9, the presence of at least one of the three studied viral genes could not be detected in the cardiac tissue samples.

Myocytic suffering was observed in 8 out of the 35 patients tested molecularly, with 6 of them showing positivity for all three viral genes, one being positive for 2 out of 3 viral genes, and one being positive for only one viral gene. (Figure 31) The viral genome could be detected in 3 out of 4 tissue specimens that exhibited lesions consistent with myocarditis. In 8 out of 12 specimens from the study group tested using molecular techniques, there was an association between the presence of pericardial inflammatory phenomena and the detection of the S, N, and ORF1ab genes. In 5 out of 7 cases, an association was observed between the presence of neutrophils in the myocardial vessel lumens and the detection of the three viral genes. Vascular lesions, such as microthromboses or vasculitic reactions, were highly associated with myocardial tissue PCR positivity, with 3 out of 4 cases exhibiting this correlation. (Figure 31)

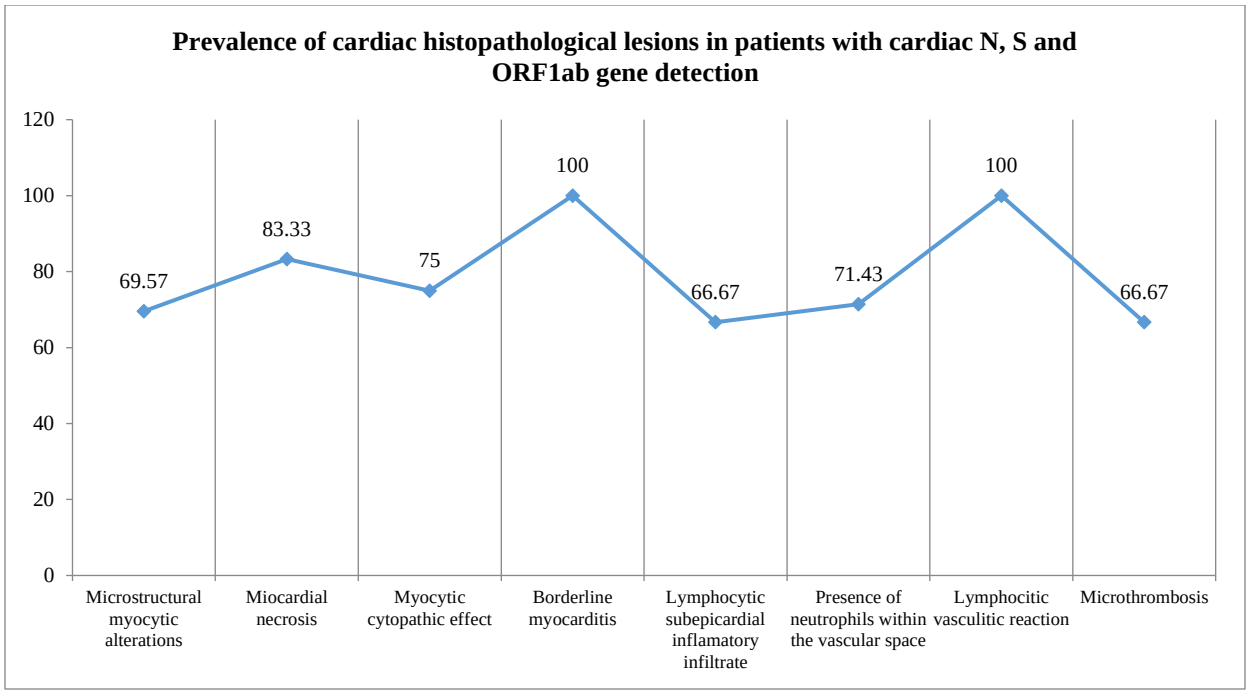

Figure 31: Prevalence of cardiac histopathological lesions in patients with cardiac N, S and ORF1ab gene detection

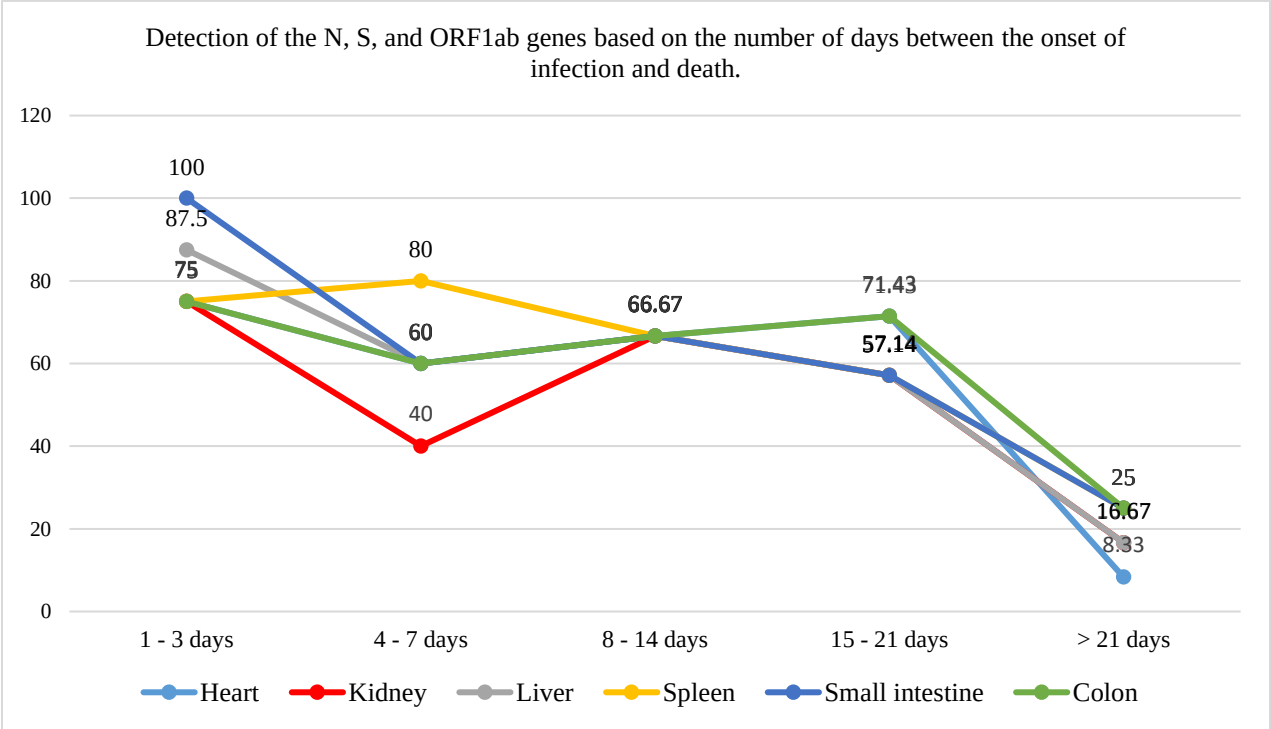

Figure 32: Detection of the N, S, and ORF1ab genes based on the number of days between the onset of infection and death.

Following the rt-PCR examination of renal tissue specimens, it was established that 16 out of 35 cases were positive for the S, N, and ORF1ab genes, 7 cases were positive for only two of these genes, and 5 cases were positive for only one gene. (Figure 29) In 7 cases, no viral genes could be detected in the examined tissue materials. Among these 35 patients tested molecularly, 9 patients had acute tubular necrosis lesions in the renal tissue. Of these, 6 tested positive for all three viral genes studied. Vasculitic reactions in the renal vascular walls and microthromboses in the renal vascular bed were 100% associated with the detection of the viral genome by PCR in renal tissue. (Figure 34) Similar to cardiac tissue, the detection of the N, S, and ORF1ab genes was observed in patients with severe SARS-CoV-2 infection, with a fulminant course. Among the 16 positive cases, 6 had a short interval between the onset of infection and death, ranging from 1 to 3 days. Two cases had an interval of 4-7 days between the onset and death, 2 cases had a 8-14 day interval, 4 cases had an interval between 15 and 21 days, and only 2 cases had an onset more than 21 days before death, with the longest duration being 68 days. (Figure 32) The statistical analysis revealed a negative, inverse correlation between the detection of the three viral genes and a longer onset-to-death interval of more than 21 days. (Figure 35)

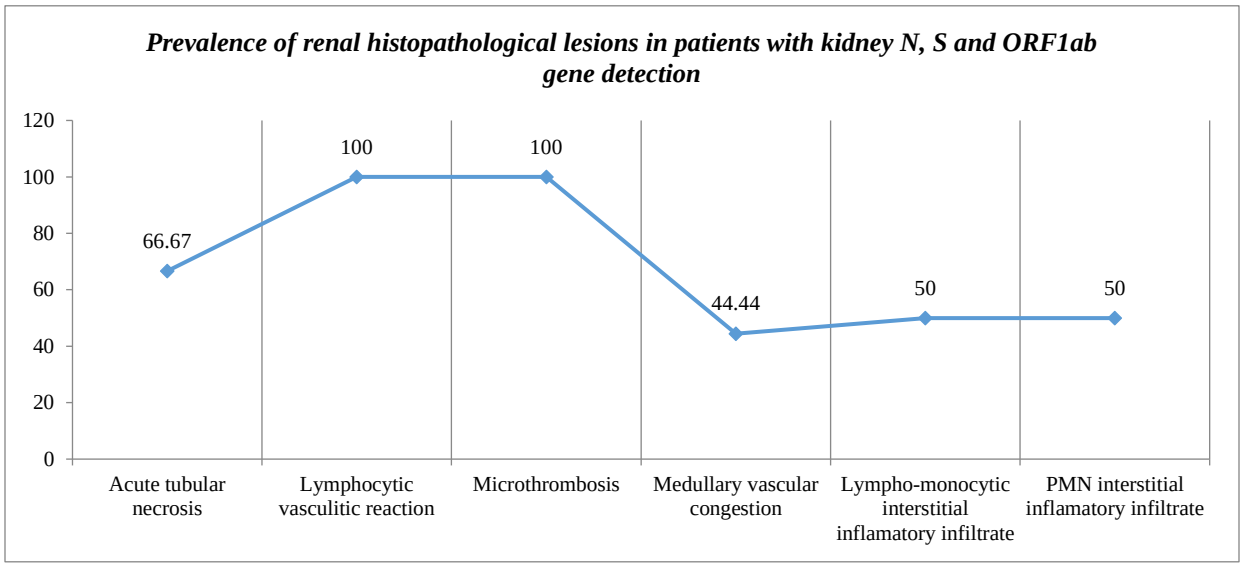

Figure 34: Prevalence of renal histopathological lesions in patients with kidney N, S and ORF1ab gene detection

In the case of liver tissue, the detection of all three viral genes was observed in 18 out of 35 patients. Two viral genes were detected in 6 patients, and only a single viral gene was found in

3 patients. (Figure 29) A little over 50% association was observed between the detection of the viral genome in the liver and necroinflammatory lesions such as granulo-vacuolar dystrophy (4 out of 7 cases), hepatocyte damage (5 out of 9 cases), and the presence of lymphocytic inflammatory infiltrate in the portal space (9 out of 17 cases). Considering the number of days between the onset of infectious symptoms and death, similar to other organs studied up to this point, a higher proportion of positive results in the liver tissue was observed in patients with a short onset-to-death interval. There were 7 cases with an interval of 1 to 3 days, and only two cases with an onset-to-death interval of more than 21 days, with the longest interval being 52 days. (Figure 32)

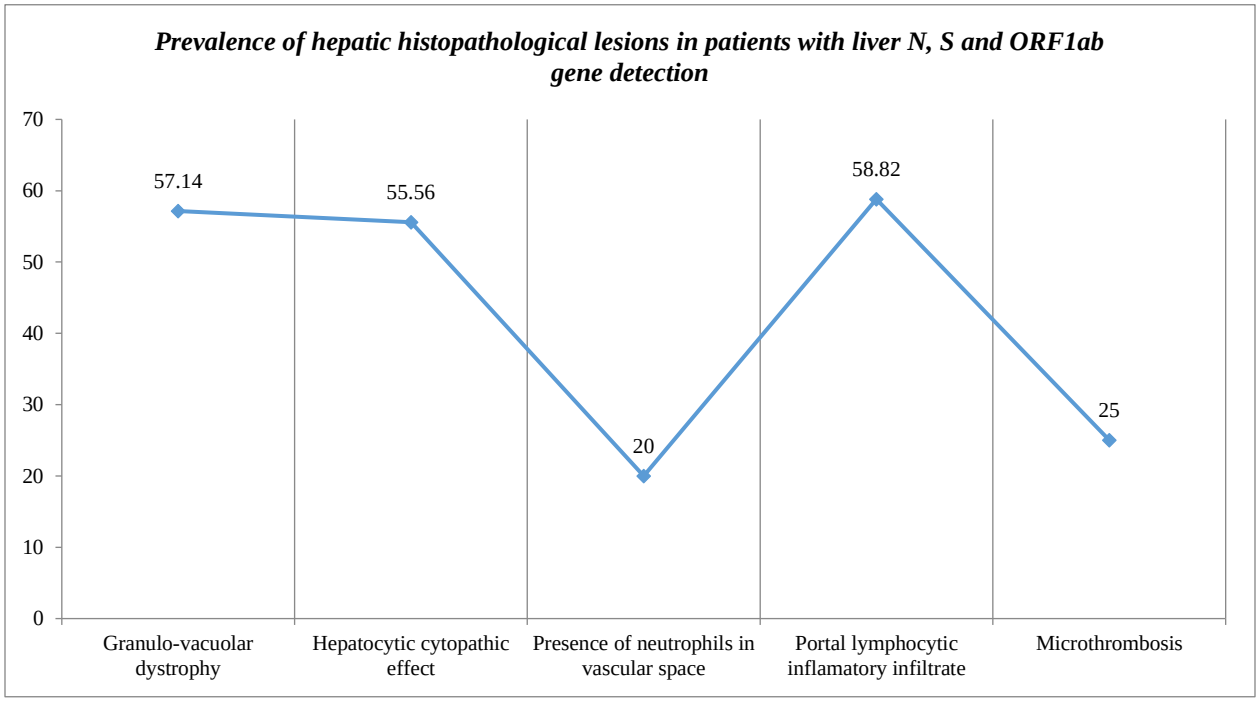

Figure 36: Prevalence of hepatic histopathological lesions in patients with liver N, S and ORF1ab gene detection

The examination of splenic tissue using molecular detection techniques for the viral genome showed a significant proportion of patients in the study group who tested positive for all three genes studied. Specifically, 19 out of 35 cases showed positivity for all three genes. Two out of the three viral genes were detected in 8 patients, while only 4 cases showed positivity for one of the genes, N, S, or ORF1ab. (Figure 29) A little over 50% of cases that exhibited marked atrophy

of the white pulp, which includes a total of 12 out of 23 cases, showed positivity in the rt-PCR testing of splenic tissue for all three viral genes. Similarly, cases with white pulp hypoplasia, represented by fewer and smaller lymphoid follicles without the presence of germinal centers, were associated with the detection of all three viral genes in a total of 6 out of 9 cases through molecular examination. (Figure 39) Patients with a rapid and fulminant course of infection showed a significantly higher proportion of positivity for the N, S, and ORF1ab genes compared to those with a slow and unfavorable course. Similar to the other organs studied, statistical analysis revealed a strong negative correlation between the presence of the viral genome in the spleen and the long time interval from the onset of infection to death. This correlation was demonstrated with a phi coefficient $\Phi = -0.425$ and supported by a chi-squared $X2\ (1, 35) = 6.311$ ($p = 0.012$). (Figure 40)

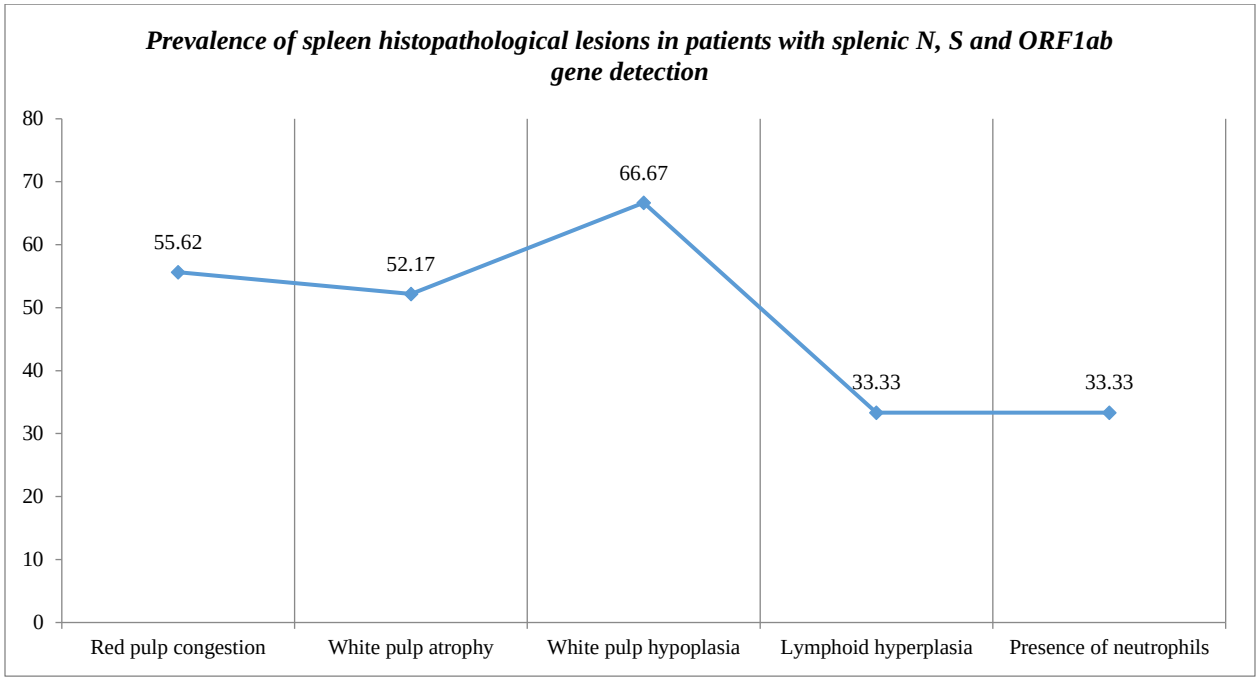

Figure 39: Prevalence of spleen histopathological lesions in patients with splenic N, S and ORF1ab gene detection

The examination of post-mortem samples from the small intestine using the polymerase chain reaction (PCR) technique revealed that, after lung tissue, the small intestine had the second highest proportion of positivity for the three genes of the SARS-CoV-2 virus studied. Specifically, 20 out of 35 cases showed positivity for all three viral genes. Two out of the three viral genes were detected in only 3 patients, and a single viral gene was present in just 4 patients. (Figure 29)

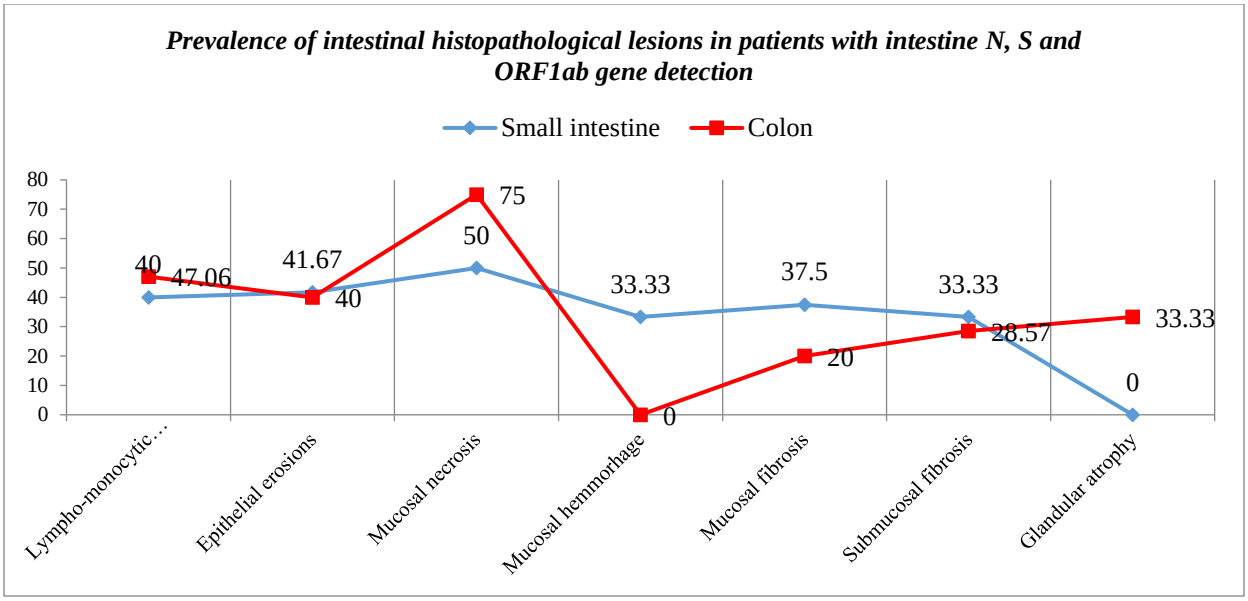

Figure 41: Prevalence of intestinal histopathological lesions in patients with intestine N, S and ORF1ab gene detection

4.9. IMMUNOHISTOCHEMICAL EXAMINATION FOR DETECTION OF VIRAL NUCLEOCAPSID

The highest positivity for the anti-nucleocapsid SARS-CoV-2 antibody was observed, as expected, at the pulmonary level. In 48 out of 56 cases, the presence of viral nucleocapsid at the cellular level could be detected. (Figure 45) The most intense positivity was observed at the level of pneumocytes in all 48 cases. (Figure 13)

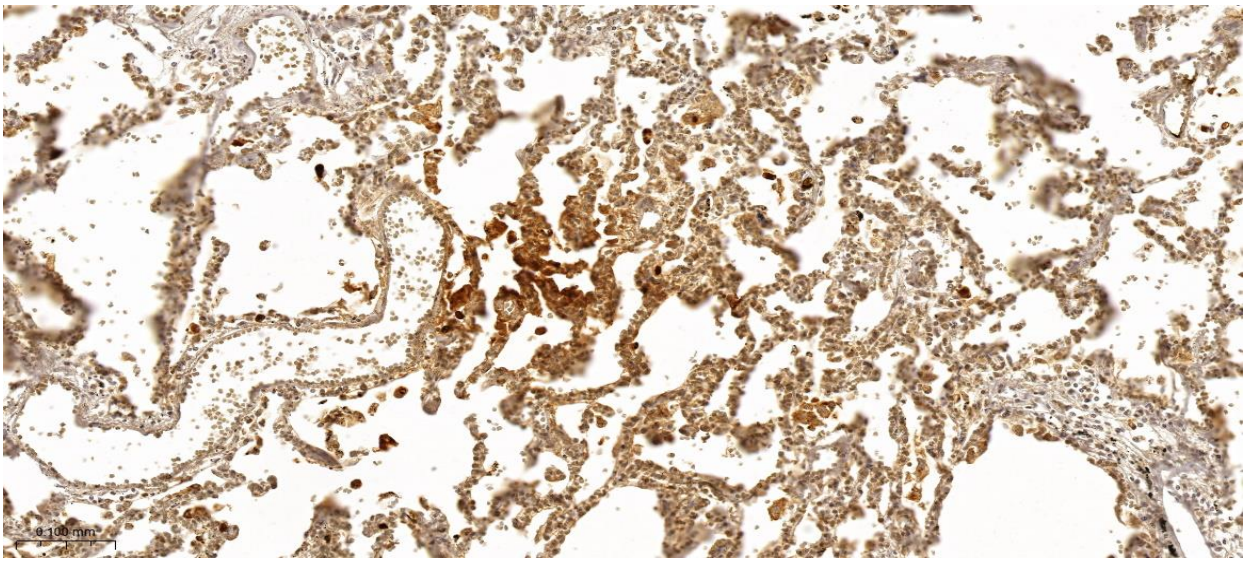

Image 13 - IHC SARS-CoV-2 11X (Lung): Intense, widespread pneumocytic positivity.

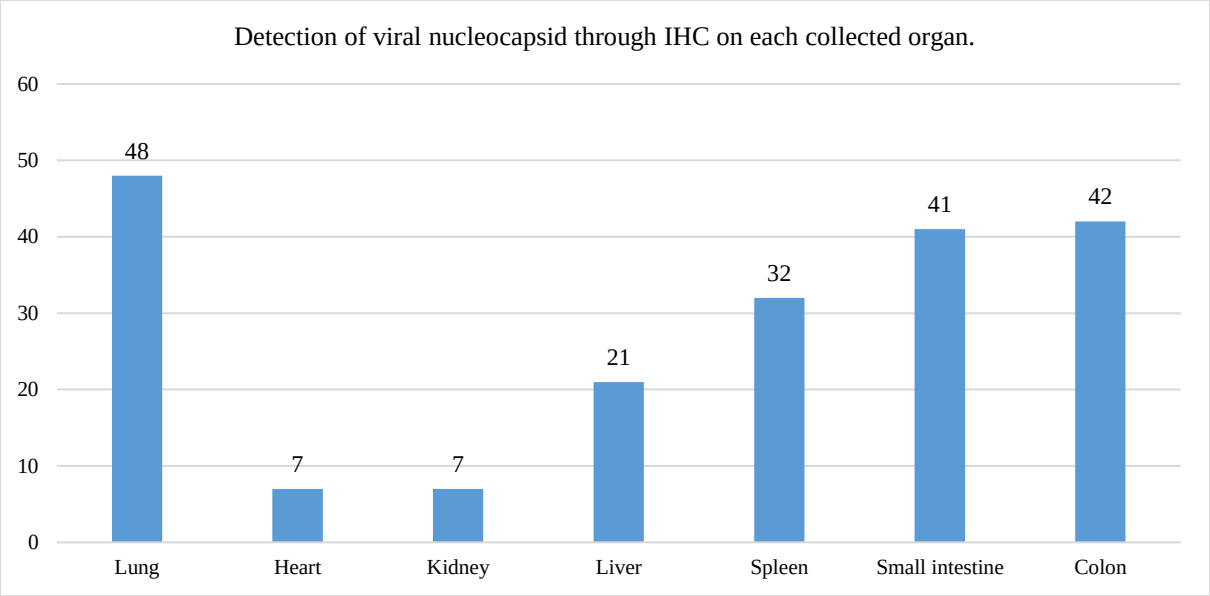

Figure 45: Detection of viral nucleocapsid through IHC on each collected organ.

The next highest frequency of positivity, following pneumocytes, was observed at the level of hyaline membranes in patients presenting these histopathological changes, where 29 cases were positive, with 21 showing strong positivity and 8 exhibiting weak positivity. (Figure 47) In the study group, 22 cases showed positivity for the anti-nucleocapsid antibody at the alveolar macrophage level. (Figure 48) Another type of lung cell that showed an affinity for the SARS-CoV-2 virus was the fibroblast, with nucleocapsid detection in 19 cases, of which 12 had weak positivity and only 7 had strong positivity.

Vascular microthrombi were observed in 20 patients, of which 14 showed numerous pneumocytes that were highly positive (>1 cell/400x microscopic field) during immunohistochemical examination. The close relationship between the extensive detection of nucleocapsid at the pneumocyte level and the formation of vascular microthrombi was demonstrated through statistical analysis, revealing a chi-squared value of $X2\ (1, 56) = 8.095$, with $p = 0.004$ and a Phi coefficient $\Phi = 0.380$. At the same time, statistical measurements assessed the relationship between the extensive detection of nucleocapsid at the pulmonary level and the detection of pneumocytes with viral cytopathic effects, including the formation of syncytial giant pneumocyte cells.

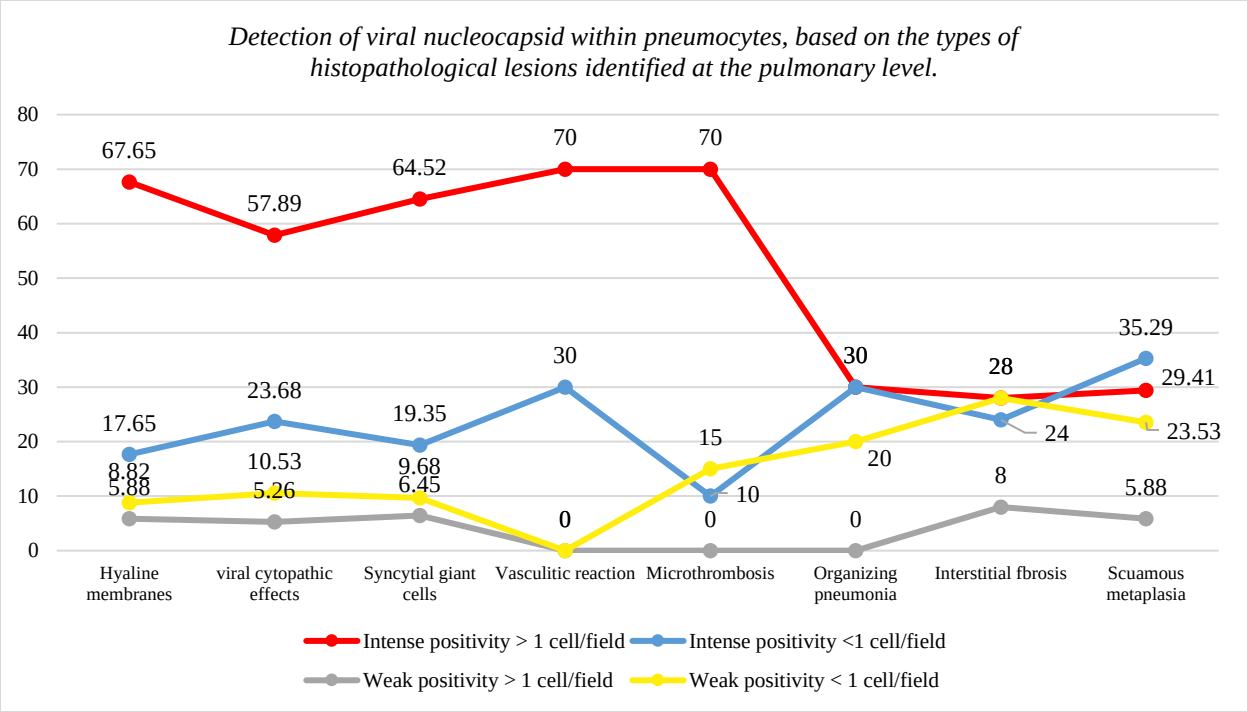

Figure 50: Detection of viral nucleocapsid within pneumocytes, based on the types of histopathological lesions identified at the pulmonary level.

The description indicates that there is a relationship between the detection of viral nucleocapsids in pneumocytes and the time interval between the onset of the infectious disease and death. It has been observed that there is an immunohistochemical pattern where the intensity and extent of pneumocytes that test positive for the SARS-CoV-2 virus are greater in patients with an infectious onset within 1 - 3 days before death. The intensity and degree of pneumocyte involvement reach a plateau in patients with an infectious onset between 4 and 21 days, with minor fluctuations. After 21 days, there is a sudden decrease in intensity and extent, with only 3 out of 21 cases showing pneumocytes that are strongly positive and extending beyond one cell per field (as shown in Figure 53). This suggests that the intensity and extent of pneumocyte involvement change over time during the course of the infection.

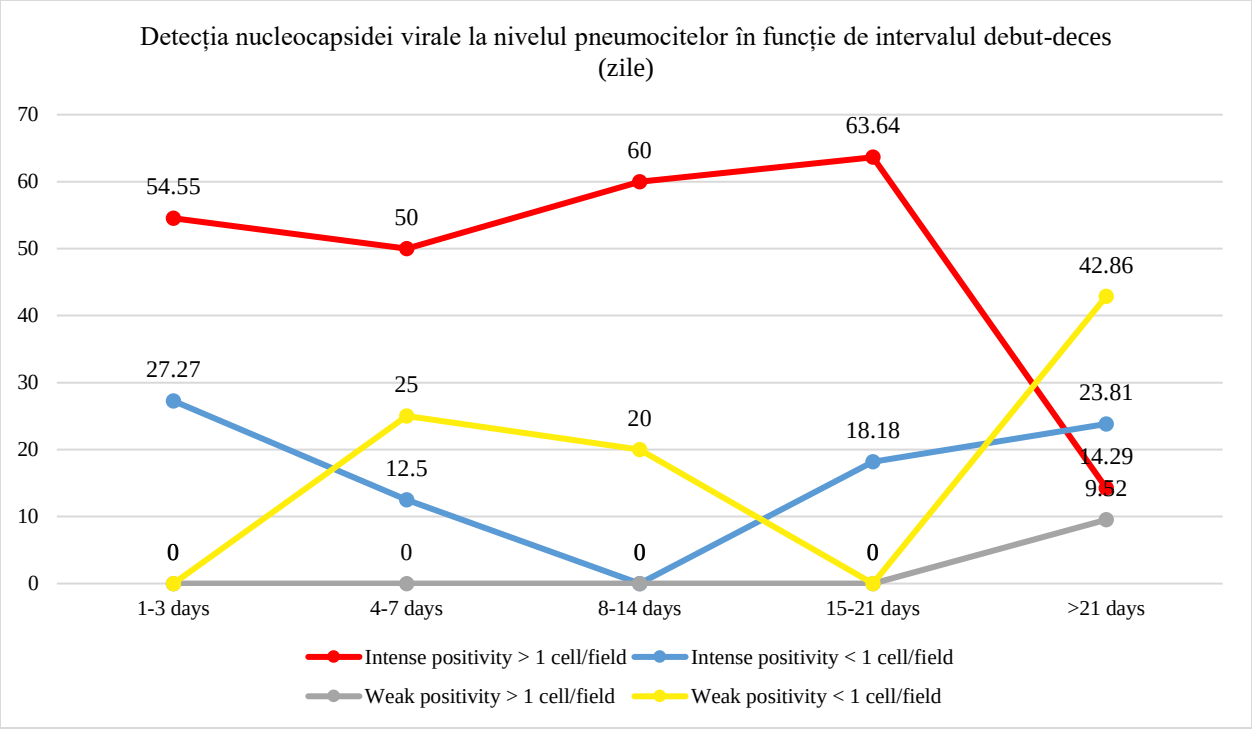

Figure 53: Gradul de detecție a nucleocapsidei virale la nivelul pneumocitelor în funcție de intervalul de zile dintre debutul bolii și deces

Following immunohistochemical analysis using the anti-nucleocapsid antibody on cardiac specimens, positivity was observed in only 7 patients. Nucleocapsid was detected at a high intensity within interstitial fibroblasts in all 7 cases and in interstitial macrophages in 6 out of 7 cases.

When comparing these results to the molecular analysis, out of the study group tested through PCR, nucleocapsid presence at the cellular level was only demonstrated in 5 patients. Among these, all three viral genes studied (N, S, and ORF1ab) were detected in 4 cases.

Regarding the correlation between immunohistochemical results and histopathological findings, it was observed that the histopathological findings were not triggered by the presence of the virus at the myocardial level, except for myocarditis lesions. However, there was a correlation between the presence of the viral nucleocapsid and myocardial microstructural lesions and cytopathic effects.

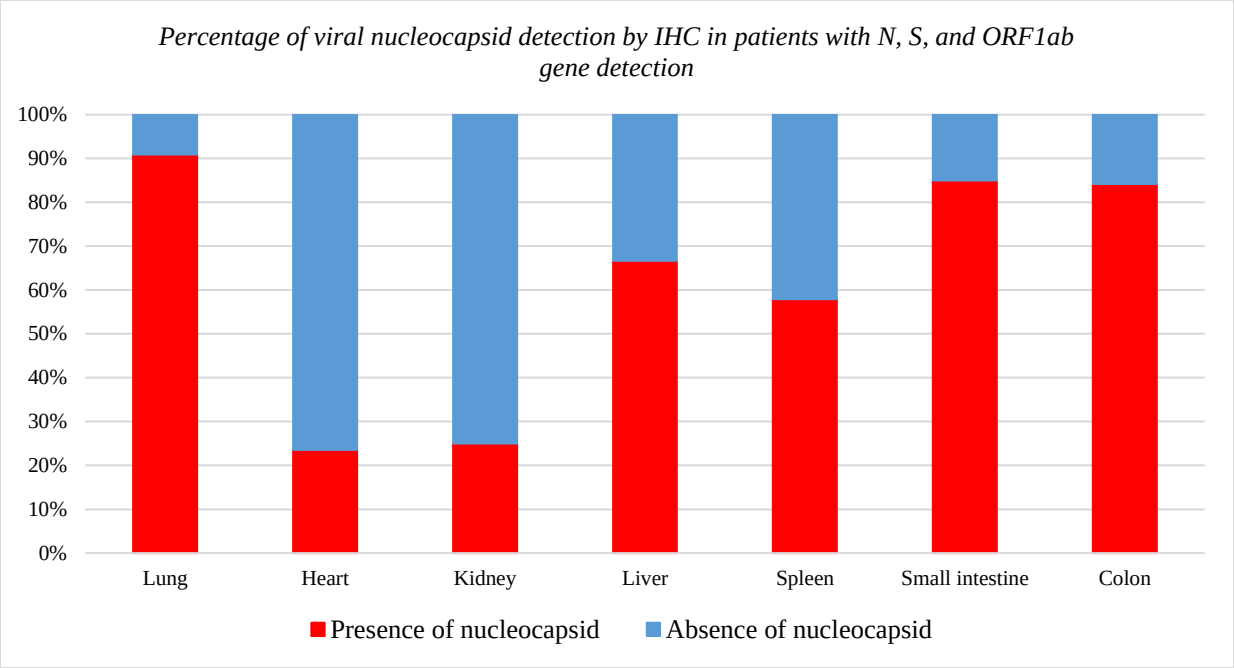

Figure 56: Percentage of viral nucleocapsid detection by IHC in patients with N, S, and ORF1ab gene detection

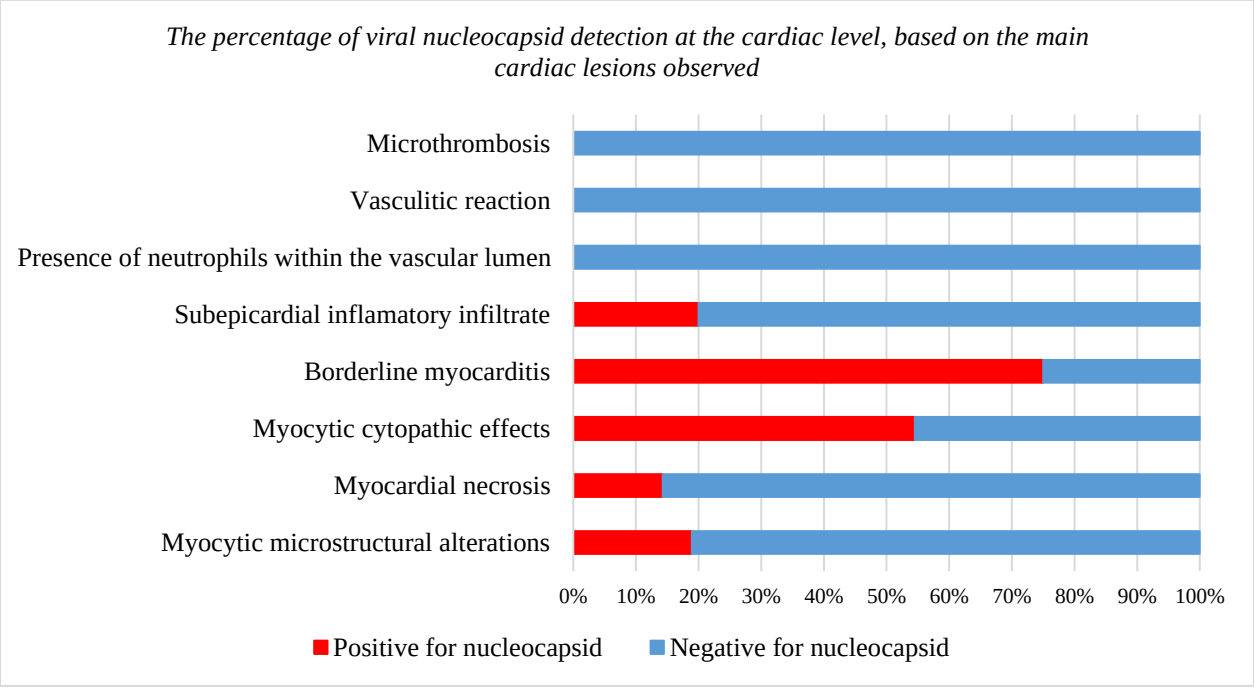

Figure 57: The percentage of viral nucleocapsid detection at the cardiac level, based on the main cardiac lesions observed.

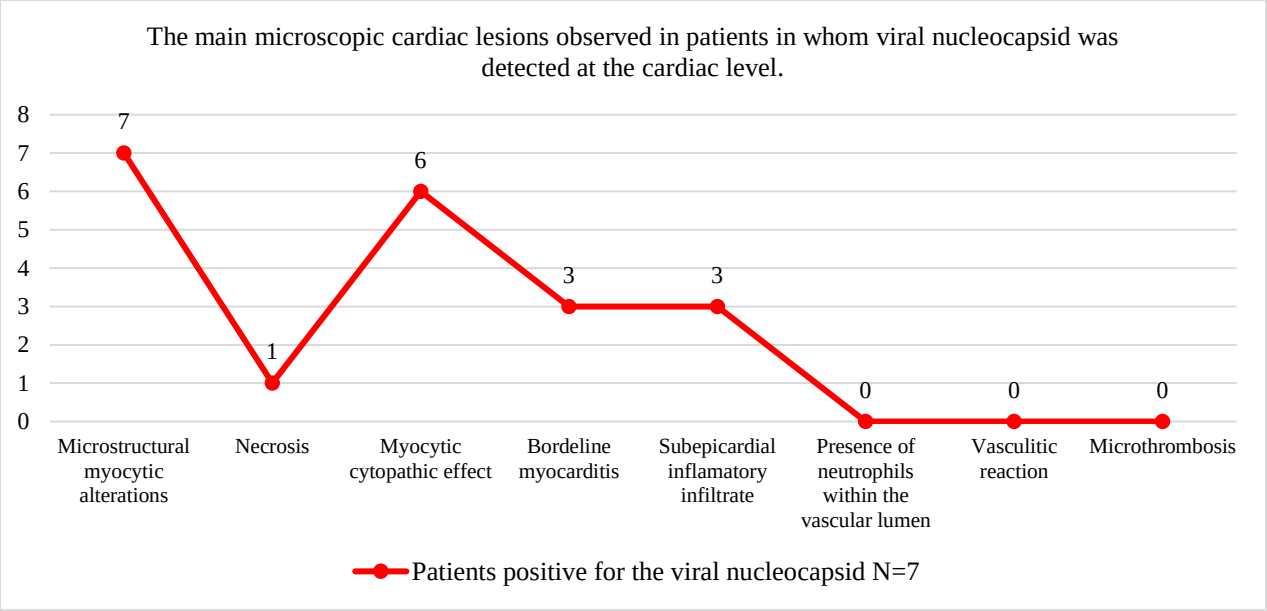

Figure 58: The main microscopic cardiac lesions observed in patients in whom viral nucleocapsid was detected at the cardiac level.

Following immunohistochemical analysis of post-mortem renal tissue, limited positivity with low intensity was observed only in the tubular epithelium in 7 out of 56 patients. Comparing the immunohistochemical results to the molecular analysis, the same pattern as in the heart was observed. Five patients from the molecularly tested group showed positivity at the tubular cell level for the viral nucleocapsid, and in 4 of these cases, the N, S, and ORF1ab genes were detected using rt-PCR. Correlating the immunohistochemical results with the histopathological analysis, it was observed that only in the case of microthromboses, there was indeed an association. In all 4 cases where the presence of vascular microthrombi was observed, viral nucleocapsid was also present in the tubular epithelium. Acute tubular necrosis was present in 5 out of 7 patients in whom the presence of nucleocapsid in renal parenchyma could be observed.

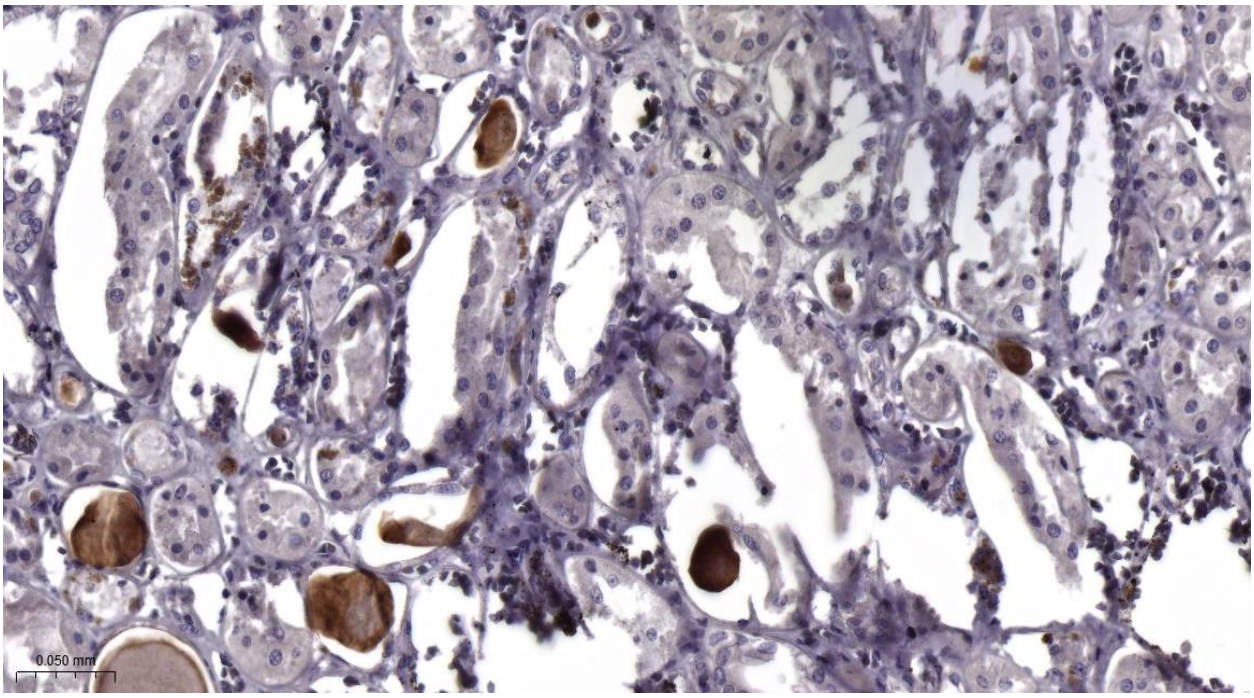

Image 14 - IHC SARS-CoV-2 21.7X (Kidney): Positivity in detached tubular cells and in hyaline casts.

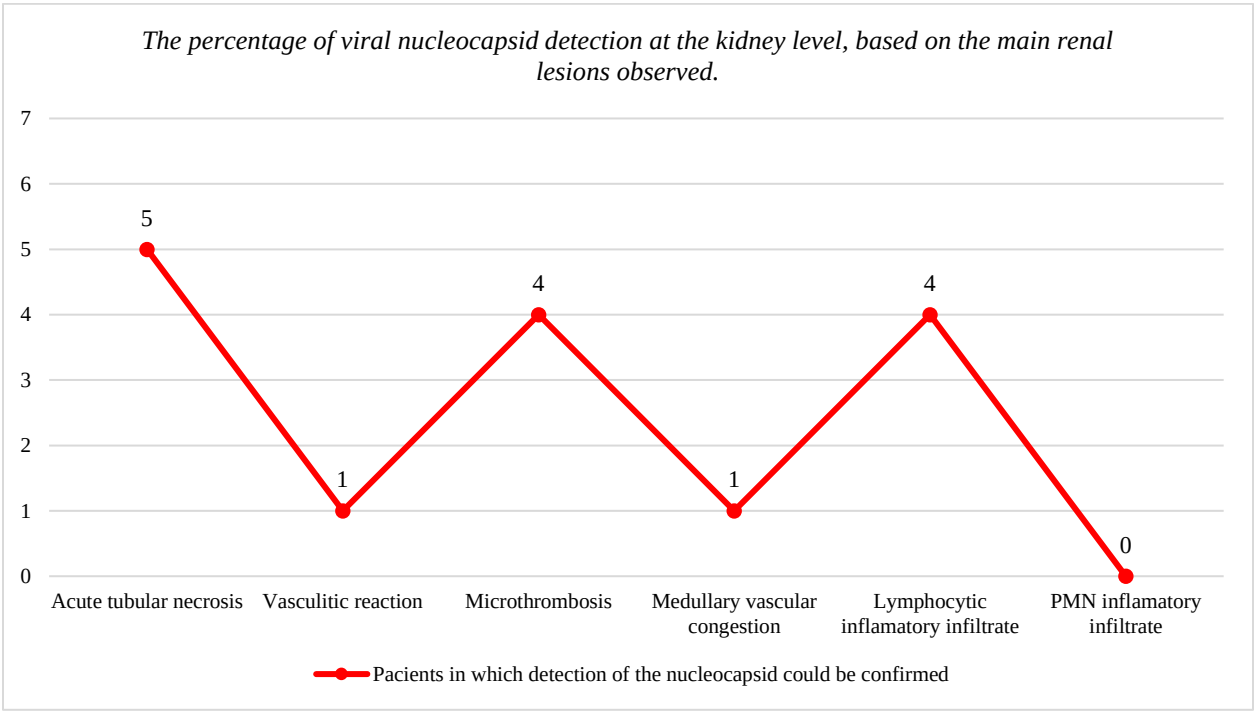

Figure 60: The percentage of viral nucleocapsid detection at the kidney level, based on the main renal lesions observed.

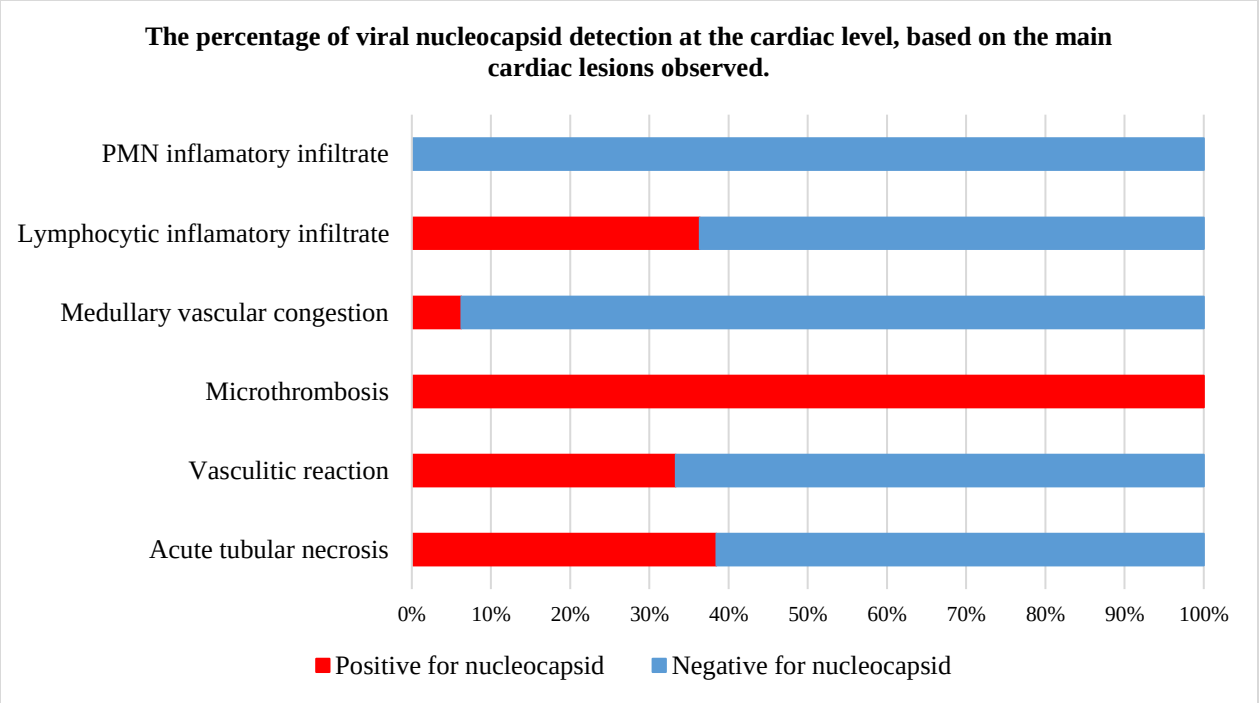

Figure 61: The percentage of viral nucleocapsid detection at the cardiac level, based on the main cardiac lesions observed.

The nucleocapsid of the SARS-CoV-2 virus was detectable in hepatic tissue using immunohistochemical techniques in three distinct cell types: hepatocytes, Kupffer cells, and interstitial fibroblasts. Among these, hepatocytes had the highest number of positive cells, with 16 cases, including 12 cases showing intense positivity and 4 cases showing weak positivity at this level. Kupffer cells followed hepatocytes in terms of nucleocapsid positivity, observed in 15 cases, all of which exhibited intense positivity. Detection of the nucleocapsid at the fibroblast level was observed in 9 cases, with 5 being intensely positive and 4 weakly positive at this level. Out of the 17 cases in the study group that showed positivity for the viral nucleocapsid in at least one of the cell types mentioned above, in 13 of them detection of the N, S, and ORF1ab genes could be established, 3 cases showed the presence of two out of the three viral genes, and in one case, the result was negative for all three viral genes.

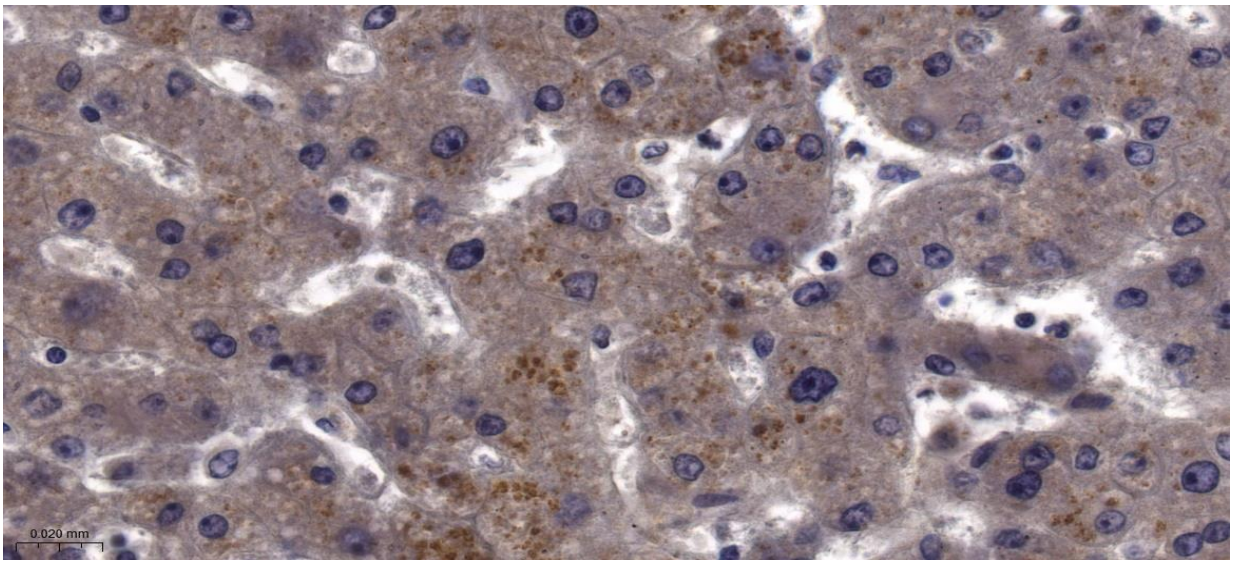

Image 15 - IHC SARS-CoV-2 48.4X (Liver): Positivity at the hepatocytic level.

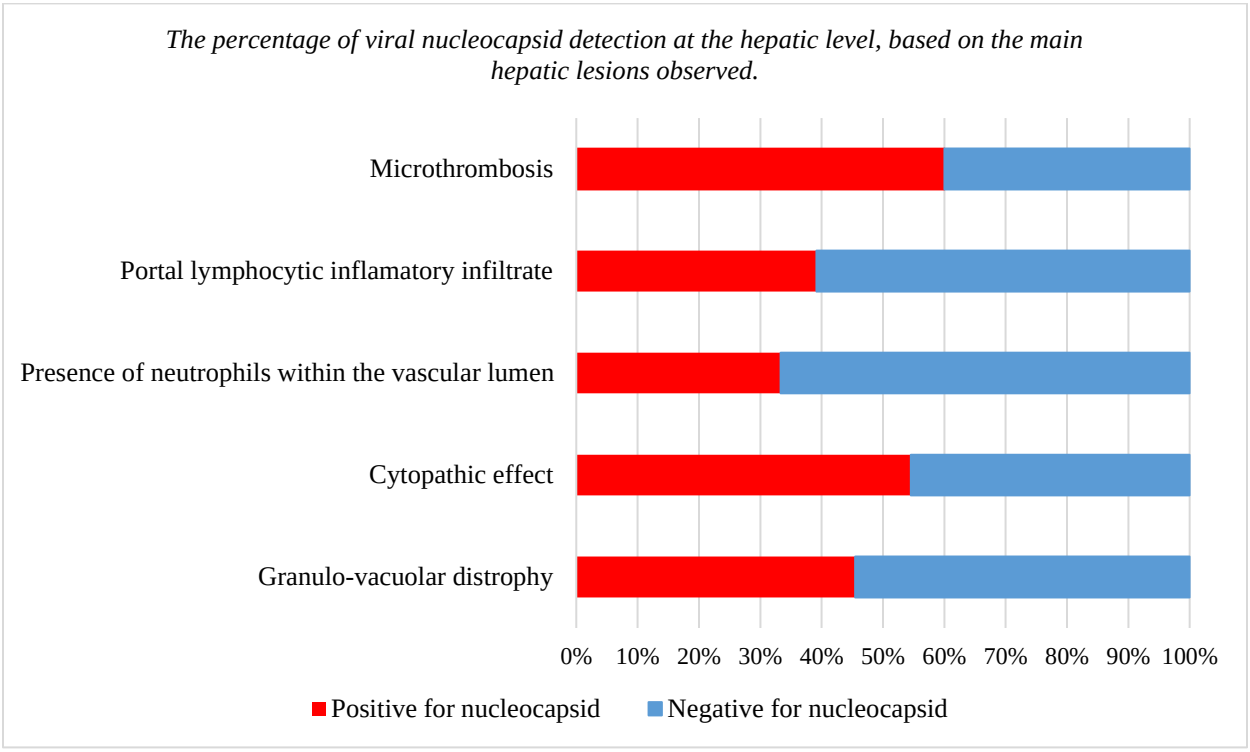

Figure 63: The percentage of viral nucleocapsid detection at the hepatic level, based on the main hepatic lesions observed.

At the splenic tissue level, the detection of the nucleocapsid through immunohistochemical techniques was found in 32 cases from the study group, and in 20 cases from the group tested through molecular techniques. Among these 20 patients, 12 presented the N, S, and ORF1ab genes

at the splenic level, 5 of them had only two out of the three studied genes detected, and the remaining 3 had only one of the three genes of the SARS-CoV-2 virus detected. Out of the 19 cases positive for all three viral genes in the rt-PCR testing, only 7 cases did not show nucleocapsid at the splenic cell level. Considering the interval between the onset of viral infection and death, the majority fell within the 4 to 7-day category, with 7 out of 8 cases. This was followed by the 15 to 21-day category, with 7 out of 11 cases positive for the nucleocapsid, and the category with an onset of over 21 days was represented by 11 out of 21 cases positive for the viral nucleocapsid.

Following the immunohistochemical analysis at the intestinal level, 42 patients showed positivity for the SARS-CoV-2 nucleocapsid antibody in the small intestine, and 41 patients in the colon. The detection of the nucleocapsid was established in stromal cells at the level of the lamina propria, primarily in macrophages. Out of the 20 patients in whom the detection of the three genes could be performed in the small intestine, 17 were positive for the viral nucleocapsid following immunohistochemical analysis. However, a discrepancy is observed in the total number of patients positive for the nucleocapsid in the molecularly tested group, where out of 28 patients, only 17 presented all three viral genes.

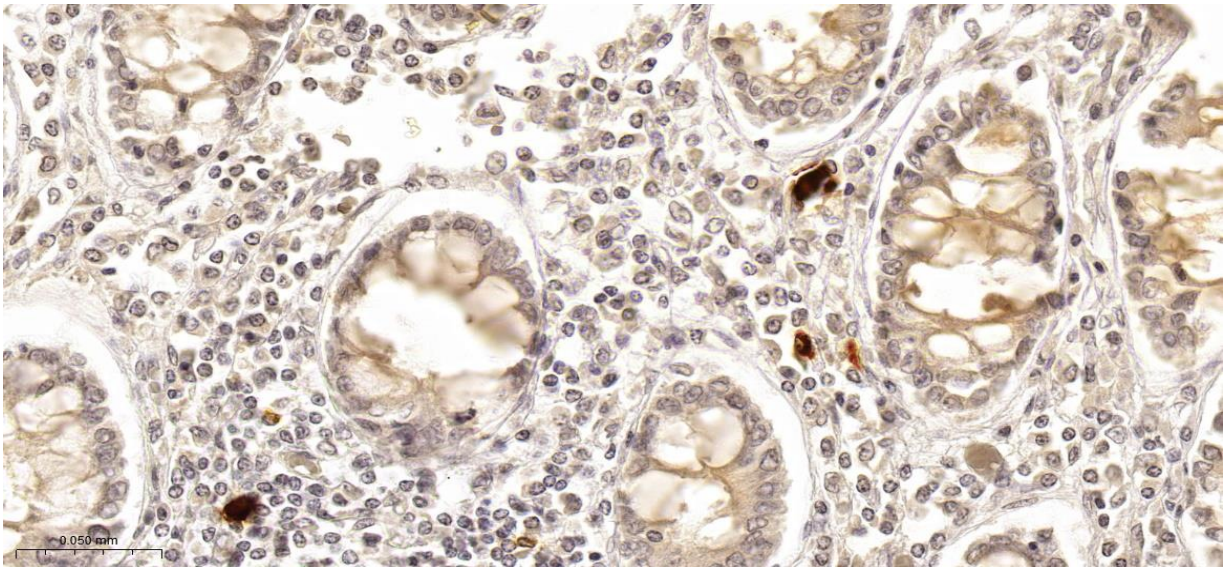

Image - IHC SARS-CoV-2 32.7X (Intestine): Positivity at the level of macrophages in the lamina propria.

4.10. HISTOPATHOLOGICAL, IMMUNOHISTOCHEMICAL, AND MOLECULAR ANALYSIS OF ANTE-PARTUM STILLBORN BABIES FROM MOTHERS WITH COVID-19 INFECTION

The current study group also included two stillborn fetuses from mothers diagnosed with SARS-CoV-2 infection. Following external and internal examination of the cadavers, no specific anomalies were observed. Histopathological examination of the placenta in the second case revealed diffuse lesions in the villi, with trophoblastic necrosis, chronic intervillositis, perivillous fibrin deposition, and a diffuse perivillous inflammatory infiltrate composed of lymphocytes and a few neutrophils. An extensive area of placental hemorrhage was also identified near the basal plate. All these microscopic anomalies correspond to the diagnosis of acute placentitis. After real-time RT-PCR analysis, the placenta, umbilical cord, brain, lungs, and liver were all positive for the N, S, and ORF1ab genes of the SARS-CoV-2 virus. The large intestine was positive exclusively for the N gene, while the kidney showed the presence of only the S gene. Through immunohistochemical analysis using the anti-SARS-CoV-2 nucleocapsid antibody, the placenta exhibited focal intense positivity in the syncytiotrophoblast. As for the umbilical cord, nucleocapsid presence was exclusively detected in the walls of blood vessels, specifically in the cytoplasm of endothelial cells. The lungs also showed intense positivity in type II pneumocytes. The first case presented with non-specific histopathological changes, and viral genome and nucleocapsid detection were inconclusive.

5. DISCUSSIONS

Following the histopathological, immunohistochemical, and molecular analysis of the current study cohort, a pathogenic, physiopathological, and morphopathological model has been partially elucidated. This model has contributed to a better understanding of the mechanisms by which the SARS-CoV-2 virus acts in the human host. However, the knowledge remains partial, and further research is necessary to develop a deeper understanding of this new viral infection that has had a significant impact on society. Future studies on this topic will be essential for improving and expanding our knowledge of this infection.

The male gender, between the ages of 60 and 80, predominates in the current study cohort. An epidemiological study published in 2021 provides useful information regarding the epidemiology of SARS-CoV-2 infection in several countries worldwide. This study refers to the

number of positively detected cases and not specifically to the number of cases diagnosed with severe pneumonia or the number of fatalities. Consequently, the highest proportion of positive cases was observed in the 50-59 age group in China and Germany, in the 20-29 age group in Korea, and in individuals over 80 years old in Italy. [105] Concerning fatalities, studies in the specialized literature, conducted on large patient samples from Germany, Belgium, Switzerland, Norway, Spain, Italy, France, or Romania, have corroborated the theory that male patients over 60 years of age have the highest risk of death as a result of SARS-CoV-2 infection. [106,107,108,109]

Regarding the statistical analysis of the hospitalization period for these patients, the majority, which accounts for 26 cases, had a short hospital stay ranging from one day or a few hours to 3 days. Similar results were also reported in a study from Belgium, which concluded that the average hospitalization period for individuals who passed away due to SARS-CoV-2 infection was 5.7 days, thus demonstrating that severe forms of SARS-CoV-2 pneumonia with a rapid progression have a high risk of fatality. [111]

Regarding the number of days between the onset of the disease and confirmation of the infectious disease in patients who could not precisely report the date of their first symptoms and death, the distribution was variable, with each interval between onset and death having roughly the same number of cases. However, the majority of cases were included in the interval where the onset of symptoms to death was more than 21 days. Similar results have been observed in the existing literature, although with a slightly shorter interval than in the current study. For example, Verity R. et al. reported an average of 17.8 days between symptom onset and death [112]. Baud D. et al. found that the highest incidence of death occurred between 2 and 8 weeks from confirmation of SARS-CoV-2 infection [113]. Madabhavi I. et al. studied deaths occurring between 6 and 41 days from symptom onset, with an average of 14 days [114]. Qiurong R. et al. observed two peaks of death incidence, one at 14 days and the other at 22 days after the onset of the infection [115].

The main comorbidities identified in the current study were predominantly cardiovascular diseases, followed by metabolic conditions, and then pulmonary diseases. These findings are consistent with other studies in the existing literature, where most authors have identified cardiovascular diseases as the most common comorbidities in patients who died due to SARS-CoV-2 infection, followed by diabetes and obesity [116,117,118,119,120,121,122,123].

Within the lungs, the entire spectrum of lesions identified during microscopic examination was categorized into three main groups: acute lesions (the most numerous), aberrant regenerative changes, and associated chronic lesions. Within acute lesions, various types of microscopic changes were observed, falling within the spectrum of either inflammatory or alveolar lesions, vascular lesions, or hemodynamic lesions. In the current study, the highest incidence was represented by the lympho-monocytic inflammatory infiltrate, present in 78.57% of cases, followed by the polymorphonuclear infiltrate, present in 62.5% of cases, and, lastly, the macrophagic infiltrate, with a percentage of 50%. In the case of alveolar lesions, a degree of type II pneumocyte hyperplasia was observed in 91.07% of cases. Viral cytopathic effects had a share of 67.87% of the total cases, followed by the presence of hyaline membranes, with a percentage of 60.71% of cases. Multinucleate giant cells were observed in 55.36% of cases. Viral cytopathic effects of pneumocytes, observed in a representative number of cases, as well as the presence of pneumocyte syncytia, suggested direct infection of these cells by the pathogen and was confirmed by the detection of viral nucleocapsid through immunohistochemical techniques in these cells in 48 cases.

Vascular lesions were part of the histopathological spectrum of SARS-CoV-2 infection at the pulmonary level, along with the previously described alveolar lesions. They were represented by the presence of microthrombi in the lumen of small or medium-sized vessels in 35.71% of cases and a lymphocytic inflammatory reaction within the walls of small intrapulmonary vessels in 17.86% of cases. Several studies in the literature confirm the presence of these lesions, including Satturwar S. et al., who described microthromboses in 59% of the studied cases and vascular lesions such as lymphocytic endotheliitis or capillaritis, similarly mediated by lymphocytes and without the presence of fibrinoid necrosis, in 21% of cases.

In the current study group, the abnormal regenerative lesions within the diffuse alveolar damage were consistently observed and were subdivided into early stages in the form of organizing pneumonia and late stages in the form of extensive interstitial fibrosis and squamous metaplasia of the alveolar epithelium. The most frequent lesions in this category were extensive interstitial fibrosis, accounting for 44.64% of cases, followed by squamous metaplasia, at 30.36%, and lastly, organizing pneumonia, at 17.86%. When considering the time interval between the onset of the infectious disease and death, it was noted that these lesions significantly increased at

15 days from onset and peaked in patients who died after 21 days from onset. These findings align with results from other studies in the literature. [134, 137, 151]

The molecular analysis for detecting the three viral genes N, S, and ORF1ab using rt-PCR from samples collected at the pulmonary level in 35 patients from the study group showed a significantly high detection rate. Specifically, all three viral genes studied were detected in the lung parenchyma in 33 out of 35 cases.

In the case of immunohistochemical analysis using the anti-nucleocapsid SARS-CoV-2 antibody, detection was observed in 48 out of 56 cases. The most intense positivity was observed in pneumocytes, specifically in type II pneumocytes. Most of these pneumocytes showed viral cytopathic effects or formed syncytial giant cells, and this was observed in 48 cases. The intense and diffuse detection of nucleocapsid in pneumocytes was highly associated with diffuse alveolar lesions in the exudative phase. However, the intensity and extent of detection in these cells sharply decreased in the fibrotic phase of diffuse alveolar lesions.

The histopathological analysis of cardiac tissue revealed various types of lesions, including myocytic lesions in 37 patients, inflammatory lesions in 22 patients, vascular lesions in only 7 patients, and associated chronic lesions in 42 patients. Among the acute myocytic, inflammatory, or vascular lesions, the highest incidence was observed in ischemic microstructural myocytic changes, accounting for 66.07% of cases. This was followed by the presence of a subepicardial lymphomonocytic inflammatory infiltrate, at a rate of 26.79%, and myocytic cytopathic changes or myocytic suffering in 19.05% of cases. True myocardial necrosis was observed in only 12.05% of cases, and microthromboses were present in 10.71% of cases. The presence of neutrophils in the vascular lumen, indicating a hyperinflammatory status, was seen in 14.29% of cases. Regarding the heart, the detection of the N, S, and ORF1ab genes was observed in only 17 out of 35 cases studied, with 4 cases detecting only 2 out of the 3 viral genes, and 5 cases demonstrating the presence of only a single viral gene. Immunohistochemical analysis revealed that nucleocapsid detection in cardiac tissue was observed in only 7 out of 56 patients, of which all 7 cases showed detection at the level of the interstitial fibroblasts, 6 out of 7 cases had detection in tissue macrophages, and only 1 case showed weak positivity in myocytes.

The main histopathological changes observed at the kidney level included chronic changes, which were representative in 30 cases, followed by acute vascular changes present in 23 cases. Inflammatory infiltrates were found in 20 patients from the study group, while acute tubular

lesions were observed in only 13 patients. The highest incidence of acute lesions was represented by interstitial lymphomonocytic inflammatory infiltrate, accounting for 37.5% of cases, followed by vascular congestion in the renal medulla at 28.57%, and acute tubular lesions at 23.21%. After thorough review of the literature, it appears that a similar histological pattern was described in other studies, but some authors reported a higher incidence of acute lesions, particularly those involving renal tubules.

For a better understanding of the mechanisms underlying kidney injury, molecular analyses and immunohistochemical tests were conducted. As a result of the examination using the rt-PCR technique on renal tissue samples, it was determined that 16 out of 35 cases tested positive for the S, N, and ORF1ab genes, 7 cases were positive for only two of these genes, and 5 cases were positive for only one viral gene. Following immunohistochemical analysis of post-mortem renal tissue samples, limited positivity with weak intensity was observed in the tubular epithelium in 7 out of 56 patients. A total of 5 patients from the group of 35 tested molecularly showed positivity in tubular epithelial cells for viral nucleocapsid, and all three viral genes were detected in 4 of them.

Following the hepatic histopathological examination, it was observed that the majority of microscopic lesions were associated with chronic changes, followed by necroinflammatory hepatocellular lesions, and to a very limited extent, vascular lesions. The presence of a lymphomonocytic inflammatory infiltrate in the portal space had the highest incidence among acute lesions, at 41%, followed by granulo-vacuolar degeneration and hepatocellular cytopathic effects, each with an incidence of 20%. The presence of neutrophils in the vascular lumen was observed in 11% of cases, and vascular microthrombi in 9% of cases. Over 50% of cases showed chronic changes associated with hepatic steatosis, followed by portal fibrosis with an incidence of 40%. This pattern of hepatic lesions was described by other authors in the literature as well. [177,181]

The detection of the three viral genes through rt-PCR was evident in 18 out of 35 patients. A slightly over 50% association was observed between the detection of the viral genome at the hepatic level and necroinflammatory lesions, such as granulo-vacuolar degeneration (4 out of 7 cases), hepatocellular cytopathic effects (5 out of 9 cases), and the presence of a lymphocytic inflammatory infiltrate in the portal space (9 out of 17 cases). The nucleocapsid of the SARS-CoV-2 virus was detectable in the liver using immunohistochemical techniques in three distinct

cell types, including hepatocytes, Kupffer cells, and interstitial fibroblasts. Among these, hepatocytes showed the highest number of positive cells in 16 cases.

The histopathological changes in the splenic parenchyma mostly involved disorganization in the white pulp. Atrophy of the white pulp had a direct proportional relationship with the slow and unfavorable progression of the viral infection, being present in just over 50% of the cases with an infectious onset more than 21 days before death and only in 7 out of 19 patients with a rapid, fulminant course.

Examination of the splenic tissue using molecular techniques for viral genome detection showed a significant proportion of patients in the study group tested positive for all three genes studied, totaling 19 out of 35 cases. Two out of three viral genes were detected in 8 patients, with only 4 cases testing positive for one of the N, S, or ORF1ab genes. The detection of nucleocapsid through immunohistochemistry techniques was observed in 32 cases out of the total of 56 patients in the study group and in 20 cases in the group tested using molecular techniques (N=35). It was primarily seen in macrophages, confirmed by CD68 positivity. Nearly 60% of the patients in whom the viral genome presence was confirmed also showed the nucleocapsid at the splenic level. Both the detection of nucleocapsid and the detection of the three viral genes studied were evident in the first 21 days after the onset of infection, followed by a sharp decrease in detection in patients with an onset more than 21 days before death.

Following the examination of the small intestine and colon, numerous changes were observed, most of which were nonspecific. At the level of the small intestine, 2 cases showed inflammatory lesions consitant with a neutrophilic infiltrate, while at the level of the colon, the same type of lesion was observed in a larger proportion, specifically in 6 specimens. A higher proportion of cases presented inflammatory lesions mediated by a lympho-monocytic inflammatory infiltrate, with a total of 21 cases in the small intestine and 24 cases in the colon, being the most frequently observed lesion. Epithelial erosions were observed in 29% and 30% of cases in the small intestine and colon, respectively. Mucosal necrosis was more commonly seen in the colon, with an incidence of 12.5%, compared to 7.14% in the small intestine. On the other hand, mucosal bleeding had a higher incidence in the small intestine compared to the colon (7.14% versus 3.57%).

The detection of the three viral genes studied was evident in 20 out of 35 cases examined in the small intestine. Two out of the three viral genes were detected in only 3 patients, and a

single viral gene was present in just 4 patients. PCR examination of the colonic tissue material revealed that all three viral genes were detected in 19 patients. A total of 42 patients showed positivity in the small intestine, and 41 patients in the colon for the anti-nucleocapsid SARS-CoV-2 antibody in the immunohistochemical analysis.

The RT-PCR analysis revealed the presence of the N, S, and Orf1ab genes in the placenta, umbilical cord, as well as in some fetal organs such as the brain, lungs, and liver. RT-PCR analysis also uncovered four cases where placental tissue was positive for the viral genes. After the molecular analysis, we aimed to confirm our results using immunohistochemical techniques to detect the viral nucleocapsid. In this way, we could definitively confirm not only the presence of viral genes in the placenta and fetal organs but also the existence of fully assembled virions, arguing in favor of active infection and replication of SARS-CoV-2 at the fetal level. Regarding the placenta, we detected the presence of the SARS-CoV-2 viral nucleocapsid in syncytiotrophoblasts, similar to several studies published in the literature. Positivity for the SARS-CoV-2 nucleocapsid was also detected in fetal lung type II pneumocytes, confirming not only vertical transmission but also the active replication process and increased affinity of the virus for this class of cells. Similar results were obtained by other researchers. The brain, heart, liver, kidneys, and intestines all tested negative for the SARS-CoV-2 virus nucleocapsid, even though the brain, lungs, and liver showed positivity for the three viral genes in the RT-PCR examination, suggesting that the virus entered the fetal circulatory system but did not replicate and did not invade the cells in these organs.

6. CONCLUSIONS

- The main age group at high risk of death is between 61 and 80 years old, followed by those aged between 41 and 60 years, and those over 80 years old. The lowest risk is seen in individuals under 20 years of age.
- The male gender presents a higher risk of death following infection with the SARS-CoV-2 virus compared to the female gender.
- The average length of hospitalization was 12 days, and the average time between the onset of the infectious disease or viral infection confirmation and death was 21 days.

- Cardiovascular comorbidities such as hypertension, atherosclerosis, and chronic heart failure are associated with the highest risk of death, followed by metabolic comorbidities, mainly obesity and diabetes, and then chronic respiratory conditions like asthma or COPD.
- The thanatogenic mechanism is typically triggered by severe viral pneumonia, followed at a significant distance by associated bacterial bronchopneumonia or sepsis, as well as pulmonary thromboembolism.
- Patients with severe SARS-CoV-2 infection may suffer from necrosis or spontaneous perforations in the digestive tract, most likely triggered by vascular wall lesions, systemic hypoxia, systemic microthromboses, or an exaggerated inflammatory response.
- From a histopathological perspective, the lung is the most affected organ of this viral infection, but microscopic lesions, directly or indirectly mediated by the virus, are also observed in the heart, kidneys, liver, spleen, and intestines.
- The histopathological pattern in SARS-CoV-2 infection at the pulmonary level consists of diffuse alveolar lesions in an exudative, regenerative, or fibrotic phase.
- The most frequently detected microscopic changes within diffuse alveolar lesions include hyperplasia of type II pneumocytes, many of which exhibit viral cytopathic effects, destruction of the alveolar epithelium with hyaline membrane formation, and the formation of multinucleated syncytial pneumocyte giant cells.
- The immune response at the pulmonary level is mediated most often by the lympho-monocytic and macrophagic systems, but in cases with a rapid and fulminant evolution, an exaggerated inflammatory status, or cases with unfavorable slow evolution and septic complications, the immune response may also be mediated by the presence of polymorphonuclear neutrophils.
- The lymphocytic inflammatory infiltrate consists mostly of CD3+ T lymphocytes.
- Pulmonary lymphocytic vasculitis reaction and microthromboses are triggered by macrophages derived from monocytes infected with the SARS-CoV-2 virus or by the systemic inflammatory response syndrome.
- Localized microthromboses are most commonly associated with the presence of the SARS-CoV-2 virus at this level, and microthromboses observed in more than one organ are associated with a high-intensity systemic inflammatory response syndrome.

- Diffuse alveolar hemorrhage or massive pulmonary edema may precede death and occur as a secondary result of vascular wall or alveolar epithelium surface lesions.
- The risk of alveolar hemorrhage is highest in patients with an infectious onset between 15 and 21 days.
- Diffuse alveolar lesions of fibrotic nature most consistently appear after 21 days from the onset of infection, but they can also be observed in the first week of infection in limited cases. These lesions are mainly represented by interstitial fibrosis, followed by squamous metaplasia and, lastly, organized pneumonia.
- The most common acute microscopic cardiac lesions were microstructural changes in myocardial fibers, followed by lymphomonocytic inflammation in the pericardium and subepicardial space, as well as cytopathic changes in myocytes.
- Lymphocytic borderline myocarditis, microthromboses, and inflammatory infiltrates in the vascular walls were observed in a limited number of patients and were associated with the presence of the virus at the myocardial level.
- The presence of neutrophils in the myocardial vascular lumen was not associated with virus detection at this level but was observed in patients with severe, fulminant viral pneumonia with rapid negative outcome or in patients with slow, unfavorable evolution with septic complications.
- Myocardial fibrosis was the most commonly associated chronic lesion observed in cardiac tissue.
- Acute tubular necrosis is the most specific injury of the renal parenchyma in patients with SARS-CoV-2 infection. It can be secondary to direct virus infection at this level or a consequence of systemic hypoxia, vascular lesions, microthromboses, and systemic inflammatory response.
- The inflammatory reaction in the renal parenchyma is mediated by the presence of the interstitial lymphomonocytic inflammatory infiltrate and may be associated with the presence of the virus at this level.
- The most frequent histopathological liver change in patients with COVID-19 infection is the presence of lymphomonocytic inflammatory infiltrates in the portal space, followed by granulo-vacuolar hepatocyte dystrophy and hepatocytic cytopathic effects.

- Associated chronic liver injuries are mostly represented by hepatic steatosis, followed by periportal fibrosis.
- Splenic lesions result from the disorganization of the red pulp, translated by marked congestion at this level, followed by alterations of the white pulp, most frequently secondary to follicular atrophy, which has a direct proportional relationship with the long-term course of the infection and is likely a consequence of the systemic lymphopenia observed in these patients.
- The histopathological changes at the intestinal level were nonspecific and mostly represented by the presence of lymphomonocytic inflammatory infiltrate in the mucosa, followed by epithelial erosions and mucosal fibrosis.
- N, S, and ORF1ab genes were most frequently detected by rt-PCR in the lungs, followed by the intestines, spleen, liver, heart, and kidneys, in this order.
- The detection of the SARS-CoV-2 virus nucleocapsid was most commonly achieved through immunohistochemical analysis in the lungs, followed by the intestines, spleen, liver, heart, and kidneys, in the mentioned order.
- Based on the correlation between rt-PCR and immunohistochemistry results, it was concluded that the SARS-CoV-2 virus is most frequently present and replicating in the lungs, followed by the intestines, liver, and spleen.
- The greatest discrepancy between the detection of the viral genome and the viral nucleocapsid was observed in the heart and kidneys, where it was concluded that the virus has low affinity for these two organs, and most patients with viral genome detection at this level were in the viremia phase.
- The cells directly targeted by the SARS-CoV-2 virus are pneumocytes, hepatocytes, renal tubular cells, pulmonary macrophages and fibroblasts, myocardial interstitial macrophages and fibroblasts, hepatic Kupffer cells, as well as splenic and intestinal macrophages.
- Vertical transmission was confirmed by detecting S, N, and ORF1ab genes in the placenta, umbilical cord, brain, lungs, and liver, as well as the identification of viral nucleocapsids in the placenta, umbilical cord, and fetal lungs.
- Fetal cells targeted by the SARS-CoV-2 virus included syncytiotrophoblasts, umbilical cord endothelial cells, and type II pneumocytes.

7. ORIGINAL ELEMENTS

Even though there have been numerous scientific papers published in the literature regarding the microscopic changes in SARS-CoV-2 viral infection from the beginning of the pandemic until now, to our knowledge, up to the present moment, no study has been elaborated that includes extensive microscopic descriptions on such a wide tissue spectrum, associated with both molecular analyses, using rt-PCR for the detection of N, S, and ORF1ab genes, and immunohistochemical analyses for the detection of viral nucleocapsid. Additionally, we have determined whether the described lesions are a direct consequence of viral invasion at the tissue level, or they are secondary to the systemic inflammatory response, or they result from early complications generated by the viral infectious process. Another element of originality was the development of a histopathological pattern generated by SARS-CoV-2 virus infection, built dynamically according to the onset of infection, a histopathological pattern that can serve as a basis for establishing certain microscopic diagnostic criteria for COVID-19. Additionally, we managed to utilize digital pathology elements by digitizing histopathological slides and analyzing them using quantification modules.

8. RESEARCH LIMITATIONS

Considering the legal aspects during the pandemic, specifically the limitation of performing autopsies on deceased patients who had previously tested positive for the SARS-CoV-2 virus, the study group was relatively small. Another limitation that arose from the small number of autopsies that could be performed was the limited number of complete autopsies, including examination of the cranial cavity for brain tissue sampling. Due to this situation, it was not possible to evaluate the brain tissue histopathologically, immunohistochemically, or molecularly in the case of patients infected with the SARS-CoV-2 virus.

Furthermore, another limitation of this study was related to the lack of sustainable funding that would have allowed for a more comprehensive molecular and immunohistochemical analysis. Therefore, molecular analyses for the detection of N, S, and ORF1ab genes could only be conducted on a sample of 35 out of 56 patients.

9. FUTURE RESEARCH DIRECTIONS

The current study, with its complexity, serves as a cornerstone for future specialized studies aimed at addressing questions that have yet to be answered even after the completion of this research. Consequently, immunohistochemical studies can be developed, either using the current sample or a new set of cases, to investigate the inflammatory molecules present in tissues affected by the novel coronavirus. Another potential study could focus on the presence of surface receptors that play a major role in cell fusion and invasion mechanisms, such as ACE2 receptors and TMPRSS2 proteins. Additionally, viral detection can be further explored using in-situ hybridization techniques designed to directly detect viral RNA in infected cells. These results can complement the viral detection findings using immunohistochemistry and polymerase chain reaction. Furthermore, it is imperative to conduct long-term studies on patients who have experienced at least one infection caused by the SARS-CoV-2 virus and have developed chronic, nonspecific symptoms. Currently, there is discussion about the phenomenon of long Covid. These studies must include histopathological analyses to identify chronic lesion foci in specific tissues and organs. Immunohistochemical or molecular studies should also be carried out to confirm or refute the long-term presence of viral RNA or specific viral genome particles and proteins.

BIBLIOGRAPHY

1. Fields, Bernard N. Knipe, David M. Howley, Peter M. (2013) Fields Virology - Volume I (6-th Ed.) Lippincott Williams & Wilkins. ISBN-13: 978-1-4511-0563-6. pp: 1-3.

2. Wang-Shick R. (2007) Molecular Pathology of Human Pathogenic Viruses (1st ed.) Elsevier. ISBN: 978-0-12-800838-6. pp: 3-5.

3. Dimmock, N. J. Easton, A. J. Leppard . K. N. (2007) Introduction to modern virology (6-th ed.) Blackwell Publishing. ISBN-13: 978-1-4051-3645-7. pp: 4-5.

4. Carter, J. Saunders, V. (2013) Virology. Principles and Applications (2nd ed.) John Wiley & Sons Ltd. ISBN 978-1-119-99143-4. pp: 27-28.

5. Flint, S. J. Enquist, L.W Racaniello, V.R. Skalka, A.M. (2009) Principles of Virology (3rd ed.) ASM Press, Washington, DC. ISBN 978-1-55581-443-4. pg 4

6. Koonin EV, Krupovic M, Agol VI. 2021.The Baltimore classification of viruses 50 yearslater: how does it stand in the light of virus evolution? Microbiol Mol Biol Rev 85:e00053-21. https://doi.org/10.1128/MMBR.00053-21.

7. Zlotnick A. Theoretical aspects of virus capsid assembly. J Mol Recognit. 2005 Nov-Dec;18(6):479-90. doi: 10.1002/jmr.754. PMID: 16193532.

8. Roos WH, Ivanovska IL, Evilevitch A, Wuite GJ. Viral capsids: mechanical characteristics, genome packaging and delivery mechanisms. Cell Mol Life Sci. 2007 Jun;64(12):1484-97. doi: 10.1007/s00018-007-6451-1. PMID: 17440680; PMCID: PMC2771126.

9. Choi YG, Rao AL. Packaging of brome mosaic virus RNA3 is mediated through a bipartite signal. J Virol. 2003 Sep;77(18):9750-7. doi: 10.1128/jvi.77.18.9750-9757.2003. PMID: 12941883; PMCID: PMC224604.

10. Catalano CE, Morais MC. Viral genome packaging machines: Structure and enzymology. Enzymes. 2021;50:369-413. doi: 10.1016/bs.enz.2021.09.006. Epub 2021 Nov 10. PMID: 34861943.

11. Chelikani V, Ranjan T, Kondabagil K. Revisiting the genome packaging in viruses with lessons from the "Giants". Virology. 2014 Oct;466-467:15-26. doi: 10.1016/j.virol.2014.06.022. Epub 2014 Jul 3. PMID: 24998349.

12. Chelikani V, Ranjan T, Zade A, Shukla A, Kondabagil K. Genome segregation and packaging machinery in Acanthamoeba polyphaga mimivirus is reminiscent of bacterial apparatus.

J Virol. 2014 Jun;88(11):6069-75. doi: 10.1128/JVI.03199-13. Epub 2014 Mar 12. PMID: 24623441; PMCID: PMC4093880.

13. Braakman I, van Anken E. Folding of viral envelope glycoproteins in the endoplasmic reticulum. Traffic. 2000 Jul;1(7):533-9. doi: 10.1034/j.1600-0854.2000.010702.x. PMID: 11208140; PMCID: PMC7190097.

14. Harrison SC. Mechanism of membrane fusion by viral envelope proteins. Adv Virus Res. 2005;64:231-61. doi: 10.1016/S0065-3527(05)64007-9. PMID: 16139596; PMCID: PMC7173036.

15. Bergelson JM. Intercellular junctional proteins as receptors and barriers to virus infection and spread. Cell Host Microbe. 2009 Jun 18;5(6):517-21. doi: 10.1016/j.chom.2009.05.009. PMID: 19527879.

16. Davies DE. Epithelial barrier function and immunity in asthma. Ann Am Thorac Soc. 2014 Dec;11 Suppl 5:S244-51. doi: 10.1513/AnnalsATS.201407-304AW. PMID: 25525727.

17. Sanders CJ, Doherty PC, Thomas PG. Respiratory epithelial cells in innate immunity to influenza virus infection. Cell Tissue Res. 2011 Jan;343(1):13-21. doi: 10.1007/s00441-010-1043-z. Epub 2010 Sep 17. PMID: 20848130.

18. Goto Y, Kiyono H. Epithelial barrier: an interface for the cross-communication between gut flora and immune system. Immunol Rev. 2012 Jan;245(1):147-63. doi: 10.1111/j.1600-065X.2011.01078.x. PMID: 22168418.

19. Tawar RG, Colpitts CC, Lupberger J, El-Saghire H, Zeisel MB, Baumert TF. Claudins and pathogenesis of viral infection. Semin Cell Dev Biol. 2015 Jun;42:39-46. doi: 10.1016/j.semcdb.2015.04.011. Epub 2015 May 7. PMID: 25960372

20. Bieniasz PD. Intrinsic immunity: a front-line defense against viral attack. Nat Immunol. 2004 Nov;5(11):1109-15. doi: 10.1038/ni1125. PMID: 15496950.

21. Majdoul S, Compton AA. Lessons in self-defence: inhibition of virus entry by intrinsic immunity. Nat Rev Immunol. 2022 Jun;22(6):339-352. doi: 10.1038/s41577-021-00626-8. Epub 2021 Oct 13. PMID: 34646033; PMCID: PMC8511856.

22. Yan N, Chen ZJ. Intrinsic antiviral immunity. Nat Immunol. 2012 Feb 16;13(3):214-22. doi: 10.1038/ni.2229. PMID: 22344284; PMCID: PMC3549670.

23. Ma Y, Galluzzi L, Zitvogel L, Kroemer G. Autophagy and cellular immune responses. Immunity. 2013 Aug 22;39(2):211-27. doi: 10.1016/j.immuni.2013.07.017. PMID: 23973220.

24. Münz C. Autophagy in immunity. Prog Mol Biol Transl Sci. 2020;172:67-85. doi: 10.1016/bs.pmbts.2020.03.005. Epub 2020 Mar 28. PMID: 32620251.

25. Feig C, Peter ME. How apoptosis got the immune system in shape. Eur J Immunol. 2007 Nov;37 Suppl 1:S61-70. doi: 10.1002/eji.200737462. PMID: 17972347.

26. Kawai T, Akira S. The role of pattern-recognition receptors in innate immunity: update on Toll-like receptors. Nat Immunol. 2010 May;11(5):373-84. doi: 10.1038/ni.1863. Epub 2010 Apr 20. PMID: 20404851.

27. Areschoug T, Gordon S. Pattern recognition receptors and their role in innate immunity: focus on microbial protein ligands. Contrib Microbiol. 2008;15:45-60. doi: 10.1159/000135685. PMID: 18511855.

28. Suresh R, Mosser DM. Pattern recognition receptors in innate immunity, host defense, and immunopathology. Adv Physiol Educ. 2013 Dec;37(4):284-91. doi: 10.1152/advan.00058.2013. PMID: 24292903; PMCID: PMC4089092.

29. Li P, Chang M. Roles of PRR-Mediated Signaling Pathways in the Regulation of Oxidative Stress and Inflammatory Diseases. Int J Mol Sci. 2021 Jul 19;22(14):7688. doi: 10.3390/ijms22147688. PMID: 34299310; PMCID: PMC8306625.

30. Ordureau A, Enesa K, Nanda S, Le Francois B, Peggie M, Prescott A, Albert PR, Cohen P. DEAF1 is a Pellino1-interacting protein required for interferon production by Sendai virus and double-stranded RNA. J Biol Chem. 2013 Aug 23;288(34):24569-80. doi: 10.1074/jbc.M113.479550. Epub 2013 Jul 11. PMID: 23846693; PMCID: PMC3750155.

31. Bell D, Young JW, Banchereau J. Dendritic cells. Adv Immunol. 1999;72:255-324. doi: 10.1016/s0065-2776(08)60023-1. PMID: 10361578

32. Banchereau J, Steinman RM. Dendritic cells and the control of immunity. Nature. 1998 Mar 19;392(6673):245-52. doi: 10.1038/32588. PMID: 9521319

33. Vivier E, Tomasello E, Baratin M, Walzer T, Ugolini S. Functions of natural killer cells. Nat Immunol. 2008 May;9(5):503-10. doi: 10.1038/ni1582. PMID: 18425107.

34. Stoermer KA, Morrison TE. Complement and viral pathogenesis. Virology. 2011 Mar 15;411(2):362-73. doi: 10.1016/j.virol.2010.12.045. Epub 2011 Feb 2. PMID: 21292294; PMCID: PMC3073741

35. Naumenko V, Turk M, Jenne CN, Kim SJ. Neutrophils in viral infection. Cell Tissue Res. 2018 Mar;371(3):505-516. doi: 10.1007/s00441-017-2763-0. Epub 2018 Jan 11. PMID: 29327081.

36. Kisielow P, von Boehmer H. Development and selection of T cells: facts and puzzles. Adv Immunol. 1995;58:87-209. doi: 10.1016/s0065-2776(08)60620-3. PMID: 7741032.

37. Luckheeram RV, Zhou R, Verma AD, Xia B. $CD4^+$T cells: differentiation and functions. Clin Dev Immunol. 2012;2012:925135. doi: 10.1155/2012/925135. Epub 2012 Mar 14. PMID: 22474485; PMCID: PMC3312336.

38. Jenkins MK, Khoruts A, Ingulli E, Mueller DL, McSorley SJ, Reinhardt RL, Itano A, Pape KA. In vivo activation of antigen-specific CD4 T cells. Annu Rev Immunol. 2001;19:23-45. doi: 10.1146/annurev.immunol.19.1.23. PMID: 11244029.

39. Andersen MH, Schrama D, Thor Straten P, Becker JC. Cytotoxic T cells. J Invest Dermatol. 2006 Jan;126(1):32-41. doi: 10.1038/sj.jid.5700001. PMID: 16417215.

40. Batista FD, Harwood NE. The who, how and where of antigen presentation to B cells. Nat Rev Immunol. 2009 Jan;9(1):15-27. doi: 10.1038/nri2454. PMID: 19079135.

41. Kurosaki T, Kometani K, Ise W. Memory B cells. Nat Rev Immunol. 2015 Mar;15(3):149-59. doi: 10.1038/nri3802. Epub 2015 Feb 13. PMID: 25677494.

42. Casali P, Schettino EW. Structure and function of natural antibodies. Curr Top Microbiol Immunol. 1996;210:167-79. doi: 10.1007/978-3-642-85226-8_17. PMID: 8565555.

43. Racine R, Winslow GM. IgM in microbial infections: taken for granted? Immunol Lett. 2009 Aug 15;125(2):79-85. doi: 10.1016/j.imlet.2009.06.003. Epub 2009 Jun 17. PMID: 19539648; PMCID: PMC2747358.

44. Vidarsson G, Dekkers G, Rispens T. IgG subclasses and allotypes: from structure to effector functions. Front Immunol. 2014 Oct 20;5:520. doi: 10.3389/fimmu.2014.00520. PMID: 25368619; PMCID: PMC4202688.

45. Schroeder HW Jr, Cavacini L. Structure and function of immunoglobulins. J Allergy Clin Immunol. 2010 Feb;125(2 Suppl 2):S41-52. doi: 10.1016/j.jaci.2009.09.046. PMID: 20176268; PMCID: PMC3670108.

46. Cascella M, Rajnik M, Aleem A, et al. Features, Evaluation, and Treatment of Coronavirus (COVID-19) [Updated 2022 Jun 30]. In: StatPearls [Internet]. Treasure Island (FL):

StatPearls Publishing; 2022 Jan-. Available from: https://www.ncbi.nlm.nih.gov/books/NBK554776/.

47. Andersen KG, Rambaut A, Lipkin WI, Holmes EC, Garry RF. The proximal origin of SARS-CoV-2. Nat Med. 2020 Apr;26(4):450-452. doi: 10.1038/s41591-020-0820-9. PMID: 32284615; PMCID: PMC7095063.

48. Day T, Gandon S, Lion S, Otto SP. On the evolutionary epidemiology of SARS-CoV-2. Curr Biol. 2020 Aug 3;30(15):R849-R857. doi: 10.1016/j.cub.2020.06.031. Epub 2020 Jun 11. PMID: 32750338; PMCID: PMC7287426.

49. Holmes EC, Goldstein SA, Rasmussen AL, Robertson DL, Crits-Christoph A, Wertheim JO, Anthony SJ, Barclay WS, Boni MF, Doherty PC, Farrar J, Geoghegan JL, Jiang X, Leibowitz JL, Neil SJD, Skern T, Weiss SR, Worobey M, Andersen KG, Garry RF, Rambaut A. The origins of SARS-CoV-2: A critical review. Cell. 2021 Sep 16;184(19):4848-4856. doi: 10.1016/j.cell.2021.08.017. Epub 2021 Aug 19. PMID: 34480864; PMCID: PMC8373617.

50. Astuti I, Ysrafil. Severe Acute Respiratory Syndrome Coronavirus 2 (SARS-CoV-2): An overview of viral structure and host response. Diabetes Metab Syndr. 2020 Jul-Aug;14(4):407-412. doi: 10.1016/j.dsx.2020.04.020. Epub 2020 Apr 18. PMID: 32335367; PMCID: PMC7165108.

51. Zhang J, Xiao T, Cai Y, Chen B. Structure of SARS-CoV-2 spike protein. Curr Opin Virol. 2021 Oct;50:173-182. doi: 10.1016/j.coviro.2021.08.010. Epub 2021 Sep 8. PMID: 34534731; PMCID: PMC8423807.

52. Chai J, Cai Y, Pang C, Wang L, McSweeney S, Shanklin J, Liu Q. Structural basis for SARS-CoV-2 envelope protein recognition of human cell junction protein PALS1. Nat Commun. 2021 Jun 8;12(1):3433. doi: 10.1038/s41467-021-23533-x. PMID: 34103506; PMCID: PMC8187709.

53. Saville JW, Berezuk AM, Srivastava SS, Subramaniam S. Three-Dimensional Visualization of Viral Structure, Entry, and Replication Underlying the Spread of SARS-CoV-2. Chem Rev. 2022 Jul 21:acs.chemrev.1c01062. doi: 10.1021/acs.chemrev.1c01062. Epub ahead of print. PMID: 35863749; PMCID: PMC9344915.

54. Alharbi SN, Alrefaei AF. Comparison of the SARS-CoV-2 (2019-nCoV) M protein with its counterparts of SARS-CoV and MERS-CoV species. J King Saud Univ Sci. 2021

Mar;33(2):101335. doi: 10.1016/j.jksus.2020.101335. Epub 2021 Jan 7. PMID: 33432259; PMCID: PMC7787911.

55. Bai Z, Cao Y, Liu W, Li J. The SARS-CoV-2 Nucleocapsid Protein and Its Role in Viral Structure, Biological Functions, and a Potential Target for Drug or Vaccine Mitigation. Viruses. 2021 Jun 10;13(6):1115. doi: 10.3390/v13061115. PMID: 34200602; PMCID: PMC8227405.

56. Brant AC, Tian W, Majerciak V, Yang W, Zheng ZM. SARS-CoV-2: from its discovery to genome structure, transcription, and replication. Cell Biosci. 2021 Jul 19;11(1):136. doi: 10.1186/s13578-021-00643-z. PMID: 34281608; PMCID: PMC8287290.

57. Huston NC, Wan H, de Cesaris Araujo Tavares R, Wilen C, Pyle AM. Comprehensive in-vivo secondary structure of the SARS-CoV-2 genome reveals novel regulatory motifs and mechanisms. bioRxiv [Preprint]. 2020 Jul 10:2020.07.10.197079. doi: 10.1101/2020.07.10.197079. Update in: Mol Cell. 2021 Jan 1;: PMID: 32676598; PMCID: PMC7359520.

58. Kim D, Lee JY, Yang JS, Kim JW, Kim VN, Chang H. The Architecture of SARS-CoV-2 Transcriptome. Cell. 2020 May 14;181(4):914-921.e10. doi: 10.1016/j.cell.2020.04.011. Epub 2020 Apr 23. PMID: 32330414; PMCID: PMC7179501.

59. Lippi G, Mattiuzzi C, Henry BM. Updated picture of SARS-CoV-2 variants and mutations. Diagnosis (Berl). 2021 Dec 23;9(1):11-17. doi: 10.1515/dx-2021-0149. PMID: 34958184.

60. Lauring AS, Hodcroft EB. Genetic Variants of SARS-CoV-2-What Do They Mean? JAMA. 2021 Feb 9;325(6):529-531. doi: 10.1001/jama.2020.27124. PMID: 33404586

61. Emrani J, Ahmed M, Jeffers-Francis L, Teleha JC, Mowa N, Newman RH, Thomas MD. SARS-COV-2, infection, transmission, transcription, translation, proteins, and treatment: A review. Int J Biol Macromol. 2021 Dec 15;193(Pt B):1249-1273. doi: 10.1016/j.ijbiomac.2021.10.172. Epub 2021 Oct 28. PMID: 34756970; PMCID: PMC8552795.

62. Hafiz M. N. Iqbal, Kenya D. Romero-Castillo, Muhammad Bilal and Roberto Parra-Saldivar, The Emergence of Novel Coronavirus and its Replication Cycle - An Overview, J. Pure Appl. Microbiol., 2020; 14(1).

63. Shang J, Wan Y, Luo C, Ye G, Geng Q, Auerbach A, Li F. Cell entry mechanisms of SARS-CoV-2. Proc Natl Acad Sci U S A. 2020 May 26;117(21):11727-11734. doi: 10.1073/pnas.2003138117. Epub 2020 May 6. PMID: 32376634; PMCID: PMC7260975.

64. Zhao Z, Qin P, Huang YW. Lysosomal ion channels involved in cellular entry and uncoating of enveloped viruses: Implications for therapeutic strategies against SARS-CoV-2. Cell Calcium. 2021 Mar;94:102360. doi: 10.1016/j.ceca.2021.102360. Epub 2021 Jan 23. PMID: 33516131; PMCID: PMC7825922.

65. Lu S, Ye Q, Singh D, Villa E, Cleveland DW, Corbett KD. The SARS-CoV-2 Nucleocapsid phosphoprotein forms mutually exclusive condensates with RNA and the membrane-associated M protein. bioRxiv [Preprint]. 2020 Jul 31:2020.07.30.228023. doi: 10.1101/2020.07.30.228023. Update in: Nat Commun. 2021 Jan 21;12(1):502. PMID: 32766587; PMCID: PMC7402048.

66. Bailey AL, Diamond MS. A Crisp(r) New Perspective on SARS-CoV-2 Biology. Cell. 2021 Jan 7;184(1):15-17. doi: 10.1016/j.cell.2020.12.003. Epub 2020 Dec 17. PMID: 33338422; PMCID: PMC7746090.

67. Forchette L, Sebastian W, Liu T. A Comprehensive Review of COVID-19 Virology, Vaccines, Variants, and Therapeutics. Curr Med Sci. 2021;41(6):1037-1051. doi:10.1007/s11596-021-2395-1

68. Hu B, Guo H, Zhou P, Shi ZL. Characteristics of SARS-CoV-2 and COVID-19 [published correction appears in Nat Rev Microbiol. 2022 May;20(5):315]. Nat Rev Microbiol. 2021;19(3):141-154. doi:10.1038/s41579-020-00459-7

69. V'kovski P, Kratzel A, Steiner S, Stalder H, Thiel V. Coronavirus biology and replication: implications for SARS-CoV-2. Nat Rev Microbiol. 2021;19(3):155-170. doi:10.1038/s41579-020-00468-6

70. Yang H, Rao Z. Structural biology of SARS-CoV-2 and implications for therapeutic development. Nat Rev Microbiol. 2021;19(11):685-700. doi:10.1038/s41579-021-00630-8

71. Bai Z, Cao Y, Liu W, Li J. The SARS-CoV-2 Nucleocapsid Protein and Its Role in Viral Structure, Biological Functions, and a Potential Target for Drug or Vaccine Mitigation. Viruses. 2021;13(6):1115. Published 2021 Jun 10. doi:10.3390/v13061115

72. Chai J, Cai Y, Pang C, et al. Structural basis for SARS-CoV-2 envelope protein recognition of human cell junction protein PALS1. Nat Commun. 2021;12(1):3433. Published 2021 Jun 8. doi:10.1038/s41467-021-23533-x

73. Shang J, Wan Y, Luo C, et al. Cell entry mechanisms of SARS-CoV-2. Proc Natl Acad Sci U S A. 2020;117(21):11727-11734. doi:10.1073/pnas.2003138117

74. Astuti I, Ysrafil. Severe Acute Respiratory Syndrome Coronavirus 2 (SARS-CoV-2): An overview of viral structure and host response. Diabetes Metab Syndr. 2020;14(4):407-412. doi:10.1016/j.dsx.2020.04.020

75. Redondo N, Zaldívar-López S, Garrido JJ, Montoya M. SARS-CoV-2 Accessory Proteins in Viral Pathogenesis: Knowns and Unknowns. Front Immunol. 2021;12:708264. Published 2021 Jul 7. doi:10.3389/fimmu.2021.708264

76. Lamers MM, Haagmans BL. SARS-CoV-2 pathogenesis. Nat Rev Microbiol. 2022;20(5):270-284. doi:10.1038/s41579-022-00713-0

77. Harrison AG, Lin T, Wang P. Mechanisms of SARS-CoV-2 Transmission and Pathogenesis. Trends Immunol. 2020;41(12):1100-1115. doi:10.1016/j.it.2020.10.004

78. Gusev E, Sarapultsev A, Solomatina L, Chereshnev V. SARS-CoV-2-Specific Immune Response and the Pathogenesis of COVID-19. Int J Mol Sci. 2022;23(3):1716. Published 2022 Feb 2. doi:10.3390/ijms23031716

79. Oprinca GC, Oprinca-Muja LA, Mihalache M, Birlutiu RM, Birlutiu V. Is SARS-CoV-2 Directly Responsible for Cardiac Injury? Clinical Aspects and Postmortem Histopathologic and Immunohistochemical Analysis. Microorganisms. 2022;10(7):1258. Published 2022 Jun 21. doi:10.3390/microorganisms10071258

80. Boeraș I, Curtean-Bănăduc A, Bănăduc D, Cioca G. Anthropogenic Sewage Water Circuit as Vector for SARS-CoV-2 Viral ARN Transport and Public Health Assessment, Monitoring and Forecasting-Sibiu Metropolitan Area (Transylvania/Romania) Study Case. Int J Environ Res Public Health. 2022;19(18):11725. Published 2022 Sep 17. doi:10.3390/ijerph191811725

81. Chrétien J, Basset F, Jaubert F, Soler P, Danel C. Cellular biology and pathology of type II pneumocytes. Int Arch Allergy Appl Immunol. 1985;76 Suppl 1:49-61. doi:10.1159/000233735

82. Fehrenbach H. Alveolar epithelial type II cell: defender of the alveolus revisited. Respir Res. 2001;2(1):33-46. doi:10.1186/rr36

83. Stanley MW, Henry-Stanley MJ, Gajl-Peczalska KJ, Bitterman PB. Hyperplasia of type II pneumocytes in acute lung injury. Cytologic findings of sequential bronchoalveolar lavage. Am J Clin Pathol. 1992;97(5):669-677. doi:10.1093/ajcp/97.5.669

84. Albrecht T, Fons M, Boldogh I, et al. Effects on Cells. In: Baron S, editor. Medical Microbiology. 4th edition. Galveston (TX): University of Texas Medical Branch at Galveston; 1996. Chapter 44. Available from: https://www.ncbi.nlm.nih.gov/books/NBK7979/

85. Leroy H, Han M, Woottum M, et al. Virus-Mediated Cell-Cell Fusion. Int J Mol Sci. 2020;21(24):9644. Published 2020 Dec 17. doi:10.3390/ijms21249644

86. Lin L, Li Q, Wang Y, Shi Y. Syncytia formation during SARS-CoV-2 lung infection: a disastrous unity to eliminate lymphocytes. Cell Death Differ. 2021;28(6):2019-2021. doi:10.1038/s41418-021-00795-y

87. Mandal RV, Mark EJ, Kradin RL. Megakaryocytes and platelet homeostasis in diffuse alveolar damage. Exp Mol Pathol. 2007;83(3):327-331. doi:10.1016/j.yexmp.2007.08.005

88. von Ranke FM, Zanetti G, Hochhegger B, Marchiori E. Infectious diseases causing diffuse alveolar hemorrhage in immunocompetent patients: a state-of-the-art review. Lung. 2013;191(1):9-18. doi:10.1007/s00408-012-9431-7

89. Cordier JF. Organising pneumonia. Thorax. 2000;55(4):318-328. doi:10.1136/thorax.55.4.318

90. Smith ML. Update on Pulmonary Fibrosis: Not All Fibrosis Is Created Equally. Arch Pathol Lab Med. 2016;140(3):221-229. doi:10.5858/arpa.2015-0288-SA

91. Ogino S, Franks TJ, Yong M, Koss MN. Extensive squamous metaplasia with cytologic atypia in diffuse alveolar damage mimicking squamous cell carcinoma: a report of 2 cases. Hum Pathol. 2002;33(10):1052-1054. doi:10.1053/hupa.2002.128246

92. Molfino NA, Jeffery PK. Chronic obstructive pulmonary disease: histopathology, inflammation and potential therapies. Pulm Pharmacol Ther. 2007;20(5):462-472. doi:10.1016/j.pupt.2006.04.003

93. Tuder RM, Stacher E, Robinson J, Kumar R, Graham BB. Pathology of pulmonary hypertension. Clin Chest Med. 2013;34(4):639-650. doi:10.1016/j.ccm.2013.08.009

94. Cooper LT Jr. Myocarditis. N Engl J Med. 2009;360(15):1526-1538. doi:10.1056/NEJMra0800028

95. Roberts WC. Pericardial heart disease: its morphologic features and its causes. Proc (Bayl Univ Med Cent). 2005;18(1):38-55. doi:10.1080/08998280.2005.11928030

96. Kossard S. Defining lymphocytic vasculitis. Australas J Dermatol. 2000;41(3):149-155. doi:10.1046/j.1440-0960.2000.00419.x

97. Espeland T, Lunde IG, H Amundsen B, Gullestad L, Aakhus S. Myocardial fibrosis. Myokardfibrose. Tidsskr Nor Laegeforen. 2018;138(16):10.4045/tidsskr.17.1027. Published 2018 Oct 12. doi:10.4045/tidsskr.17.1027

98. Tejado BSM, Jou C. Histopathology in HCM. Glob Cardiol Sci Pract. 2018;2018(3):20. Published 2018 Aug 12. doi:10.21542/gcsp.2018.20

99. Rosen S, Stillman IE. Acute tubular necrosis is a syndrome of physiologic and pathologic dissociation. J Am Soc Nephrol. 2008;19(5):871-875. doi:10.1681/ASN.2007080913

100. Afsar B, Ortiz A, Covic A, Solak Y, Goldsmith D, Kanbay M. Focus on renal congestion in heart failure. Clin Kidney J. 2016;9(1):39-47. doi:10.1093/ckj/sfv124

101. Panqueva, L., & Pilar, R.D. (2016). Useful Algorithms for Histopathological Diagnosis of Liver Disease Based on Patterns of Liver Damage.

102. Amzolini AM, Forţofoiu MC, Barău Abu-Alhija A, et al. Triglyceride and glucose index: a useful tool for non-alcoholic liver disease assessed by liver biopsy in patients with metabolic syndrome?. Rom J Morphol Embryol. 2021;62(2):475-480. doi:10.47162/RJME.62.2.13

103. Suttie AW. Histopathology of the spleen. Toxicol Pathol. 2006;34(5):466-503. doi:10.1080/01926230600867750

104. Hermida MD, de Melo CVB, Lima IDS, Oliveira GGS, Dos-Santos WLC. Histological Disorganization of Spleen Compartments and Severe Visceral Leishmaniasis. Front Cell Infect Microbiol. 2018;8:394. Published 2018 Nov 13. doi:10.3389/fcimb.2018.00394

105. Salzberger B, Buder F, Lampl B, et al. Epidemiology of SARS-CoV-2. Infection. 2021;49(2):233-239. doi:10.1007/s15010-020-01531-3

106. Pantea Stoian A, Pricop-Jeckstadt M, Pana A, et al. Death by SARS-CoV 2: a Romanian COVID-19 multi-centre comorbidity study. Sci Rep. 2020;10(1):21613. Published 2020 Dec 10. doi:10.1038/s41598-020-78575-w

107. Gebhard C, Regitz-Zagrosek V, Neuhauser HK, Morgan R, Klein SL. Impact of sex and gender on COVID-19 outcomes in Europe. Biol Sex Differ. 2020 May 25;11(1):29. doi: 10.1186/s13293-020-00304-9. PMID: 32450906; PMCID: PMC7247289.

108. Néant N, Lingas G, Le Hingrat Q, et al. Modeling SARS-CoV-2 viral kinetics and association with mortality in hospitalized patients from the French COVID cohort. Proc Natl Acad Sci U S A. 2021;118(8):e2017962118. doi:10.1073/pnas.2017962118

109. Grippo F, Navarra S, Orsi C, et al. The Role of COVID-19 in the Death of SARS-CoV-2-Positive Patients: A Study Based on Death Certificates. J Clin Med. 2020;9(11):3459. Published 2020 Oct 27. doi:10.3390/jcm9113459

110. Bonafè M, Prattichizzo F, Giuliani A, Storci G, Sabbatinelli J, Olivieri F. Inflamm-aging: Why older men are the most susceptible to SARS-CoV-2 complicated outcomes. Cytokine Growth Factor Rev. 2020;53:33-37. doi:10.1016/j.cytogfr.2020.04.005

111. Faes C, Abrams S, Van Beckhoven D, et al. Time between Symptom Onset, Hospitalisation and Recovery or Death: Statistical Analysis of Belgian COVID-19 Patients. Int J Environ Res Public Health. 2020;17(20):7560. Published 2020 Oct 17. doi:10.3390/ijerph17207560

112. Verity R, Okell LC, Dorigatti I, et al. Estimates of the severity of coronavirus disease 2019: a model-based analysis [published correction appears in Lancet Infect Dis. 2020 Apr 15;:] [published correction appears in Lancet Infect Dis. 2020 May 4;:]. Lancet Infect Dis. 2020;20(6):669-677. doi:10.1016/S1473-3099(20)30243-7

113. Baud D, Qi X, Nielsen-Saines K, Musso D, Pomar L, Favre G. Real estimates of mortality following COVID-19 infection. Lancet Infect Dis. 2020;20(7):773. doi:10.1016/S1473-3099(20)30195-X

114. Madabhavi I, Sarkar M, Kadakol N. COVID-19: a review. Monaldi Arch Chest Dis. 2020;90(2):10.4081/monaldi.2020.1298. Published 2020 May 14. doi:10.4081/monaldi.2020.1298

115. Ruan Q, Yang K, Wang W, Jiang L, Song J. Clinical predictors of mortality due to COVID-19 based on an analysis of data of 150 patients from Wuhan, China [published correction appears in Intensive Care Med. 2020 Apr 6;:]. Intensive Care Med. 2020;46(5):846-848. doi:10.1007/s00134-020-05991-x

116. Elezkurtaj S, Greuel S, Ihlow J, et al. Causes of death and comorbidities in hospitalized patients with COVID-19. Sci Rep. 2021;11(1):4263. Published 2021 Feb 19. doi:10.1038/s41598-021-82862-5

117. Qiu P, Zhou Y, Wang F, et al. Clinical characteristics, laboratory outcome characteristics, comorbidities, and complications of related COVID-19 deceased: a systematic review and meta-analysis. Aging Clin Exp Res. 2020;32(9):1869-1878. doi:10.1007/s40520-020-01664-3

118. Djaharuddin I, Munawwarah S, Nurulita A, Ilyas M, Tabri NA, Lihawa N. Comorbidities and mortality in COVID-19 patients. Gac Sanit. 2021;35 Suppl 2:S530-S532. doi:10.1016/j.gaceta.2021.10.085

119. Peña JE, Rascón-Pacheco RA, Ascencio-Montiel IJ, et al. Hypertension, Diabetes and Obesity, Major Risk Factors for Death in Patients with COVID-19 in Mexico. Arch Med Res. 2021;52(4):443-449. doi:10.1016/j.arcmed.2020.12.002

120. Phelps M, Christensen DM, Gerds T, et al. Cardiovascular comorbidities as predictors for severe COVID-19 infection or death. Eur Heart J Qual Care Clin Outcomes. 2021;7(2):172-180. doi:10.1093/ehjqcco/qcaa081

121. Koya SF, Ebrahim SH, Bhat LD, et al. COVID-19 and Comorbidities: Audit of 2,000 COVID-19 Deaths in India. J Epidemiol Glob Health. 2021;11(2):230-232. doi:10.2991/jegh.k.210303.001

122. Khan MMA, Khan MN, Mustagir MG, Rana J, Islam MS, Kabir MI. Effects of underlying morbidities on the occurrence of deaths in COVID-19 patients: A systematic review and meta-analysis. J Glob Health. 2020;10(2):020503. doi:10.7189/jogh.10.020503

123. Potere N, Valeriani E, Candeloro M, et al. Acute complications and mortality in hospitalized patients with coronavirus disease 2019: a systematic review and meta-analysis. Crit Care. 2020;24(1):389. Published 2020 Jul 2. doi:10.1186/s13054-020-03022-1

124. Fitzek A, Schädler J, Dietz E, et al. Prospective postmortem evaluation of 735 consecutive SARS-CoV-2-associated death cases. Sci Rep. 2021;11(1):19342. Published 2021 Sep 29. doi:10.1038/s41598-021-98499-3

125. Kim AR, Lee J, Park S, et al. Comparison of the causes of death associated with delta and Omicron SARS-CoV-2 variants infection. J Infect Public Health. 2023;16(1):133-135. doi:10.1016/j.jiph.2022.11.030

126. De Nardi P, Parolini DC, Ripa M, Racca S, Rosati R. Bowel perforation in a Covid-19 patient: case report. Int J Colorectal Dis. 2020;35(9):1797-1800. doi:10.1007/s00384-020-03627-6

127. Al Argan RJ, Alqatari SG, Al Said AH, et al. Gastrointestinal perforation secondary to COVID-19: Case reports and literature review. Medicine (Baltimore). 2021;100(19):e25771. doi:10.1097/MD.0000000000025771

128. Chaugale SB, Singhal V, Kapoor D, Singh A. Gastrointestinal complications (gangrene or perforation) after corona virus disease 2019 - A series of ten patients. Indian J Gastroenterol. 2022;41(3):307-312. doi:10.1007/s12664-021-01218-z

129. Giuffrè M, Bozzato AM, Di Bella S, et al. Spontaneous Rectal Perforation in a Patient with SARS-CoV-2 Infection. J Pers Med. 2020;10(4):157. Published 2020 Oct 8. doi:10.3390/jpm10040157

130. Elhence A, Ghoshal UC. Gastrointestinal perforation and vascular thrombosis in patients with corona virus disease-19: A life-threatening problem. Indian J Gastroenterol. 2022;41(3):218-223. doi:10.1007/s12664-022-01265-0

131. Ranchal P, Yates E, Gupta R, Aronow WS. Tocilizumab-Associated Bowel Perforation in SARS-CoV-2 Infection. Am J Ther. 2022;29(6):e699-e702. doi:10.1097/MJT.0000000000001273

132. Vikse J, Henry BM. Tocilizumab in COVID-19: Beware the risk of intestinal perforation. Int J Antimicrob Agents. 2020;56(1):106009. doi:10.1016/j.ijantimicag.2020.106009

133. Rojo M, Cano-Valderrama O, Picazo S, et al. Gastrointestinal Perforation After Treatment With Tocilizumab : An Unexpected Consequence of COVID-19 Pandemic. Am Surg. 2020;86(6):565-566. doi:10.1177/0003134820926481

134. Yao XH, Luo T, Shi Y, et al. A cohort autopsy study defines COVID-19 systemic pathogenesis. Cell Res. 2021;31(8):836-846. doi:10.1038/s41422-021-00523-8

135. Poletti V, Casoni GL, Cancellieri A, Piciucchi S, Dubini A, Zompatori M. Diffuse alveolar damage. Pathologica. 2010;102(6):453-463.

136. Septimiu-Radu S, Gadela T, Gabriela D, et al. A Systematic Review of Lung Autopsy Findings in Elderly Patients after SARS-CoV-2 Infection. J Clin Med. 2023;12(5):2070. Published 2023 Mar 6. doi:10.3390/jcm12052070

137. Tian S, Xiong Y, Liu H, Niu L, Guo J, Liao M, Xiao SY. Pathological study of the 2019 novel coronavirus disease (COVID-19) through postmortem core biopsies. Mod Pathol. 2020;33:1007–1014. doi: 10.1038/s41379-020-0536-x. [PMC free article] [PubMed] [CrossRef] [Google Scholar]

138. Zhang H, Zhou P, Wei Y, Yue H, Wang Y, Hu M, Zhang S, Cao T, Yang C, Li M, Guo G, Chen X, Chen Y, Lei M, Liu H, Zhao J, Peng P, Wang CY, Du R. Histopathologic changes and SARS-CoV-2 immunostaining in the lung of a patient with COVID-19. Annals of Internal

Medicine. 2020;172(9):629–632. doi: 10.7326/M20-0533. [PMC free article] [PubMed] [CrossRef] [Google Scholar]

139. Barton LM, Duval EJ, Stroberg E, Ghosh S, Mukhopadhyay COVID-19 Autopsies, Oklahoma, USA. Am J Clin Pathol. 2020;153:725–733. doi: 10.1093/ajcp/aqaa062. [PMC free article] [PubMed] [CrossRef] [Google Scholar]

140. Fitzek A, Sperhake J, Edler C, Schröder AS, Heinemann A, Heinrich F, Ron A, Mushumba H, Lütgehetmann M, Püschel K. Evidence for systematic autopsies in COVID-19 positive deceased: case report of the first German investigated COVID-19 death. Rechtsmedizin. 2020;30:184–189. doi: 10.1007/s00194-020-00401-4. [PMC free article] [PubMed] [CrossRef] [Google Scholar]

141. Hanley LS, Lucas SB, Youd E, Swift B, Osborn M. Autopsy in suspected COVID-19 cases. J Clin Pathol. 2020;73:239–242. doi: 10.1136/jclinpath-2020-206522. [PubMed] [CrossRef] [Google Scholar]

142. Suess C, Hausmann R (2020) Gross and histopathological pulmonary findings in a COVID-19 associated death during self-isolation. Int J Leg Med. 10.1007/s00414-020-02319-8 [PMC free article] [PubMed]

143. Buchrieser J, Schwartz O. Pregnancy complications and Interferon-induced transmembrane proteins (IFITM): balancing antiviral immunity and placental development. C R Biol. 2021;344(2):145-156. Published 2021 Jul 2. doi:10.5802/crbiol.54

144. Hernández JM, Podbilewicz B. The hallmarks of cell-cell fusion. Development. 2017;144(24):4481-4495. doi:10.1242/dev.155523

145. Zhang Z, Zheng Y, Niu Z, et al. SARS-CoV-2 spike protein dictates syncytium-mediated lymphocyte elimination. Cell Death Differ. 2021;28(9):2765-2777. doi:10.1038/s41418-021-00782-3

146. Buchrieser J, Dufloo J, Hubert M, et al. Syncytia formation by SARS-CoV-2-infected cells. EMBO J. 2021;40(3):e107405. doi:10.15252/embj.2020107405

147. Rajah MM, Bernier A, Buchrieser J, Schwartz O. The Mechanism and Consequences of SARS-CoV-2 Spike-Mediated Fusion and Syncytia Formation. J Mol Biol. 2022;434(6):167280. doi:10.1016/j.jmb.2021.167280

148. Borczuk AC, Salvatore SP, Seshan SV, et al. COVID-19 pulmonary pathology: a multi-institutional autopsy cohort from Italy and New York City. Mod Pathol. 2020;33(11):2156-2168. doi:10.1038/s41379-020-00661-1

149. Damiani S, Fiorentino M, De Palma A, et al. Pathological post-mortem findings in lungs infected with SARS-CoV-2. J Pathol. 2021;253(1):31-40. doi:10.1002/path.5549

150. Calabrese F, Pezzuto F, Fortarezza F, et al. Pulmonary pathology and COVID-19: lessons from autopsy. The experience of European Pulmonary Pathologists. Virchows Arch. 2020;477(3):359-372. doi:10.1007/s00428-020-02886-6

151. Satturwar S, Fowkes M, Farver C, et al. Postmortem Findings Associated With SARS-CoV-2: Systematic Review and Meta-analysis. Am J Surg Pathol. 2021;45(5):587-603. doi:10.1097/PAS.0000000000001650

152. Aguiar D, Lobrinus JA, Schibler M, Fracasso T, Lardi C. Inside the lungs of COVID-19 disease. Int J Legal Med. 2020;134(4):1271-1274. doi:10.1007/s00414-020-02318-9

153. Falasca L, Nardacci R, Colombo D, et al. Postmortem Findings in Italian Patients With COVID-19: A Descriptive Full Autopsy Study of Cases With and Without Comorbidities. J Infect Dis. 2020;222(11):1807-1815. doi:10.1093/infdis/jiaa578

154. Gawelek KL, Padera R, Connors J, Pinkus GS, Podznyakova O, Battinelli EM. Cardiac megakaryocytes in SARS-CoV-2-positive autopsies. Histopathology. 2022;81(5):600-624. doi:10.1111/his.14734

155. Iwamura C, Hirahara K, Kiuchi M, et al. Elevated Myl9 reflects the Myl9-containing microthrombi in SARS-CoV-2-induced lung exudative vasculitis and predicts COVID-19 severity. Proc Natl Acad Sci U S A. 2022;119(33):e2203437119. doi:10.1073/pnas.2203437119

156. Iba T, Connors JM, Levy JH. The coagulopathy, endotheliopathy, and vasculitis of COVID-19. Inflamm Res. 2020;69(12):1181-1189. doi:10.1007/s00011-020-01401-6

157. Damiani E, Carsetti A, Casarotta E, et al. Microvascular alterations in patients with SARS-COV-2 severe pneumonia. Ann Intensive Care. 2020;10(1):60. Published 2020 May 20. doi:10.1186/s13613-020-00680-w

158. Yang Y, Wu Y, Meng X, et al. SARS-CoV-2 membrane protein causes the mitochondrial apoptosis and pulmonary edema via targeting BOK. Cell Death Differ. 2022;29(7):1395-1408. doi:10.1038/s41418-022-00928-x

159. Löffler C, Mahrhold J, Fogarassy P, Beyer M, Hellmich B. Two Immunocompromised Patients With Diffuse Alveolar Hemorrhage as a Complication of Severe Coronavirus Disease 2019. Chest. 2020;158(5):e215-e219. doi:10.1016/j.chest.2020.06.051

160. Wendisch D, Dietrich O, Mari T, et al. SARS-CoV-2 infection triggers profibrotic macrophage responses and lung fibrosis. Cell. 2021;184(26):6243-6261.e27. doi:10.1016/j.cell.2021.11.033

161. Parimon T, Espindola M, Marchevsky A, Rampolla R, Chen P, Hogaboam CM. Potential mechanisms for lung fibrosis associated with COVID-19 infection. QJM. 2023;116(7):487-492. doi:10.1093/qjmed/hcac206

162. Margaroli C, Benson P, Sharma NS, et al. Spatial mapping of SARS-CoV-2 and H1N1 lung injury identifies differential transcriptional signatures. Cell Rep Med. 2021;2(4):100242. doi:10.1016/j.xcrm.2021.100242

163. Maffia-Bizzozero S, Cevallos C, Lenicov FR, et al. Viable SARS-CoV-2 Omicron sub-variants isolated from autopsy tissues. Front Microbiol. 2023;14:1192832. Published 2023 May 22. doi:10.3389/fmicb.2023.1192832

164. Caniego-Casas T, Martínez-García L, Alonso-Riaño M, et al. RNA SARS-CoV-2 Persistence in the Lung of Severe COVID-19 Patients: A Case Series of Autopsies. Front Microbiol. 2022;13:824967. Published 2022 Jan 31. doi:10.3389/fmicb.2022.824967

165. Musso N, Falzone L, Stracquadanio S, et al. Post-Mortem Detection of SARS-CoV-2 RNA in Long-Buried Lung Samples. Diagnostics (Basel). 2021;11(7):1158. Published 2021 Jun 24. doi:10.3390/diagnostics11071158

166. Beltempo P, Curti SM, Maserati R, Gherardi M, Castelli M. Persistence of SARS-CoV-2 RNA in post-mortem swab 35 days after death: A case report. Forensic Sci Int. 2021;319:110653. doi:10.1016/j.forsciint.2020.110653

167. Owusu D, Pomeroy MA, Lewis NM, et al. Persistent SARS-CoV-2 RNA Shedding Without Evidence of Infectiousness: A Cohort Study of Individuals With COVID-19. J Infect Dis. 2021;224(8):1362-1371. doi:10.1093/infdis/jiab107

168. Schaefer IM, Padera RF, Solomon IH, et al. In situ detection of SARS-CoV-2 in lungs and airways of patients with COVID-19. Mod Pathol. 2020;33(11):2104-2114. doi:10.1038/s41379-020-0595-z

169. Martines RB, Ritter JM, Matkovic E, et al. Pathology and Pathogenesis of SARS-CoV-2 Associated with Fatal Coronavirus Disease, United States. Emerg Infect Dis. 2020;26(9):2005-2015. doi:10.3201/eid2609.202095

170. Bussani R, Zentilin L, Correa R, et al. Persistent SARS-CoV-2 infection in patients seemingly recovered from COVID-19. J Pathol. 2023;259(3):254-263. doi:10.1002/path.6035

171. Zou X., Fang M., Li S., Wu L., Gao B., Gao H., Ran X., Bian Y., Li R., Yu S., et al. Characteristics of Liver Function in Patients With SARS-CoV-2 and Chronic HBV Coinfection. Clin. Gastroenterol. Hepatol. 2021;19:597–603. doi: 10.1016/j.cgh.2020.06.017. [PMC free article]

172. Lindner D., Fitzek A., Bräuninger H., Aleshcheva G., Edler C., Meissner K., Scherschel K., Kirchhof P., Escher F., Schultheiss H.-P., et al. Association of Cardiac Infection With SARS-CoV-2 in Confirmed COVID-19 Autopsy Cases. JAMA Cardiol. 2020;5:1281–1285. doi: 10.1001/jamacardio.2020.3551.

173. Kawakami R., Sakamoto A., Kawai K., Gianatti A., Pellegrini D., Nasr A., Kutys B., Guo L., Cornelissen A., Mori M., et al. Pathological Evidence for SARS-CoV-2 as a Cause of Myocarditis: JACC Review Topic of the Week. J. Am. Coll. Cardiol. 2021;77:314–325. doi: 10.1016/j.jacc.2020.11.031

174. Zhang X., Tan Y., Ling Y., Lu G., Liu F., Yi Z., Jia X., Wu M., Shi B., Xu S., et al. Viral and host factors related to the clinical outcome of COVID-19. Nature. 2020;583:437–440. doi: 10.1038/s41586-020-2355-0.

175. Das M, Bristow MR, Chung MK. The Essential Vulnerability of Human Cardiac Myocytes to SARS-CoV-2. JACC Basic Transl Sci. 2021;6(4):346-349. Published 2021 Apr 27. doi:10.1016/j.jacbts.2021.02.010

176. Rivero J, Merino-López M, Olmedo R, et al. Association between Postmortem Kidney Biopsy Findings and Acute Kidney Injury from Patients with SARS-CoV-2 (COVID-19). Clin J Am Soc Nephrol. 2021;16(5):685-693. doi:10.2215/CJN.16281020

177. Mahjani M, Parvin M, Ghobadi S, et al. Postmortem Histopathologic Findings and SARS-CoV-2 Detection in Autopsy Kidneys of Patients With COVID-19: A Systematic Review and Meta-Analysis. Am J Clin Pathol. 2023;159(5):429-436. doi:10.1093/ajcp/aqad001

178. orge D, Bernardi S, Arcangeli M, Bianchi S. Histopathological Features of SARS-CoV-2 in Extrapulmonary Organ Infection: A Systematic Review of Literature. Pathogens. 2022;11(8):867. Published 2022 Jul 31. doi:10.3390/pathogens11080867

179. Wang M, Xiong H, Chen H, Li Q, Ruan XZ. Renal Injury by SARS-CoV-2 Infection: A Systematic Review. Kidney Dis (Basel). 2021;7(2):100-110. doi:10.1159/000512683

180. Massoth LR, Desai N, Szabolcs A, et al. Comparison of RNA In Situ Hybridization and Immunohistochemistry Techniques for the Detection and Localization of SARS-CoV-2 in Human Tissues. Am J Surg Pathol. 2021;45(1):14-24. doi:10.1097/PAS.0000000000001563

181. Lau WL, Zuckerman JE, Gupta A, Kalantar-Zadeh K. The COVID-Kidney Controversy: Can SARS-CoV-2 Cause Direct Renal Infection?. Nephron. 2021;145(3):275-279. doi:10.1159/000513789

182. Pesti A, Danics K, Glasz T, et al. Liver alterations and detection of SARS-CoV-2 RNA and proteins in COVID-19 autopsies. Geroscience. 2023;45(2):1015-1031. doi:10.1007/s11357-022-00700-6

183. Bahadur G, Bhat M, Acharya S, et al. Retrospective observational RT-PCR analyses on 688 babies born to 843 SARS-CoV-2 positive mothers, placental analyses and diagnostic analyses limitations suggest vertical transmission is possible. Facts Views Vis Obgyn. 2021;13(1):53-66. Published 2021 Mar 31. doi:10.52054/FVVO.13.1.001

184. Marinho PS, da Cunha AJLA, Chimelli L, et al. Case Report: SARS-CoV-2 Mother-to-Child Transmission and Fetal Death Associated With Severe Placental Thromboembolism. Front Med (Lausanne). 2021;8:677001. Published 2021 Aug 16. doi:10.3389/fmed.2021.677001

185. Dubucs C, Groussolles M, Ousselin J, et al. Severe placental lesions due to maternal SARS-CoV-2 infection associated to intrauterine fetal death. Hum Pathol. 2022;121:46-55. doi:10.1016/j.humpath.2021.12.012

186. di Gioia C, Zullo F, Bruno Vecchio RC, et al. Stillbirth and fetal capillary infection by SARS-CoV-2. Am J Obstet Gynecol MFM. 2022;4(1):100523. doi:10.1016/j.ajogmf.2021.100523

187. Lesieur E, Torrents J, Fina F, et al. Congenital Infection of Severe Acute Respiratory Syndrome Coronavirus 2 With Intrauterine Fetal Death: A Clinicopathological Study With Molecular Analysis. Clin Infect Dis. 2022;75(1):e1092-e1100. doi:10.1093/cid/ciab840

188. Patanè L, Cadamuro M, Massazza G, et al. Evidence of vertical transmission of SARS-CoV-2 and interstitial pneumonia in second-trimester twin stillbirth in asymptomatic woman. Case report and review of the literature. Am J Obstet Gynecol MFM. 2022;4(3):100589. doi:10.1016/j.ajogmf.2022.100589

189. Linehan L, O'Donoghue K, Dineen S, White J, Higgins JR, Fitzgerald B. SARS-CoV-2 placentitis: An uncommon complication of maternal COVID-19. Placenta. 2021;104:261-266. doi:10.1016/j.placenta.2021.01.012

190. Mao Q, Chu S, Shapiro S, Young L, Russo M, De Paepe ME. Placental SARS-CoV-2 distribution correlates with level of tissue oxygenation in COVID-19-associated necrotizing histiocytic intervillositis/perivillous fibrin deposition. Placenta. 2022;117:187-193. doi:10.1016/j.placenta.2021.12.002.